National Library of Canada
Bibliothèque nationale du Canada

Canadian Theses Service
Service des thèses canadiennes

Ottawa, Canada
K1A 0N4

NOTICE

The quality of this microform is heavily dependent upon the quality of the original thesis submitted for microfilming. Every effort has been made to ensure the highest quality of reproduction possible.

If pages are missing, contact the university which granted the degree.

Some pages may have indistinct print especially if the original pages were typed with a poor typewriter ribbon or if the university sent us an inferior photocopy.

Reproduction in full or in part of this microform is governed by the Canadian Copyright Act, R.S.C. 1970, c. C-30, and subsequent amendments.

AVIS

La qualité de cette microforme dépend grandement de la qualité de la thèse soumise au microfilmage. Nous avons tout fait pour assurer une qualité supérieure de reproduction.

S'il manque des pages, veuillez communiquer avec l'université qui a conféré le grade.

La qualité d'impression de certaines pages peut laisser à désirer, surtout si les pages originales ont été dactylographiées à l'aide d'un ruban usé ou si l'université nous a fait parvenir une photocopie de qualité inférieure.

La reproduction, même partielle, de cette microforme est soumise à la Loi canadienne sur le droit d'auteur, SRC 1970, c. C-30, et ses amendements subséquents.

NL-339 (r. 88/04) c

Canada

National Library of Canada
Bibliothèque nationale du Canada

Canadian Theses Service
Service des thèses canadiennes

Ottawa, Canada
K1A 0N4

The author has granted an irrevocable non-exclusive licence allowing the National Library of Canada to reproduce, loan, distribute or sell copies of his/her thesis by any means and in any form or format, making this thesis available to interested persons.

L'auteur a accordé une licence irrévocable et non exclusive permettant à la Bibliothèque nationale du Canada de reproduire, prêter, distribuer ou vendre des copies de sa thèse de quelque manière et sous quelque forme que ce soit pour mettre des exemplaires de cette thèse à la disposition des personnes intéressées.

The author retains ownership of the copyright in his/her thesis. Neither the thesis nor substantial extracts from it may be printed or otherwise reproduced without his/her permission.

L'auteur conserve la propriété du droit d'auteur qui protège sa thèse. Ni la thèse ni des extraits substantiels de celle-ci ne doivent être imprimés ou autrement reproduits sans son autorisation.

ISBN 0-315-56063-0

Canada

Detection of Onset of Instabilities for an Early Warning Safety Monitor for Articulated Freight Vehicles

Alain Piché

A Thesis

in

The Department

of

Mechanical Engineering

Presented in Partial Fulfillment of the Requirements
for the degree of Master of Engineering at
Concordia University
Montréal, Québec, Canada

January 1990

© Alain Piché, 1990

ABSTRACT

Detection of Onset of Instabilities for an Early Warning Safety Monitor for Articulated Freight Vehicles

Alain Piché

The directional dynamics of articulated freight vehicles is investigated in order to determine the key vehicle response parameters related to onset of rollover. Roll stability of an articulated vehicle is investigated via computer simulation for low speed cornering and high speed directional maneuvers. Attempts are made to relate the onset of roll instability to various vehicle response parameters. These vehicle response parameters are thoroughly reviewed in view of their reliability and ease of on-line acquisition. A comprehensive database on the properties and geometry of the vehicle is compiled. Sensitivity of response parameters to variations in vehicle parameters is evaluated in order to arrive at a set of key response variables that can best describe the onset of roll instability. The study concludes that the sprung mass lateral acceleration and rearmost axle's roll angle response can best relate to onset of roll instability experienced during cornering and high-speed directional maneuvers, respectively. Vehicle jackknife, caused by wheel lockup at the tractor's rear axles, is investigated through simulation of a comprehensive vehicle dynamics software, referred to as "Phase IV Model". Directional response characteristics of the articulated vehicle are evaluated for braking-in-a-turn maneuver in order to express the onset of vehicle jackknife via measurable vehicle response parameters. Directional behavior of the vehicle is further investigated for variations in braking force distribution and two necessary conditions are derived that

can detect the onset of vehicle jackknife. The key operational parameters related to the occurrence of accidents involving heavy vehicles are thus identified and the design of an early warning monitor is proposed. The microprocessor based early warning safety monitor can warn the driver of an impending instability such that an appropriate corrective action may be taken to avert the occurrence of an accident.

ACKNOWLEDGEMENT

The financial supports received from FCAR's "Bourse de maitrise en genie et autres sciences appliquées" and CONCAVE Research Center, and the technical supports provided by Dr. S. Rakheja and Dr. T.S. Sankar are greatly acknowledged.

TABLE OF CONTENTS

LIST OF FIGURES

LIST OF TABLES

NOMENCLATURE

$\vec{a}_c$	Fifth wheel acceleration (m/s^2)
$\vec{a}_{mUi}$	Acceleration of the i^{th} unsprung mass (m/s^2)
$\vec{a}_{mSk}$	Acceleration of the k^{th} sprung mass (m/s^2)
$\vec{a}_{mUi/Ri}$	i^{th} unsprung mass acceleration with respect to the roll center (m/s^2)
$\vec{a}_{Ri/mSk}$	Acceleration of the i^{th} roll center with respect to the center of gravity of the k^{th} sprung mass (m/s^2)
AT_{ij}	Aligning torque generated at the tire-road interface of the j^{th} tire on axle i (N·m)
a_y	Lateral acceleration (g's)
$\bar{a}_y$	Safe value of lateral acceleration (g's)
a_y^c	Rollover threshold of the compliant vehicle (g's)
a_y^*	Rollover threshold of a rigidly suspended vehicle (g's)
A_i	Dual tire spacing on axle i (m)
$[A_{ij}]_k$	Transformation matrix from the k^{th} sprung mass body fixed coordinate system to the inertial coordinate system
BTORQ	Total brake torque on the tandem set (N·m)
C	Compliance factor
$\bar{C}$	Mean value of compliance factor
C^*	Threshold value of compliance factor
C_{FR}	Tractor frame Coulomb friction (N)
$\vec{d}$	Vector of vehicle dimensions, positions and velocities
$\vec{f}_c$	Vector of constraint forces
F_{ij}	Force due to the j^{th} suspension spring on axle i (N)
F_r	Approximate lateral force at the tractor drive axles (N)

F_{Rl}	Force acting through the roll center in a direction parallel to the $\vec{j}_u$ axis (N)
FSHIFT	Dynamic load transfer ratio
F_{sl}	Suspension force transmitted to the sprung mass for axle i (N)
F_{yl}	Total lateral force at the tire-road interface of axle i (N)
F_{ylj}	Lateral force at the tire-road interface of the j^{th} tire on axle i (N)
F_{zlj}	Vertical force at the tire-road interface of the j^{th} tire on axle i (N)
F_{5y}	Lateral constraint force acting on the fifth wheel (N)
g	Gravitational acceleration (9.81 m/s^2)
h	Height of the vehicle center of gravity above ground level (m)
HR_l	Vertical distance of roll center from the ground plane (m)
H_{Ul}	Vertical distance of the center of gravity of the i^{th} unsprung mass from the ground plane (m)
I_{XXSk}	Roll mass moment of inertia of the sprung mass k ($kg \cdot m^2$)
I_{YYSk}	Pitch mass moment of inertia of the sprung mass k ($kg \cdot m^2$)
I_{ZZl}	Total yaw mass moment of inertia of the tractor ($kg \cdot m^2$)
I_{ZZSk}	Yaw mass moment of inertia of the sprung mass k ($kg \cdot m^2$)
I_{ZZUl}	Yaw mass moment of inertia of the i^{th} unsprung mass ($kg \cdot m^2$)
K_{lj}	Vertical stiffness of the j^{th} suspension spring on axle i (N/m)
K_{FR}	Torsional stiffness of tractor frame (N·m/rad)
$KOVT_{lj}$	Roll resisting stiffness at the tire-road interface of the j^{th} tire on axle i (N·m/rad)
KRS_l	Auxiliary roll stiffness of the suspension spring on axle i (N·m/rad)

KT_{ij}	Vertical stiffness of the j^{th} tire on axle i (N/m)
KYT_{ij}	Lateral stiffness of the j^{th} tire on axle i (N/m)
K_S	Torsional stiffness of the fifth wheel (N·m/rad)
m_1	Total mass of the tractor (k_g)
M	Inertia matrix
m_{Sk}	Sprung mass k (kg)
m_{Ui}	Unsprung mass of axle i (kg)
M_{FR}	Roll moment transmitted through the frame (N·m)
M_{x1}	Roll moment acting on the tractor at the fifth wheel (N·m)
M_{x2}	Roll moment acting on the semitrailer kingpin (N·m)
M_{y2}	Pitch moment acting on the semitrailer kingpin (N·m)
N	Vehicle dimensions matrix
OVT_{ij}	Roll resisting moment at the tire-road interface of the j^{th} tire on axle i (N·m)
p_{Sk}	Roll rate of the k^{th} sprung mass (rad/s)
p_{Ui}	Roll rate of the i^{th} unsprung mass (rad/s)
q_{Sk}	Pitch rate of the k^{th} sprung mass (rad/s)
r_{Sk}	Yaw rate of the k^{th} sprung mass (rad/s)
r_{Ui}	Yaw rate of the i^{th} unsprung mass (rad/s)
R_i	Rolling radius of the tires on axle i (m)
s_i	Half of the lateral distance between suspension springs on axle i (m)
SF	Vertical suspension force in the absence of braking for walking beam suspension (N)
$\overline{SF}$	Total suspension force during braking for walking beam suspension (N)
TD	Tandem spread of the axle (m)

T_i Half of the lateral distance between the inner tires on axle i (m)

T_{ij} Transformation matrix of the constraint equation

u_{Sk} Longitudinal velocity of the k^{th} sprung mass (m/s)

$u_{tire_{ij}}$ Forward velocity of the j^{th} tire on axle i (m/s)

v_{axle_i} Lateral velocity of axle i (m/s)

v_{Sk} Lateral velocity of the k^{th} sprung mass (m/s)

w_{Sk} Vertical velocity of the k^{th} sprung mass (m/s)

W Total weight of the sprung and unsprung masses (N)

W_{Si} Weight of the i^{th} sprung mass (N)

W_{Ui} Weight of the i^{th} unsprung mass (N)

$WAXL_i$ Load carried by axle i (N)

W_{FR} Vertical shear force acting through the tractor frame (N)

W_S Vertical load on the fifth wheel (N)

$\ddot{\vec{x}}$ Acceleration vector (m/s^2)

x_{Ri} Longitudinal distance between the roll center i and the center of gravity of the sprung mass (m)

x_{Ui} Longitudinal distance from the sprung mass center of gravity to axle i (m)

x_S Longitudinal distance between the tractor center of gravity and the fifth wheel (m)

y_i Lateral displacement of axle i due to the lateral compliance of the tire (m)

z_{FRi} Vertical distance between the torsional axis of the tractor frame and ground plane (m)

z_{Ri} Vertical distance between the sprung mass center of gravity and the roll center of axle i (m)

z_{Ui} Vertical distance between the roll center and the center of gravity of axle i (m)

z_{Uoi} Vertical distance between the i^{th} roll center and i^{th} axle center of gravity at $t = 0$ (m)

z_{Si} Vertical distance from the fifth wheel coupling to the ground plane (m)

α Safety factor

α_{ji} Sideslip angle of the j^{th} tire on axle i (rad)

δ_1 Front wheel steer angle (rad)

Δ_{ij} Vertical deflection of the j^{th} tire on axle i (m)

Δ_{oi} Vertical deflection of tires on axle i at $t = 0$ (m)

Δz_{Sk} Vertical deflection of the k^{th} sprung mass center of gravity along the inertial axis $\vec{k}_n$ (m)

ϕ Roll angle (rad)

ϕ_{Sk} Roll angle of the k^{th} sprung mass (rad)

ϕ_{Ui} Roll angle of the i^{th} unsprung mass (rad)

ψ_{Sk} Yaw angle of the k^{th} sprung mass (rad)

θ_{Sk} Pitch angle of the k^{th} sprung mass (rad)

σ Standard deviation

γ Articulation angle (rad)

$\dot{}$ First derivative with respect to time

$\ddot{}$ Second derivative with respect to time

CHAPTER 1

INTRODUCTION AND LITERATURE REVIEW

1.1 GENERAL

For reasons of economy, the Canadian trucking industry has indicated a continuing interest in increasing the sizes and load carrying capacities of freight vehicles. In the last few years, the vehicle weights and dimensions regulations have been relaxed considerably in Canada. Many studies carried out for the trucking industry and policy makers have established that:

(a) Handling and control characteristics of articulated freight vehicles are adversely affected by the increased weights and dimensions [1].

(b) The rollover immunity of articulated freight vehicles is so low that a moderately severe maneuver often causes significant magnitude of lateral forces, and yaw and roll moments that may lead to instability. The rollover immunity of articulated freight vehicles is further deteriorated by the increased weights and dimensions [2].

As with all motor vehicles, the driver control is limited to braking, acceleration and steering inputs. A combination of these controls is required to operate the vehicle under routine or non-routine, often severe, avoidance maneuvers when the driver is confronted with a potential crash threat. In the case of most four-wheel vehicles, relatively severe levels of either steering and/or braking must be made to induce dynamic instabilities. However, this is not the case with heavy vehicles, they are proportionally more involved in single vehicle

accidents (rollovers, loss-of-control, jackknifes, and collisions with roadside fixed objects) than passenger cars and light trucks. A review of heavy vehicle accident files revealed that heavy trucks were involved in 28% of single vehicle accidents as compared with 19% for passenger vehicles [3]. Almost 60% of the heavy vehicle accidents were associated with rollover [4]. Review of highway accident files further revealed that 9% of the multiple vehicle accidents involving heavy freight vehicles resulted in rollover of the heavy vehicle, while the 33% of single vehicle accidents involving heavy vehicles resulted in rollover. The vehicle rollover often occurs at low speeds during a cornering maneuver [5,6].

The high center of gravity of many freight vehicles, especially when laden, and the dynamic characteristics of articulated vehicles are the primary contributory factors to vehicle accidents leading to rollover and jackknife. Heavy vehicle instabilities can be classified in two broad classes based upon the type of maneuver: (i) roll instability and (ii) yaw instability, as shown in Figure 1.1. The roll instability can be further described in terms of low speed and high speed roll instability. The low speed roll instability is experienced during steady turning maneuvers when the centrifugal forces imposed on the vehicle exceed the rollover threshold of the vehicle. Such a roll instability often leads to either vehicle rollover or vehicle running off the road or a combination of both. High speed roll instability is often caused by the rapid steer inputs when the driver is confronted with a potential crash threat. Sudden lane changes at high speeds generate diverging directional response which may lead to rollover in the absence of corrective steering action. The roll instabilities are

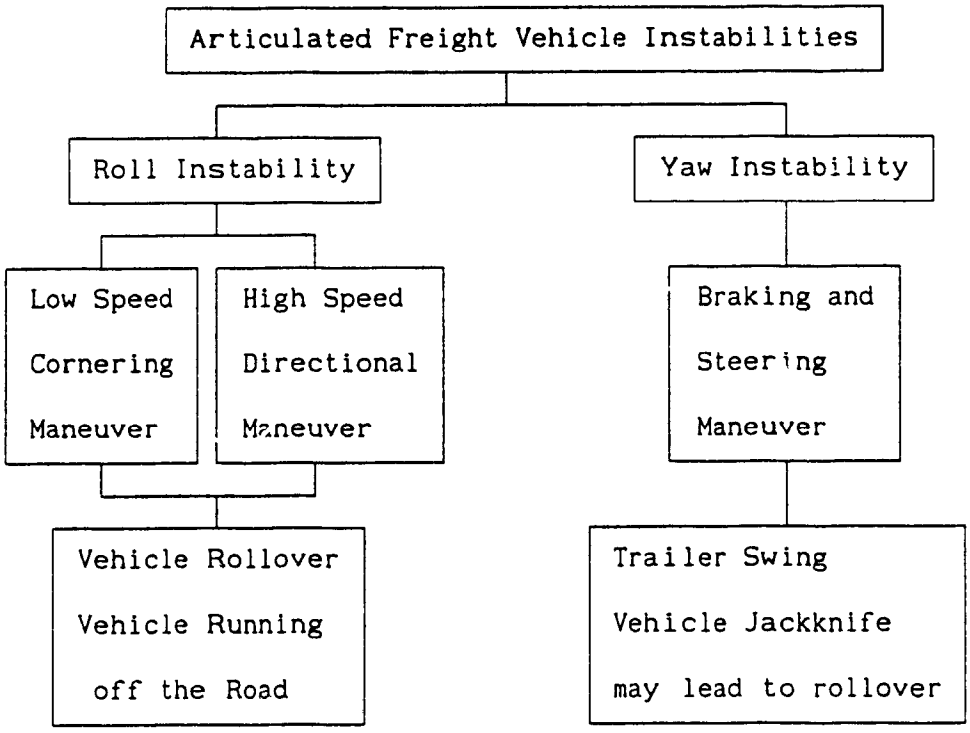

FIGURE 1.1: Articulated Freight Vehicle Instabilities Classification

often initiated at the rearmost axle of the articulated freight vehicles and the driver often remains unaware of such impending instability due to the excessive size of the vehicle.

The yaw instability, caused by either braking or combined braking and steering maneuvers, can lead to vehicle jackknife. The primary cause of yaw instability is the rearward bias of the braking forces typical in the heavy vehicle brake system design, increasing the probability of tractor rear wheels to experience lockup. When lockup occurs, the tires lose their ability to generate cornering forces and the vehicle experiences yaw instability. Unstable yaw response along with rapid corrective steering maneuvers of the heavy vehicle often leads to vehicle jackknife followed by a rollover.

Consequently, in view of the recently relaxed weights and dimensions, and increased population of heavy articulated vehicles on the highways, there exists an increased concern over their operational safety. Their potential instabilities and extremely high inertia pose high risks to highway safety and commercial property. The driver often remains unaware of the impending roll instabilities at the trailer axles and the directional instabilities caused by the vehicle jackknife are quite rapid to be detected by the driver. A delay in corrective action causes risks to the driver, the vehicle and the highway safety

Thus there exists a need to monitor the dynamics of heavy vehicle during their operation, in order to warn the driver of the impending instabilities. The driver could then take an appropriate corrective action to minimize the severity of instabilities and to maximize the preservation of the vehicle and the highway safety

In an attempt to minimize the potential risks to highway safety, it has been proposed that the efforts should be directed towards development of effective methods to assess the relative stability performance of various highway vehicle combinations. The assessment method must account for static and dynamic characteristics of the vehicle, and search for motion cues that the driver can either sense or fail to sense prior to an instability [7]. However, no serious attempts have yet been made to identify the vital motion cues associated with onset of vehicle instability that the drivers can either sense or fail to sense.

Alternatively, the onset of vehicle instabilities can be related to certain vehicle response parameters. These vital response parameters can be continuously monitored to generate an early warning to the vehicle driver, such that an appropriate corrective action can be taken to ensure the safety of the driver, vehicle and the highway.

In view of the unreasonable risks posed by the highway accidents involving heavy freight vehicles, the roll and yaw directional dynamics of such vehicles has drawn extensive research investigations [8,9,10,11]. However, studies on determination of vital response parameters related to the onset of vehicle instability and development of an early warning monitor are limited to only a few [12,13]. A brief review of the relevant literature on directional dynamics of articulated freight vehicles is presented in the following section.

1.2 REVIEW OF PREVIOUS INVESTIGATIONS

The handling and stability of heavy trucks and articulated vehicles have been extensively investigated by various researchers during the

last two decades. Vlk [8] conducted a review of the literature on the lateral dynamics of articulated vehicles and concluded that only few investigations focused on the directional dynamics of such vehicles.

In view of changing weights and dimensions, and risks posed by accidents involving such vehicles, numerous analytical and experimental studies have been conducted to study rollover dynamics, directional dynamics, directional performance, etc. The influence of size and weight variables on the stability and control characteristics of heavy trucks and tractor-trailer combinations has been investigated by Ervin *et al.* [14]. The computer simulation results were validated via a limited number of field tests.

Vlk [15] examined the yaw stability of articulated vehicles during cornering. A simplified analysis of the transient turning behavior of two types of articulated vehicles showed that the tractor-semitrailer preserves stability under driving speeds exceeding 70 km/h, whereas the truck-trailer appears to become oscillatory unstable at driving speeds beyond 60 km/h. The studies conducted by Nalecz and Genin [9] concluded that heavy vehicles, in general, begin to show unstable behavior as the lateral acceleration approaches 3 to 4 m/s^2 (0.3 to 0.4 g).

Vlk [11] developed a simplified model to study the steady turning performance of freight vehicle combinations. A vertical load analogy was proposed to represent the location of the center of gravity of various units. His approach was applied to study the steady turning performance of a truck-trailer in which the trailer employed a dolly with a turntable. The study concluded that folding about the front articulation point of the truck-trailer was quite typical. Schmid [16] concluded that the resultant tire side forces should be applied behind

the center of gravity of the truck in order to ensure the yaw stability of the truck-trailer combination. If this condition is unfulfilled, the truck tends to deviate from the desired path above a certain speed.

A jackknife type of instability results when the tractor's rear wheels experience lockup. It is conceptually similar to a spinout response of a four-wheel vehicle. A second articulation instability, called trailer swing results when all the trailer wheels experience lockup. The trailer rotates out of alignment relatively slowly, often without being noticed by the driver, since no significant disturbances in the tractor motion occur [17].

A common mode of failure for heavy vehicles is rollover. A roll instability is attained whenever the overturning moment, generated by the centrifugal forces, exceeds the net stabilizing moment. For heavily laden vehicles, the rollover threshold is so low that rollover can easily occur at medium level maneuvers on paved surfaces. Typically laden heavy vehicles can roll over during turning maneuvers when the lateral acceleration approaches roughly 4 m/s^2 [9].

1.2.1 Developments in Vehicle Dynamics Simulation Models

In the sixties, yaw plane models of articulated vehicles were developed as systems of linear equations to describe the directional dynamics of the vehicle combinations. Schmid [16] investigated the lateral dynamics and was one of the first to publish comprehensive mechanical equivalent models of complete truck-trailers. Because of the available computing possibilities, he made many assumptions and therefore provided statements of limited quality about the directional stability of such complex systems. The four degrees-of-freedom linear

vehicle dynamic model was expressed by a characteristic equation. The roots of the characteristic equation provided the marginal speed of the vehicle related to divergent instability. However, this model was only valid when the turntable point was directly above the trailer front axle.

A comprehensive linear yaw plane model of various heavy vehicle combinations has been developed by UMTRI (University of Michigan Transportation Research Institute) [18]. The model represents the vehicle combination by a system of linear equations. The vehicles are assumed to behave as rigid bodies moving at constant forward velocity in the horizontal plane. The articulation angles are assumed to be small and the surface is assumed to have uniform frictional properties. The cornering forces and aligning moments generated at the tire-road interface are assumed as linear functions of the sideslip angle of the tire, and the braking and tractive forces are considered negligible.

Ervin *et al.* [14] investigated the rearward amplification of an articulated vehicle, defined as the ratio of the trailer lateral acceleration to the tractor lateral acceleration, using the yaw plane model subject to a sinusoidal steering input. The results of the study represented only first-order estimate of the rearward amplification behavior due to the linear assumption. However, severe maneuvers leading to large slip angles (greater than 3 degrees) and the load transfer from the inner to the outer track could not be simulated using this model.

Mallikarjunarao and Fancher [18] developed characteristic equations for the linear yaw plane model and investigated the vehicle stability via an eigenvalue analysis. The linear model was used to determine the

damping ratios, natural frequencies, peak lateral acceleration response and transient directional response of the various elements of the articulated vehicle combination during an emergency lane change maneuver. The directional behavior of the Michigan tanker, evaluated using the linear yaw plane model, was compared to that of other freight vehicles to demonstrate the potentials of a modified hitch.

Vlk [8] indicated that while many research papers and reports described the development of various computer simulation models to analyze the lateral dynamics of articulated vehicles, there exist relatively few published studies on the comparison of these models. The influence of size and weight variables on the stability and control of heavy trucks and tractor-trailer combinations was examined by Ervin *et al.* [14] using computer simulations. Their computer simulation studies were validated via a limited number of field tests. These models clearly predicted the periodic yaw response of the trailer about its equilibrium position but did not yield information about aperiodic trailer swing and jackknife due to a lack of a bounded and thus nonlinear tire model.

In the seventies, the research trend was towards the development of increasingly sophisticated computer simulation models to handle complex tire models. Since the directional dynamics of a vehicle combination is strongly related to the forces generated at the tire-road interface, nonlinear tire models were used in the lateral stability analyses of the vehicle subject to simultaneous braking and steering maneuvers [19]. Johnson and Huston [20] developed an articulated vehicle model incorporating nonlinear tire characteristics to investigate its directional stability. Leucht [21] developed a nonlinear mathematical

model to study the steering and braking dynamics of articulated vehicles. The equations of motion were similar to those of the linear yaw plane model. However, the dynamic load transfer (longitudinal as well as lateral) and the nonlinear cornering force-slip angle relationship of pneumatic tires were incorporated. Bernard [22] developed a vehicle model for the simulation of steady turning and braking-in-a-turn maneuvers giving special considerations to the tire-road interface modeling. A high degree of correlation between freight vehicle test data and simulation results was also demonstrated for steady turning and braking-in-a-turn maneuvers. Susemihl and Krauter [23] developed a nonlinear vehicle model allowing the evaluation of current design features, such as fifth wheel reactions and automatic antilock systems.

It has been shown that the vehicle rollover is strongly related to the rollover threshold acceleration of the vehicle established during a steady turning maneuver. A static roll model of the articulated vehicle was developed by Mallikarjunarao *et al.* [24] to determine the rollover threshold of articulated vehicles during steady turning maneuvers. A system of equations describing the static equilibrium of the vehicle in the roll plane is solved iteratively for small increments in roll angle of the semitrailer's sprung mass. The multiple axle suspensions were modeled by grouping the axles in three composite axles. The lumped composite axles represented a tractor front axle, a single tractor rear axle (by grouping the tandem axle), and a single semitrailer axle (by grouping the trailer axles) [18]. The static roll model validity was demonstrated by Mallikarjunarao *et al.* [24] with the aid of extensive tilt table test results. The computer simulations were conducted to

demonstrate the significance of suspension spring backlash in view of the roll stiffness. The parametric study concluded that the spring backlash affects the vehicle roll considerably and it is therefore necessary to incorporate this effect in simulation studies.

Winkler *et al.* [25] emphasized that vehicle testing or on-highway experience is extremely essential to confirm significant findings of computer models, specifically for maneuver levels beyond the valid range of the mathematical models. The yaw-roll vehicle model developed to predict the directional response of articulated vehicle combinations, provided a good correlation with the test results up to lateral accelerations of roughly 2 m/s^2, assuming constant forward speed [26]. For more severe maneuvers, at which wheel lift-off is experienced, comparisons with experimental results indicated that the model provided a conservative estimate of the lateral acceleration. The yaw response of the analytical model compared fairly well with that established from field tests. However, the timing and duration of the predicted motions showed discrepancies of considerable magnitude.

A comprehensive three-dimensional vehicle model, referred to as the "Phase IV Model", was developed by UMTRI [26], to simulate the directional dynamics of heavy vehicle combinations subject to braking and steering maneuvers. The model is capable of simulating the directional dynamics of trucks, tractor-semitrailers, doubles and triples. It represents the UMTRI's latest thinking in computer modeling of the braking and steering response of commonly used commercial vehicles. The dynamics of the vehicle combinations are represented by differential equations derived from Newtonian mechanics, that are solved for successive time increments by digital integration.

The mathematical model incorporates up to 71 degrees-of-freedom. The number of degrees-of-freedom is dependent on the vehicle configuration and derives from the following:

(a) six degrees-of-freedom (three translational and three rotational) for the sprung mass of the truck or the tractor;

(b) three rotational degrees-of-freedom for the semitrailer (the other three translational degrees-of- freedom of the semitrailer are effectively eliminated by dynamic constraints at the hitch);

(c) five degrees-of-freedom for each of the two full trailers allowed;

(d) two degrees-of-freedom (bounce and roll) for each of the 13 axles allowed;

(e) a rotational degree-of-freedom for each of the 26 wheels allowed.

For the simulation of lateral dynamics behavior, the model incorporates state-of-the-art representation of cornering force characteristics of the tires and vehicle suspension properties of significance to the cornering behavior. The program can be operated either for an open-loop or a closed-loop steering maneuver on roads of specified grade or cross-slope.

Computer simulations of the vehicle model for idealized steering and braking inputs demonstrated the influence of deceleration rate, brake-torque distribution, diverse loading conditions and time delays associated with application of brake at various axles on the directional response of heavy vehicles.

1.2.2 Roll Stability Analyses

In view of the changing weights and dimensions, the roll stability of freight vehicle combinations has drawn considerable attention from the policy makers and the industry. Numerous studies presented evidences linking the nominal roll stability of heavy articulated vehicles to the involvement of such vehicles in rollover accidents [27]. Almost 60% of articulated vehicle rollovers led to fatalities among the drivers and the number of rollovers occurring on dry pavements is considerably larger than those on wet pavements [28]. The likelihood of a vehicle rollover is strongly related to its rollover threshold, defined as the lateral acceleration level which is sufficient to provide an overturning moment exceeding the net stabilizing moment. Ervin *et al.* [29] investigated the lateral acceleration threshold values of articulated vehicles at which vehicle rollover may be expected.

The static rollover threshold of a rigid heavy vehicle (no suspension and tire deflections) is estimated as the ratio of half the effective track width to the trailer center of gravity height. The rollover threshold of such rigid vehicles is in the order of 6 m/s^2. Compliant tires lead to a lower value of rollover threshold (roughly 5 m/s^2), while the compliant tires and suspensions cause a further decrease in the threshold value to around 3.3 m/s^2 [30]. The rollover threshold of a vehicle is further influenced by the suspension properties and suspension geometry, in particular the roll center height.

The mechanisms influencing freight vehicle roll stability in a steady turn are well understood. As a vehicle undergoes a turn, it experiences a centrifugal force pulling outward from the center of the

turn through its center of gravity. This force tends to roll the vehicle outward from the turn, and if large enough, will cause the inside tires to lift off. The roll angle of the sprung mass then increases rapidly, due to spring backlash, leading to vehicle rollover. In addition to the centrifugal force, the lateral load shift encountered during vehicle roll tends to reduce the net stabilizing moment and thus lowers the rollover threshold [31].

Miller and Barter [32] attempted a simple theoretical analysis of the articulated vehicle rollover by neglecting all the dynamic forces and assuming that rollover occurs when the wheels on all the axles experience lift-off. It was observed that, while negotiating a roundabout, vehicles stable on the first half of the curve may roll over during the second half. The parametric study clearly indicated that the most important single parameter to be controlled is the trailer center of gravity height, which should be kept as low as possible to achieve the highest rollover threshold. An increase in effective tire track tends to improve the rollover threshold limit of the vehicle combination by increasing the magnitude of the stabilizing moment. However, the effective tire track is limited by roads design. The lateral accelerations measured during field tests, conducted at various speeds and turn radii, correlated well with those evaluated from the steady-state calculations made in their study. Their study further concluded that the speeds which drivers estimated quite safe were often quite close to the vehicle's rollover limit. Almost all the drivers involved in rollover accidents were surprised with the outcome and the lack of warning they had.

Mallikarjunarao *et al.* [24] investigated the rollover stability of heavy vehicles and showed that the calculated roll angles, except for small discrepancies, matched test data fairly well. The highest level of lateral acceleration achieved corresponded to the trailer tires lift-off. The rollover thresholds were also found to agree with test results.

Ervin [2] studied the static roll characteristics of heavy trucks and established that the rollover threshold of vehicle with non-compliant tires and suspension is related to the tire track width, center of gravity height and vehicle roll angle. The rollover threshold of an articulated vehicle is further lowered due to compliant tires and suspensions. Softer suspensions yield even lower value of rollover threshold due to low roll stiffness. The measure of the load transfer ratio serves as a continuous analog indicator of the proximity to total wheel lift-off and is used to distinguish between different vehicles subjected to the same maneuver [1].

Since the fifth wheel coupling between the tractor and semitrailer is quite stiff in the roll plane and the springs are stiffer on the semitrailer axles, the greatest load transfer occurs on the semitrailer axles. This load transfer at the semitrailer axles and the linear nature of the steering behavior up to the rollover limit implies a danger that the driver is given no warning of the impending rollover situation [33]. A study on Michigan double tanker, comprising of a tractor, a semitrailer and a pup trailer, revealed that the roll coupling between the pup trailer and the semitrailer is the key factor in increasing its roll stiffness and thus the roll stability of the pup trailer [34].

The focus of prior works on the analysis of roll stability of heavy vehicles was primarily directed towards static phenomena, and specifically on the rollover in a steady turn. However, there exits a need to examine the dynamics associated with rollover in order to assess the adequacy of the static roll plane models [31].

Verma and Gillespie [35] showed that the roll dynamics of such vehicles is dependent on the time history of applied lateral force and induced vertical bounce motions. Rollover can occur at lateral acceleration levels less than the rollover threshold due to roll resonance. The limiting dynamic acceleration is dependent upon the vehicle's suspension characteristics, especially the backlash in the suspension springs. Finally, it is suggested that the rollover limit of a vehicle combination should be estimated from the vehicle's dynamic response.

Macadam [36] investigated the relationship between directional and roll stability of heavy trucks during steady turning maneuvers. Findings of the computer-based study suggested that yaw divergence will lead to rollover in the absence of corrective steering action or reduced speed, and the primary mechanism responsible to precipitate yaw divergent behavior is the nonlinear sensitivity of the cornering properties of truck tires to vertical loads.

1.2.3 Directional Stability Analyses of Articulated Vehicles

Several analytical models, of varying complexities have been developed to obtain the general directional stability limits of heavy vehicle combinations. Diboll and Hagen [37] grouped the variables associated with the design and operation of a heavy vehicle into five

dimensionless parameters: the ratio of lateral energy input at the wheels to the trailer forward kinetic energy; the Strouhal number relating size, frequency and velocity; the structural damping ratio; a measure of the trailer moment of inertia; and the distance from the articulation point to the center of gravity of the trailer. These dimensionless parameters were used to determine the damping required to ensure lateral stability. The most important parameters appear to be the first two, (ratio of lateral energy input at the wheels to the kinetic energy of the trailer, and Strouhal number) both of which include the trailer velocity. The first parameter showed that as the velocity is increased more damping is required to retain lateral stability. The second parameter indicated that a higher natural frequency in the lateral mode will allow a higher velocity before an instability is reached. This lateral frequency is greatly affected by the lateral stiffness of the articulation mechanism. Tractor-semitrailer combinations often employ stiff lateral springs and articulation mechanisms to achieve high lateral resonant frequency.

Kashmerick [38], Gillespie and Winkler [39] showed that dual tires rotating at a common spin velocity with a tandem axle result in a yawing moment opposing vehicle turning. Typically the path curvature gain, defined as the ratio of the steady state curvature response to the front wheel steer angle, derived for tandem axle truck shows that these additional turning resistances do not depend upon the vehicle speed and thus modify only the Ackerman angle required to negotiate a steady turn. The understeer coefficient therefore remains unchanged by the dual tires and tandem axles, however the vehicle yaw damping is increased.

Numerous studies conducted on the directional stability of heavy vehicle combinations lead to the conclusion that the trailer's parameters are far more significant than those of the towing vehicle in view of the stability. A study by Collins and Wong [40] indicated that hitch loading, trailer length, mass, mass moment of inertia and small variations in the tractor tire pressure influence the trailer stability. Even in the absence of a braking input, it is possible for a vehicle to exhibit a spinout response caused by the development of an unfavorable balance in the lateral forces generated at the front and rear axle tires during cornering. Many heavy trucks begin to show a directionally unstable response to steering at lateral acceleration levels around 3 to 4 m/s^2 when operating at normal highway speeds.

Johnson *et al.* [41] established that the roll degree-of-freedom of a vehicle is extremely important and must be included in the lateral stability model of the vehicle. Their analytical study demonstrated that roll freedom, roll steer and drawbar flexibility have dramatic effects on the vehicle stability. Another study further concluded that the effects of variations in the cornering stiffness and roll steer coefficients were far more significant than those of variations in other parameters [42].

Crolla and Hales [43] investigated the lateral stability characteristics of a tractor-trailer via an eigenvalue analysis. The influence of different forward velocities on the lateral stability of existing tractor-trailer combinations was investigated. The results of the classical study of yaw oscillations of a trailer towed by a car of infinite mass have been used quite extensively in the recreational

vehicle industry [44]. The study also proposed the minimum damping or minimum hitch load criteria to improve yaw stability performance.

Mikulcik [45] developed a set of algebraic equations to determine the stability boundaries of a car-trailer system. The analytical model is also applicable to articulated freight vehicles. The study identified the group of parameters pertinent to the combination stability, using the coefficients of the characteristic equation. A general criterion governing both the oscillatory and aperiodic stability was derived using Routh's methodology. The graphical representation showed a stable region bounded by limits of oscillatory and aperiodic stability. A parametric sensitivity analysis was conducted to evaluate comparative stability and the relative effects of parameter changes.

Huston and Johnson [46] investigated the rearward amplification and resulting trailer swing of vehicle combinations. The study established that the trailer swing becomes dominant when the center of gravity of the trailer mass is moved to the rear. Fancher [47] developed a simple yaw plane model, including the locations of all axles installed on a unit, and established that the magnitude of amplification and thus the trailer swing increases with an increase in the number of articulation points and a decrease in the trailer length.

The maneuverability limit of a vehicle is reached when the moments due to side forces about the vertical axis are unable to maintain the vehicle in a dynamic equilibrium as it performs a prescribed maneuver for given vehicle parameters, speed, braking, and environmental factors. As the vehicle approaches its maneuverability limit, the articulation angle increases rapidly leading to jackknife or trailer swing [48].

Pflug [49] established that the lateral dynamics of articulated vehicles is worsened considerably when the trailer yaw mass moment of inertia is increased in relation to its mass. The study recommended that the load in partly laden trailers should be located such that the overall center of gravity does not deviate considerably from the position of the center of gravity of the trailer's body. Tousi *et al.* [50] showed that the lateral bending stiffness of the frame affects the lateral stability limits of articulated vehicles with relatively stiff tires.

Due to their high center of gravity relative to the wheel track, laden freight vehicles are prone to roll instabilities rather than yaw instabilities when cornering on a dry road. The lateral acceleration of a tractor-semitrailer vehicle, encountered during a directional maneuver, does not approach its rollover threshold limit on a wet road. The reduced coefficient of friction of wet roads results in tire skid before the rollover threshold is reached, causing yaw instability.

1.2.4 Stability Analyses during Braking Maneuvers

During the past two decades, many investigators developed detailed, complex models to analyze the steering and braking performance of heavy freight vehicles. Due to the unreasonable risks associated with the instability of such vehicles, the handling and directional performance of articulated vehicle was the subject of many investigations during that period. The wheel lockup at the rear axle of the towing vehicle, facilitated by the removal of its dynamic load, specifically poses a dangerous situation. Wheel lockup leads to a complete loss of the tire side forces at the rear axle and a rapid increase in the tractor yaw

angle. This divergent motion is called jackknife [51]. The tractor jackknife is encountered when the ratio of the magnitude of yaw response of the tractor to the magnitude of yaw response of the semitrailer approaches a large value. Schmid [16] defined the jackknife effect as the articulation angular acceleration. Compared with other instability modes, the tractor jackknife is the most dangerous, most rapid, and least controllable by the driver. The instability manifests itself in a very rapid rotation, requiring one or two seconds for the tractor to rotate through almost 120 degrees. This results in the cab striking the trailer body.

For this reason, wheel lockup at the rear axle of the towing vehicle must be prevented. Consequently, excessive braking at the front axle is favorable due to increase in the front axle load under braking, however the directional control is lost when the front wheels experience lockup. On the other hand, when the trailer wheels are locked, the restoring effect is lost and the trailer exhibits a diverging yaw motion. This divergent motion is called trailer swing [17,51]. The vehicle combination also exhibits an instability even when all the wheels experience lockup at the same time. The vehicle will become unstable when there is a yaw angle disturbance at the beginning of the braking maneuver [52]. This directional behavior of an articulated vehicle can be attributed to the cornering properties of the pneumatic tires. Cornering forces developed by the tires approach zero when the wheels experience lockup and thus the tires do not react to steering and remain unable to correct the vehicle attitude as it begins to deviate from a desired path.

The cornering forces generated by the tires are nonlinear functions of the normal load, braking force and sideslip angles [53]. Huston and Johnson [54] developed a relationship to estimate the cornering stiffness values of tires and demonstrated that variations in cornering stiffness caused by changes in normal loads significantly affect the critical speed of a vehicle combination.

Pacejka [55] presented the dynamic properties of a rolling tire in the form of transfer functions and differential equations. He indicated that the tire response depends on the tire compliance and its inertial properties. Segel and Ervin [56] investigated the influence of tire factors on truck stability and concluded that certain heavy trucks can experience diverging yaw motion during steady turning at severity levels far below those needed to achieve limiting response of passenger cars. The influence of distribution of roll stiffness along the vehicle combination on its directional stability was investigated. The study concluded that the fore-aft roll stiffness distribution was the primary mechanism serving to aggravate the heavy truck yaw instability and the shear-force-related properties of the truck tires cause the trucks to respond differently to parametric variations than typical passenger cars. Both analysis and experiments showed that the cornering stiffness and its variations with normal load are the primary properties of a tire governing the vehicle understeer in small disturbances maneuvers.

Computer simulations of the vehicle model for idealized steering and braking inputs demonstrated the influence of deceleration rate, brake-torque distribution, diverse loading conditions, and time delays associated with application of brake at various axles on the directional response of heavy vehicles [57]. The varying loading conditions were

identified as the major cause of undesirable directional response under normal operations with a fixed brake-torque distribution. The study showed that brake-torque distribution, load-sensitive brake-torque control, and brake application times are design variables that can improve the overall behavior of the vehicle under realistic loading conditions.

Instabilities associated with loss of control and jackknife can be identified from the vehicle response to a braking-in-a-turn maneuver. Loss of directional control is encountered when the path of the tractor center of gravity follows a straight line. The time history of the tractor yaw angle is required to determine if a vehicle has a tendency to jackknife, while the time history of the articulation angle is required to determine if the trailer has a tendency to swing.

1.2.5 Stability with Antilock Braking

Locked wheel stops are neither the most efficient nor the shortest stops achieved during braking. Slowing the vehicles by rapid brake modulation allows a more stable and shorter stopping distance because the tires are held at the point of incipient skid. At this point, the coefficient of friction is at its highest value and allows the greatest deceleration rate and most efficient braking. Rapid brake modulation to provide maximum braking is only developed by certain antilock devices [58]. The onset of a locked wheel is detected from the state of the drive wheels, and the corrective action consists of a corrective braking using the antilock systems at all the axles. A more effective approach consists of braking in a stabilizing technique [23]. In this approach,

the stabilizing yaw moment is actively developed through braking when the onset of a jackknife is detected.

A typical antilock braking system requires an accurate measurement of the vehicle road speed as a reference for wheel slip control. Johnston [59] described a Doppler radar system to measure the vehicle speed. The Doppler radar's output is compared with that of the wheel speed sensors to generate a command signal to control the brakes. The onset of wheel lock, however, cannot be anticipated far enough in advance to provide useful warning to the driver [13].

A decade after the antilock portion of the Federal Motor Vehicle Safety Standard (FMVSS) was struck down, efforts on development of effective antilock braking systems began to surface again [60]. Several studies demonstrated that antilock braking system prevents wheels lockup when braking, and provides directional stability, steer control and optimum stopping distances [61,62]. A standard antilock braking system consists of an electronic control unit that manipulates the speed signals of all wheel sensors and determines the reference speeds adapted to the vehicle speed, wheel deceleration/acceleration and slip signals. The wheel speed sensors, usually reluctance-type magnetic pickups, are installed in the rear drive axle carrier [63,64].

1.2.6 Determination of Onset of Vehicle Instability

Since the introduction of electronic controls in the automotive industry, considerable efforts have been mounted to develop sensors and display devices to improve vehicle performance and driver comfort. Smart electronic control systems are now being developed to improve performance, economy and safety of heavy-duty trucks [30]. Important

accident scenarios include: rollover due to sudden lane changes or high speed cornering, loss of directional control due to locked wheel during sudden stops or steering axle tire failure, or brake failure. Important parameters to be monitored include: speed, braking system performance (reservoir pressure, lining condition, integrity of air supply system), front axle tire pressure, steering, and the pressure at the fifth wheel. Of the major in-transit accident scenarios, only rollover and wheel lockup involve driver-vehicle interactions. The driver-vehicle interaction in rollover or wheel lockup, however, presents the potential for the recognition of hazardous situations using on-board measurements in time to allow the driver to take corrective action.

The study conducted by Miller and Barter [32] revealed that speeds estimated as safe by the drivers during a steady turn were often quite close to the vehicle's rollover limit. Almost all the drivers involved in rollover accidents felt that they had no warning of the impending rollover. The lack of warning of the impending roll instability has been attributed to the large load transfer at the semitrailer axles [33]. The jackknife instability, associated with the locked wheel at the tractor's rear axle, is perhaps the most dangerous, most rapid and least controllable by the driver. The relative yaw movement of the trailer with respect to the tractor is extremely rapid to be detected by the driver.

In view of the hazards posed by an accident involving heavy vehicles and the lack of warning on the onset of vehicle instability, it has been recognized that some form of early warning to the driver is extremely vital to ensure the safety of the vehicle, driver and the highway [13]. However, only a few efforts have been made to identify

the key motion parameters related to the onset of the roll and yaw instability of the vehicle.

Croce *et al.* [65] established the measurable parameters describing the onset of vehicle jackknife, through computer simulations of a linear model of the vehicle. The study established that abrupt increase in tractor yaw angle, increase in trailer yaw velocity and tire skid at the tractor rear axles, can best describe the onset of jackknife. An increase in the articulation angle without a corresponding change in the tractor yaw angle and tire skid at the semitrailer axles have been related to onset of the trailer swing [16]. The onset of vehicle rollover has been related to magnitude of lateral acceleration approaching 3 to 4 m/s^2, roll frequency approaching the roll resonant frequency, abrupt increase in roll angle and excessive deflection of the suspension springs. However, majority of these parameters are either extremely sensitive to vehicle design and operational factors or require comprehensive instrumentation.

Since industry continues to attach great importance to improve the heavy vehicle safety, Carracher [66] indicated that further progress towards development of an electronic safety monitor is expected in the near future. Some of these parameters are already monitored and controlled with devices mounted on these vehicles. Antilock braking systems monitor speeds of the wheels and the vehicle to control the potential instability during braking. Larocque *et al.* [13] emphasized the need of a safety monitor and investigated the feasibility of a vehicle system safety monitor. Their study concluded that further research is desired in this area to increase the vehicle safety. Since

the vehicle design is dictated by profit and not safety, the stability limits of these vehicles are not expected to increase.

1.3 SCOPE OF THE THESIS

The overall objective of the thesis research is to contribute towards the development of an on-line safety monitor for heavy articulated vehicles that can provide an early warning of the impending instabilities. The specific objectives of the thesis research are:

(a) Through computer modeling and simulations, identify the key operational parameters closely related to vehicle instabilities such as rollover and jackknife.

(b) Reduce the number of identified operational parameters to a minimum and derive a set of directly measurable dynamic quantities related to the onset of vehicle instabilities.

(c) Investigate the sensitivity of the key identified parameters to variations in vehicle design and operational factors.

(d) Design an on-line safety monitor using a microprocessor and low cost reliable transducers.

In Chapter 2, the roll stability of articulated freight vehicles is investigated for steady turning. The steady turning roll stability limits of a tractor-semitrailer combination are investigated using the static roll plane model of the vehicle. The equations of motion for the model are derived and the associated assumptions are presented. This model is simulated in conjunction with a comprehensive database on vehicle geometry, and commercially employed suspension and tires. The

key measurable parameters related to onset of vehicle rollover emerging from this analyses are discussed.

The roll stability of articulated freight vehicles during lane change and evasive maneuver is investigated in Chapter 3. The high speed roll stability corresponding to lane change and evasive maneuvers is studied using the three dimensional yaw and roll plane model of the vehicle. The equations of motion for the model are derived and the simplifying assumptions are discussed. The three-dimensional vehicle model is simulated in conjunction with the database on suspension and tires compiled in the previous chapter. A number of directional response parameters related to onset of roll instability at highway speeds are identified. The identified response parameters are reviewed in relation to their ease of measurement. The key measurable parameters cognate to onset of vehicle rollover emerging from this analysis are listed.

The directional stability of the vehicle combination during braking and steering maneuvers is investigated in Chapter 4. The equations of motion of the three dimensional vehicle model are derived and the associated simplifying assumptions are discussed. A parametric sensitivity analysis is conducted to determine the influence of vehicle geometry, and tire and suspension properties on the onset of vehicle jackknife. A number of key vehicle response parameters related to onset of jackknife instability are identified. The identified vehicle response parameters are reduced to directly measurable directional response parameters.

In Chapter 5, the identified key response variables are discussed in view of their feasibility and ease of measurement. The design of the

early warning system is also presented. The sensors, data acquisition and the associated hardware including the microprocessor board are discussed. The software to compute the onset of instabilities associated with roll and jackknife is presented.

Finally, the conclusions of the study and recommendations for future work are presented in Chapter 6.

CHAPTER 2

STATIC ROLL STABILITY ANALYSIS OF HEAVY VEHICLES

2.1 GENERAL

Many research investigations conducted on articulated vehicle dynamics reveal that the vehicle rollover is strongly related to its rollover threshold during steady turning [24,32]. The rollover threshold is defined as the magnitude of maximum lateral acceleration that the vehicle can withstand. The rollover threshold is primarily affected by the center of gravity height of the trailer and the tire track width. The combined center of gravity height of the trailer sprung mass and the payload has been estimated as 2 meters corresponding to a median freight density condition. This 2-meter reference value has been extensively used to estimate vehicle roll characteristics pertaining to rollover accident data. The tire track width of the vehicle is limited by the maximum permissible vehicle width. Majority of the current heavy vehicle configurations are limited to 2.44 meters (96 inches) width. However, wider heavy vehicle combinations (2.59 meters or 102 inches) are gaining popularity in view of their increased freight volume and roll stability.

A heavy vehicle combination may exhibit roll instabilities either at low speeds during cornering or at high speeds during a directional maneuver. The roll instability at low speeds occurs during cornering, where the vehicle is subject to high levels of lateral acceleration due to short turn radius. The roll instability of a vehicle at high speeds is often caused by yaw divergence leading to vehicle rollover during a

directional maneuver. The high speed roll instability often occurs at relatively low levels of lateral acceleration.

The cornering stability of articulated vehicles is investigated via a static roll analysis while the dynamic roll stability is evaluated via a comprehensive three dimensional vehicle model in the next chapter. The analytical models are developed for a tractor-semitrailer combination since 77% of all highway freight vehicles operating on Canadian highways are tractor-semitrailers [1]. The roll stability of the vehicle combination is investigated for various loading and most frequently used tires and suspensions in order to determine feasible key operational parameters related to onset of roll instability.

2.2 MECHANICS OF VEHICLE ROLLOVER

The mechanism of vehicle rollover during turning can be illustrated through the static roll analysis. Consider a rigidly suspended vehicle with a single roll degree-of-freedom negotiating a turning maneuver, as shown in Figure 2.1. It is assumed that the vehicle achieves a steady lateral acceleration by means of lateral tire forces arising in the ground plane. The primary overturning moment ($-Wa_y h$) about the ground plane is caused by the lateral acceleration of the vehicle and a restoring moment ($F_{zi2}T_i - F_{zi1}T_i$) arises due to the lateral transfer of load between the left- and right-side tires. As the vehicle rolls about a point in the ground plane, the vehicle's center of gravity is displaced laterally thus giving rise to the lateral displacement moment ($-Wh\phi$). The summation of these moments representing the steady state equilibrium yields:

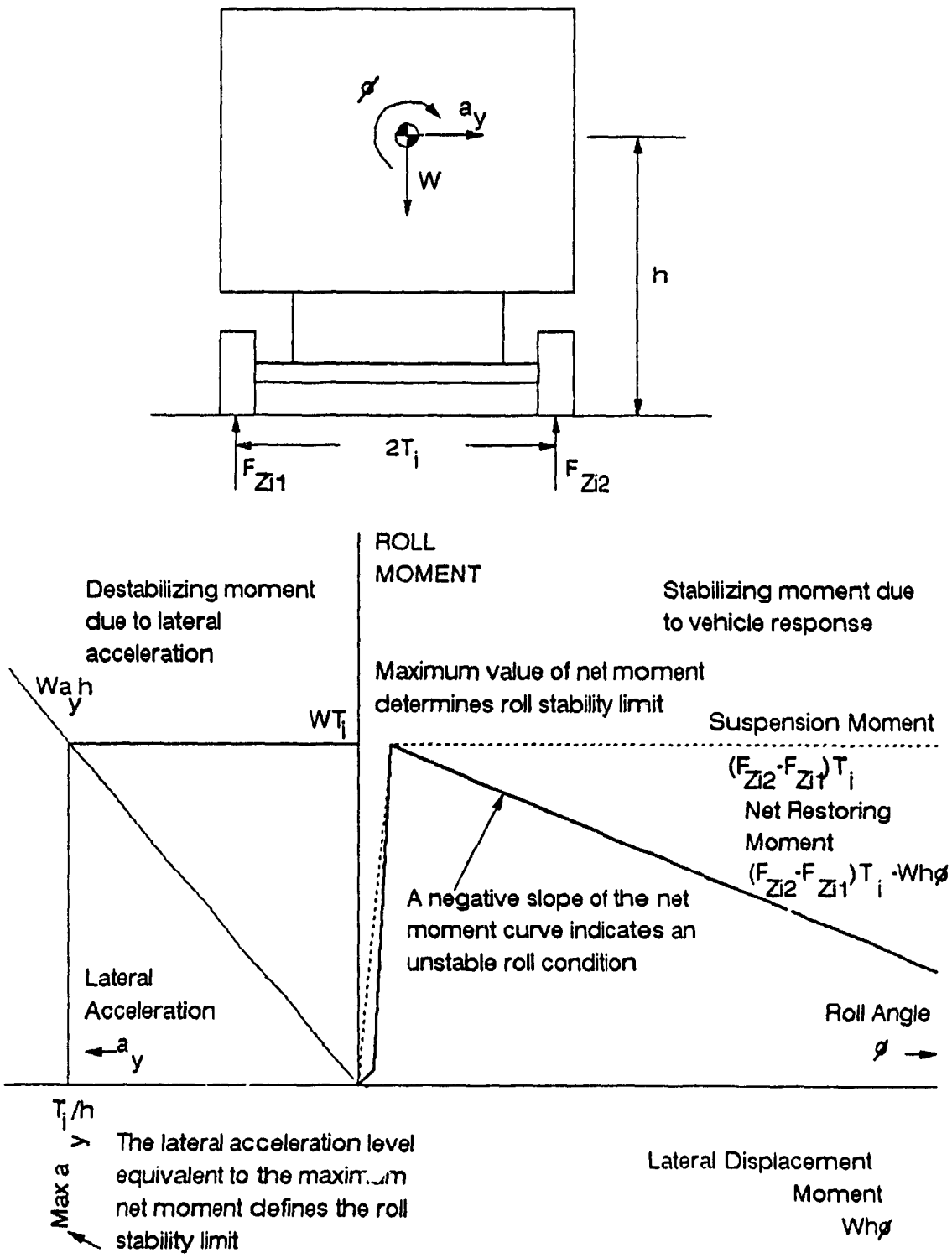

FIGURE 2.1: Roll Moment Diagram of a Rigid Vehicle

$$Wa_y h = (F_{zi2} - F_{zi1})T_i - Wh\phi \qquad (2.1)$$

The overturning, restoring and lateral displacement moments are shown graphically in Figure 2.1. The sum of restoring and lateral displacement moments yields the net stabilizing moment, derived from the vehicle response. The vehicle will become unstable in roll whenever the lateral acceleration level is sufficient to provide an overturning moment which exceeds the net stabilizing moment. In case of a rigidly suspended vehicle the maximum restoring is achieved as WT_i, when the total vertical load is transferred to the outboard tires, which occurs with almost zero roll angle.

When the overturning moment exceeds the maximum restoring moment, the rigidly suspended vehicle begins to exhibit a roll angle response. The center of gravity of the vehicle is displaced laterally as the vehicle rolls about a point in the ground plane, the lateral displacement moment increases, providing a negative slope to the net stabilizing moment curve shown on the right side of Figure 2.1. The net stabilizing moment curve reveals that a declining magnitude of the overturning moment is needed to continue the rollover response as the roll angle increases. The center of gravity is displaced until it reaches a point which is directly over the outboard wheels beyond which the vehicle is inherently unstable and rolls over without the aid of any external disturbances.

The static roll stability of a vehicle can be described by its rollover threshold, defined as the maximum value of lateral acceleration which the vehicle can withstand without rolling over. The static rollover threshold also describes the value of lateral acceleration

corresponding to the maximum net restoring moment (WT_1). From Equation (2.1), the rollover threshold can be expressed as a function of half the tire track width and the center of gravity height:

$$a_y^* = \frac{T_1}{h} \tag{2.2}$$

where a_y^* is the rollover threshold of a rigidly suspended vehicle. The rollover threshold of an articulated vehicle is a complex function of various vehicle design factors: center of gravity height, suspension characteristics, tire characteristics, number and location of axles, articulation properties, axle loads, torsional flexibility of the chassis structure, etc. Thus the determination of roll stability limit of a vehicle during low speed cornering is quite involved. Roll stability limits of articulated vehicles are computed using the static roll plane analysis software, developed by UMTRI [24].

2.3 STATIC ROLL ANALYSIS

Consider a five-axle tractor-semitrailer vehicle with a three-axle tractor and a two-axle semitrailer, as shown in Figure 2.2. The multiple axle suspensions are modeled by grouping the axles with similar suspension properties, such that multiple axles are represented by three composite axles. The lumped composite axles represent a tractor front axle, a single tractor rear axle (by grouping the tandem axle), and a single semitrailer axle (by grouping the trailer axles) [24]. The sprung weight of the tractor is modeled as two sprung weights, W_{S1} and W_{S2}, supported by the front and rear composite axles of the tractor. The two sprung weights are coupled through the torsional stiffness of

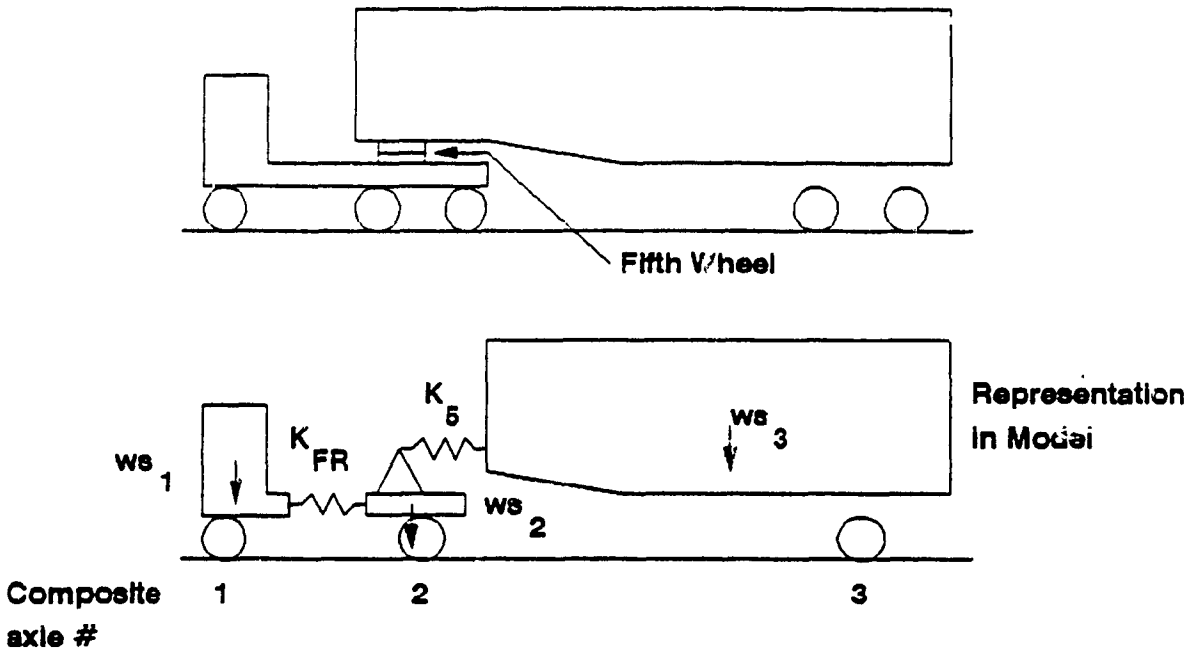

FIGURE 2.2: Idealized Representation of the Tractor-Semitrailer

the tractor frame, K_{FR}, as shown in Figure 2.2. The sprung weight of the semitrailer is coupled to the tractor sprung weight, W_{S2}, by the torsional stiffness of the fifth wheel and semitrailer structure, K_S.

The roll plane model of the vehicle is shown in Figure 2.3. A number of simplifying assumptions are made during the development of the roll plane model. The suspension springs are constrained to translate along the vertical directions parallel to $\vec{k}_{U1}$ axis of the unsprung weight. The nonlinear force-deflection characteristics of the suspension springs are linearized about the operating point using a look-up table. The typical load-deflection characteristics of a suspension spring are shown in Figure 2.4. The vertical stiffness of the tires is assumed to be linear with spring constant KT_{ij} (i=1,2,3 and j=1,...,4), where i represents the axle and j represents the tires of each composite axle. The lateral stiffness of the tires is also assumed to be linear with spring constant KYT_{ij}. At lateral accelerations close to the rollover limit of the vehicle, the load transfer to the tires located on the outside of the turn is quite significant. Thus the lateral forces developed by the tires on the inside of the turn are assumed to be negligible when compared to the lateral forces developed by the tires on the outside of the turn.

The sprung masses are permitted to rotate about their respective roll centers, which are located at a fixed distance from the sprung mass center of gravity. The relative motion between the unsprung and sprung masses is assumed to occur about the roll center. Roll angles of the sprung and unsprung masses are assumed to be small, such that $\sin \phi = \phi$ and $\cos \phi = 1$. The torsional stiffness of the tractor is assumed to be

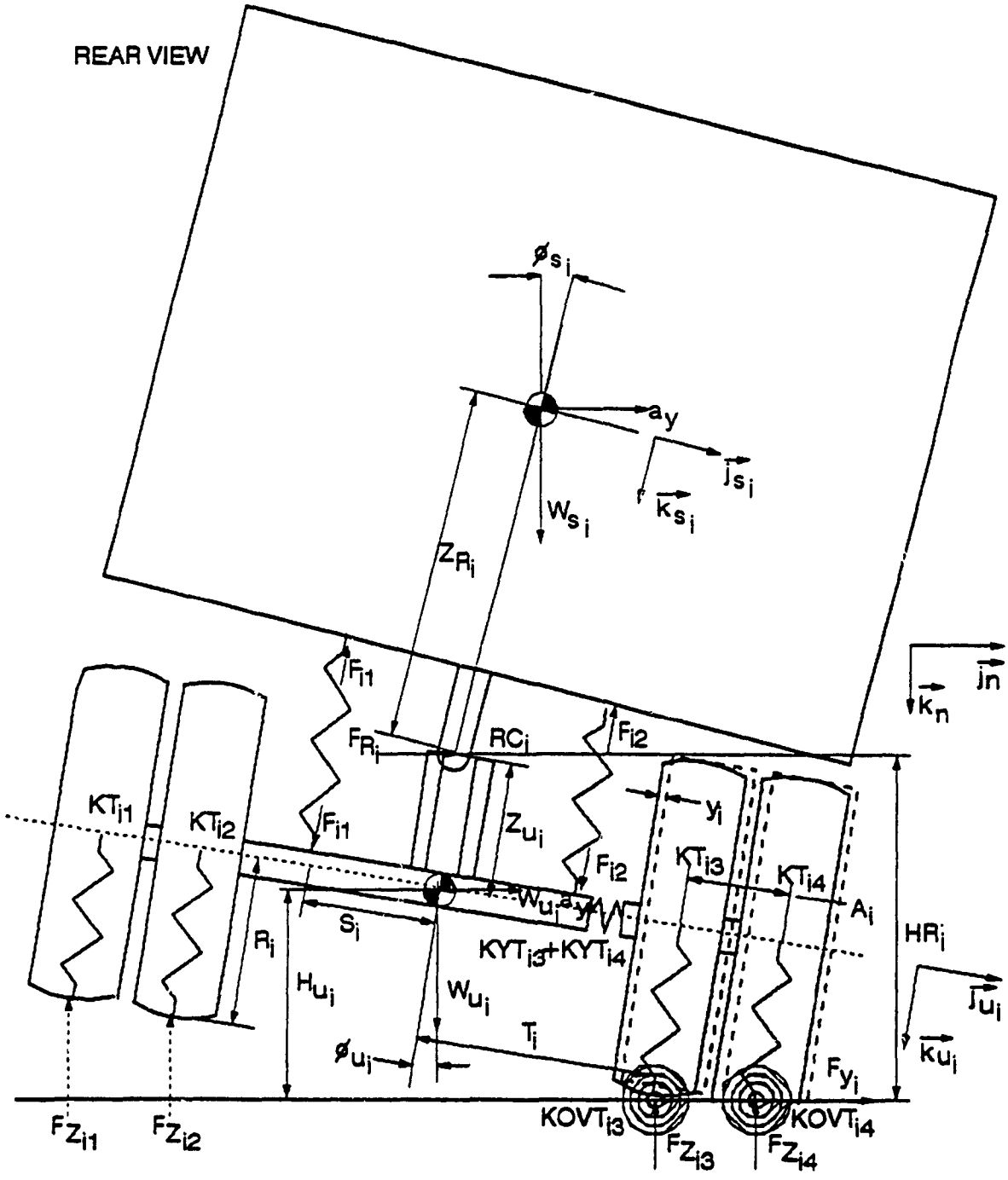

FIGURE 2.3: Forces and Moments Acting in the Y-Z Plane Containing Axle *i*

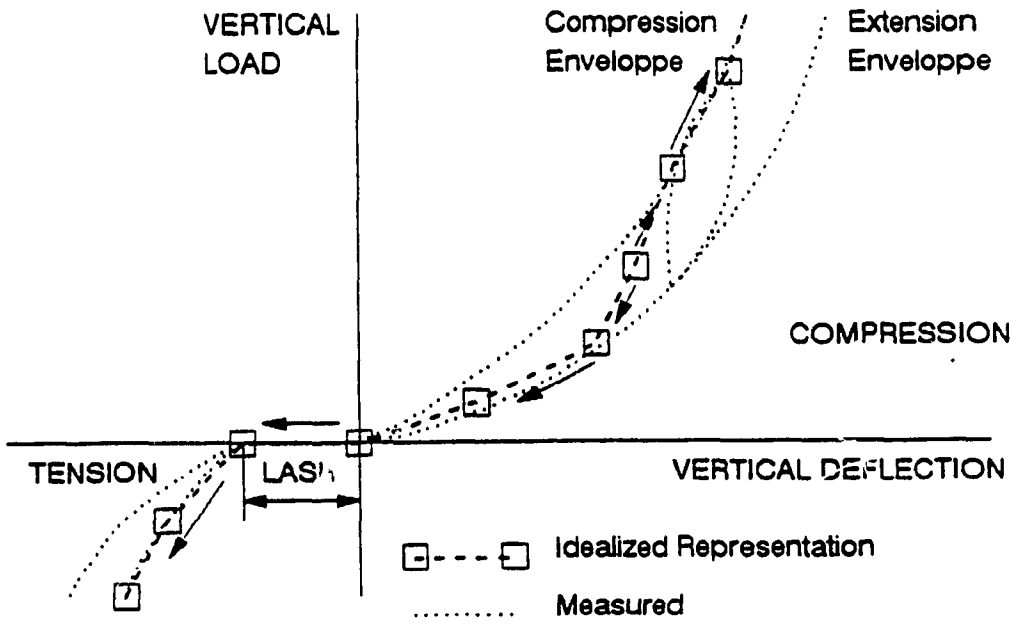

FIGURE 2.4: Typical Force-Displacement Characteristics of the Suspension Springs

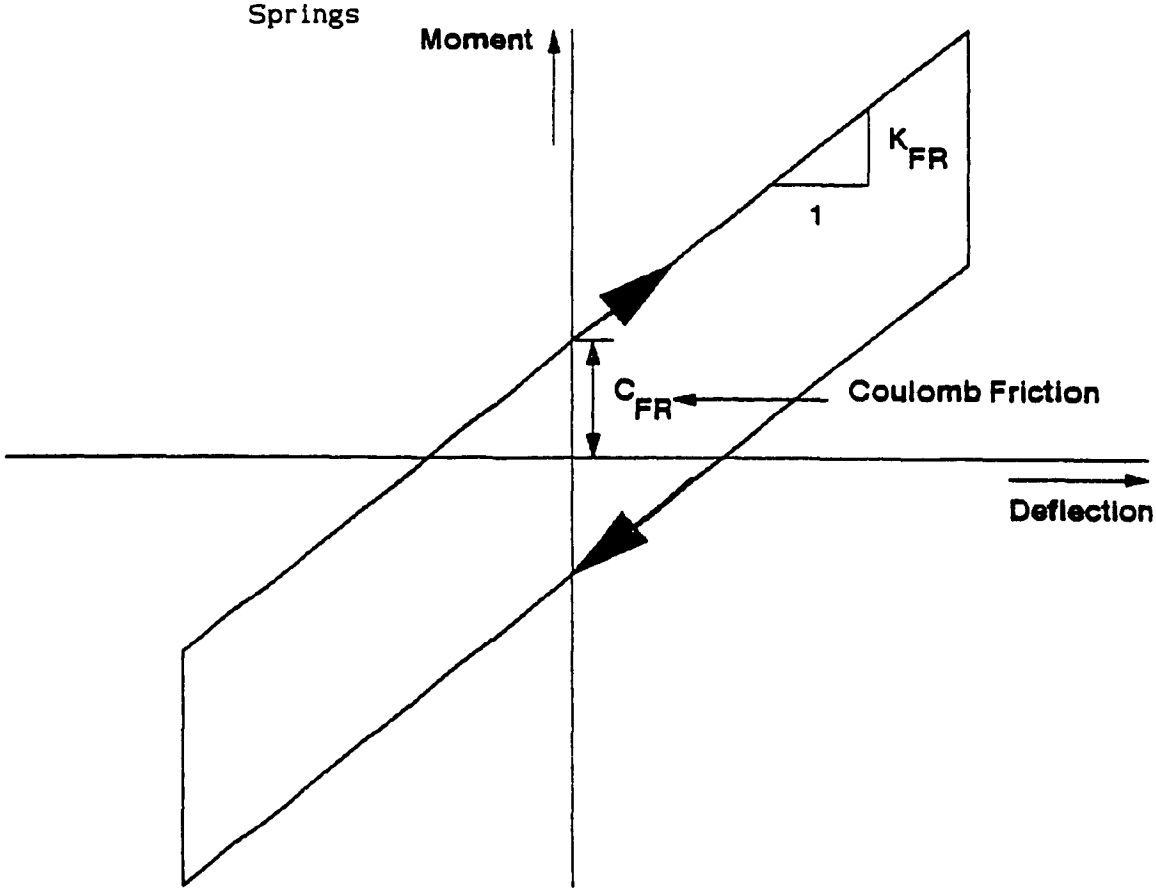

FIGURE 2.5: Idealized Representation of the Tractor Frame Stiffness

hysteretic, as shown in Figure 2.5, while the stiffness of the fifth wheel and semitrailer structure is lumped together.

The influence of the articulation angle on the roll response of the vehicle is neglected while assuming small articulation angles. The sprung masses at various axles experience different vertical deflections, thus vehicle pitching during rollover can be incorporated in the model. However, variations in the axle loads due to vehicle pitching are assumed to be negligible.

2.4 EQUATIONS OF STATIC ROLL EQUILIBRIUM

A total of fifteen equations are needed to define the static roll equilibrium of a tractor-semitrailer derived by balancing the following forces and moments:

(a) the roll moments acting on the sprung masses,

(b) the roll moments acting on the unsprung masses,

(c) the vertical forces acting on the suspension springs,

(d) the vertical forces acting on the tires, and

(e) the lateral forces acting on the tires.

2.4.1 Roll Moments Acting on the Sprung Masses

The roll moments acting on the sprung masses include moments due to suspension forces, torsional stiffness of the tractor and semitrailer structure, lateral forces acting through the roll center, and lateral components of the gravitational forces. Balancing the roll moments acting on the tractor's front sprung weight yields:

$$F_{11}[s_1+z_{R1}\sin(\phi_{S1}-\phi_{U1})] - F_{12}[s_1-z_{R1}\sin(\phi_{S1}-\phi_{U1})]$$
$$+ W_{FR}(a_y\cos\phi_{S1}-\sin\phi_{S1})z_{FR1} + M_{FR}$$
$$- F_{R1}z_{R1}\cos(\phi_{S1}-\phi_{U1}) = 0.0 \qquad (2.3)$$

where F_{1j} $(j=1,2)$ is the force due to suspension springs on the tractor front axle, M_{FR} is the roll moment transmitted through the tractor frame and W_{FR} is the vertical shear force acting through the tractor frame. Note that $W_{FR} = W_5 + W_{S2} - WAXL_2$, where $WAXL_2$ is the normal load on the tractor's rear axle.

Since the roll angles are assumed small, Equation (2.3) reduces to:

$$(F_{11}-F_{12})s_1 + (F_{11}+F_{12})z_{R1}(\phi_{S1}-\phi_{U1})$$
$$+ W_{FR}(a_y-\phi_{S1})z_{FR1} + M_{FR} - F_{R1}z_{R1} = 0.0 \qquad (2.4)$$

The effect of a small change in the sprung mass roll angle, from an equilibrium condition, is studied by rewriting the above equation in the following form:

$$(\Delta F_{11}-\Delta F_{12})s_1 + (\Delta F_{11}+\Delta F_{12})z_{R1}(\phi_{S1}-\phi_{U1}) + (F_{11}+F_{12})z_{R1}(\Delta\phi_{S1}-\Delta\phi_{U1})$$
$$- W_{FR}(\Delta a_y-\Delta\phi_{S1})z_{FR1} + \Delta M_{FR} - \Delta F_{R1}z_{R1} = 0.0 \qquad (2.5)$$

The changes in the suspension forces at axle i are related to variations in the deflections, such as $\Delta\phi_{S1}$, $\Delta\phi_{U1}$, and Δz_{U1}, in the following manner:

$$\Delta F_{ij} = \frac{\partial F_{ij}}{\partial z_{U1}}\Delta z_{U1} + \frac{\partial F_{ij}}{\partial \phi_{S1}}\Delta\phi_{S1} + \frac{\partial F_{ij}}{\partial \phi_{U1}}\Delta\phi_{U1}; \quad i=1,2,3 \text{ and } j=1,2 \qquad (2.6)$$

Equation (2.6) is expanded to obtain separate equations for the left- and right-hand side springs. The partial differentials of the suspension spring forces are then expressed in terms of local linear equivalent spring constants, corresponding to the operating spring deflections, to yield:

$$\Delta F_{i1} = K_{i1}\left[\Delta z_{Ui} - s_i(\Delta\phi_{Si}-\Delta\phi_{Ui})\right]$$

$$\Delta F_{i2} = K_{i2}\left[\Delta z_{Ui} + s_i(\Delta\phi_{Si}-\Delta\phi_{Ui})\right] \qquad (2.7)$$

and

$$\Delta F_{i1} + \Delta F_{i2} = (WAXL_i - W_{Ui})(\Delta a_y \phi_{Ui} + a_y \Delta\phi_{Ui}) \qquad (2.8)$$

where z_{Ui} is the vertical motion of the unsprung mass of axle i along the k_{Ui} axis, s_i is the half spring spacing of axle i and ϕ_{Ui} is the roll angle of the ith unsprung mass.

Similarly, variations in the lateral force, F_{Ri}, acting through the roll center, in a direction parallel to the $\vec{j}_{Ui}$ axis, is written as:

$$\Delta F_{Ri} = (WAXL_i - W_{Ui})(\Delta a_y - \Delta\phi_{Ui}); \quad i=1,2,3 \qquad (2.9)$$

Upon substituting Equations (2.7), (2.8), and (2.9) into Equation (2.5), the following equation, describing the roll moments acting on the front sprung mass of the tractor, for small deviations about a given equilibrium condition, is obtained:

$$\begin{aligned}
&(K_{11}-K_{12})s_1\Delta z_{U1} - (K_{11}+K_{12})s_1^2\Delta\phi_{S1} + (K_{11}+K_{12})s_1^2\Delta\phi_{U1} \\
&+ (F_{11}+F_{12})z_{R1}(\Delta\phi_{S1}-\Delta\phi_{U1}) + K_{FR}(\Delta\phi_{S2}-\Delta\phi_{S1}) \\
&+ (WAXL_1 - W_{U1})(\phi_{S1}-\phi_{U1})z_{R1}(\Delta a_y\phi_{U1} + a_y\Delta\varphi_{U1}) \\
&- (WAXL_1 - W_{U1})z_{R1}(\Delta a_y - \Delta\phi_{U1}) + W_{FR}z_{FR1}(\Delta a_y - \Delta\phi_{S1}) = 0.0
\end{aligned} \qquad (2.10)$$

Similarly, we derive equations for the remaining two sprung masses to obtain:

$$-W_{FR}z_{FR2}(\Delta a_y-\Delta\phi_{S2}) + K_S(\Delta\phi_{S3}-\Delta\phi_{S2}) - W_S(\Delta a_y-\Delta\phi_{S2})z_{S2}$$
$$+ (K_{21}-K_{22})s_2\Delta z_{U2} - (K_{21}+K_{22})s_2^2\Delta\phi_{S2} + (K_{21}+K_{22})s_2^2\Delta\phi_{U2}$$
$$+ (F_{21}+F_{22})z_{R2}(\Delta\phi_{S2}-\Delta\phi_{U2}) - K_{FR}(\Delta\phi_{S2}-\Delta\phi_{S1})$$
$$+ (WAXL_2-W_{U2})z_{R2}(\phi_{S2}-\phi_{U2})(\Delta a_y\phi_{U2}+a_y\Delta\phi_{U2})$$
$$- (WAXL_2-W_{U2})z_{R2}(\Delta a_y-\Delta\phi_{U2}) = 0.0 \qquad (2.11)$$

$$(K_{31}-K_{32})s_3\Delta z_{U3} - (K_{31}+K_{32})s_3^2\Delta\phi_{S3} + (K_{31}+K_{32})s_3^2\Delta\phi_{U3}$$
$$+ (F_{31}+F_{32})z_{R3}(\Delta\phi_{S3}-\Delta\phi_{U3}) - K_S(\Delta\phi_{S3}-\Delta\phi_{S2})$$
$$+ (WAXL_3-W_{U3})(\phi_{S3}-\phi_{U3})z_{R3}(\Delta a_y\phi_{U3}+a_y\Delta\phi_{U3})$$
$$- (WAXL_3-W_{U3})z_{R3}(\Delta a_y-\Delta\phi_{U3}) - W_S(\Delta a_y-\Delta\phi_{S3})z_{S3} = 0.0 \qquad (2.12)$$

Equations (2.10), (2.11), and (2.12) define the roll moments acting on the tractor's front, tractor's rear and the trailer's sprung weights, respectively, as caused by small deviations from an equilibrium condition.

2.4.2 Roll Moments Acting on the Unsprung Masses

The equation of roll equilibrium of the unsprung weights includes moments arising from suspension and tire forces, lateral forces acting through the roll center, and lateral forces developed at the tires, as shown in Figure 2.3. The equation for the roll moment of the ith unsprung mass can thus be expressed as:

$$(F_{Z11}+F_{Z12}+F_{Z13}+F_{Z14})R_i \sin \phi_{Ui} + (F_{Z11}-F_{Z14})(T_i+A_i)\cos \phi_{Ui}$$
$$+ (F_{Z12}-F_{Z13})T_i \cos \phi_{Ui} - (F_{Z13}+F_{Z14})y_i \cos \phi_{Ui} - (F_{11}-F_{12})s_i$$
$$+ F_{Ri}z_{Ui} + F_{yi}H_{Ui} + OVT_{i3} + OVT_{i4} = 0.0; \quad i=1,2,3 \qquad (2.13)$$

where F_{Zij} is the vertical force acting on tire j of axle i, T_i is half the inner tire track width, A_i is the dual tire spacing, and y_i is the lateral displacement of tires on the outside of the turn. F_{yi} is the lateral force developed at the tires of axle i, R_i is the effective tire radius on axle i and H_{Ui} is the vertical height of the unsprung mass center of gravity. Assuming the roll angles to be small, and rewriting the above equation to express a small change about an equilibrium condition, we get:

$$(\Delta F_{Z11}+\Delta F_{Z12}+\Delta F_{Z13}+\Delta F_{Z14})R_i\phi_{Ui} + (F_{Z11}+F_{Z12}+F_{Z13}+F_{Z14})R_i\Delta\phi_{Ui}$$
$$+ (\Delta F_{Z11}-\Delta F_{Z14})(T_i+A_i) - (\Delta F_{Z13}+\Delta F_{Z14})y_i - (F_{Z13}+F_{Z14})\Delta y_i$$
$$+ (-\Delta F_{11}+\Delta F_{12})s_i + (\Delta F_{Z12}-\Delta F_{Z13})T_i + \Delta F_{Ri}z_{Ui} + F_{Ri}\Delta z_{Ui} + \Delta F_{yi}H_{Ui}$$
$$+ F_{yi}\Delta H_{Ui} + \Delta OVT_{i3} + \Delta OVT_{i4} = 0.0; \quad i=1,2,3 \qquad (2.14)$$

The increments in the tire loads, ΔF_{Zij}, are related to changes in (a) the unsprung mass roll angle, $\Delta\phi_{Ui}$ and (b) the unsprung mass bounce, ΔH_{Ui}. The variations in normal forces acting on the four tires of a single axle are expressed as:

$$\Delta F_{Z11} = -KT_{i1}\left((T_i+A_i)\Delta\phi_{Ui} - \Delta H_{Ui}\right)$$
$$\Delta F_{Z12} = -KT_{i2}\left(T_i\Delta\phi_{Ui} - \Delta H_{Ui}\right)$$
$$\Delta F_{Z13} = KT_{i3}\left((T_i-y_i)\Delta\phi_{Ui} - \Delta y_i\phi_{Ui} + \Delta H_{Ui}\right)$$
$$\Delta F_{Z14} = KT_{i4}\left((T_i+A_i-y_i)\Delta\phi_{Ui} - \Delta y_i\phi_{Ui} + \Delta H_{Ui}\right); \quad i=1,2,3 \qquad (2.15)$$

The changes in the roll-resisting moment produced at the tire-road interface is given by:

$$\Delta OVT_{i3} = - KOVT_{i3}\Delta\phi_{U1}$$
$$\Delta OVT_{i4} = - KOVT_{i4}\Delta\phi_{U1}; \quad i=1,2,3 \tag{2.16}$$

where $KOVT_{ij}$ is the linear overturning stiffness of tire j on axle i.

Substituting Equations (2.7), (2.8), (2.9), (2.15), and (2.16) into Equation (2.14), the following equation is obtained describing the roll moments on an axle caused by small deviations about a given equilibrium condition:

$$\begin{aligned}
&- \Big[(K_{i1}+K_{i2})s_i^2 - WAXL_i R_i - (WAXL_i - W_{Ui})z_{Ui} + KOVT_{i3} + KOVT_{i4} \\
&+ KT_{i1}(T_i+A_i)^2 + KT_{i2}T_i^2 + KT_{i3}(T_i-y_i)^2 + KT_{i4}(T_i+A_i-y_i)^2\Big]\Delta\phi_{U1} \\
&\quad - \Big[F_{Zi3} + F_{Zi4} + \Big((KT_{i3}+KT_{i4})(T_i-y_i) + KT_{i4}A_i\Big)\phi_{Ui}\Big]\Delta y_i \\
&\quad\quad + \Big[- (K_{i1}+K_{i2})s_i + (WAXL_i - W_{Ui})(a_y - \phi_{Ui})\Big]\Delta z_{Ui} \\
&\quad\quad\quad + \Big[(KT_{i1}-KT_{i4})(T_i+A_i) + (KT_{i2}-KT_{i3})T_i \\
&\quad\quad\quad\quad - (KT_{i3}+KT_{i4})y_i + WAXL_i a_y\Big]\Delta H_{Ui} \\
&\quad\quad\quad\quad - \Big[(WAXL_i - W_{Ui})HR_i + W_{Ui}H_{Ui}\Big]\Delta a_y \\
&\quad\quad\quad + (K_{i1}+K_{i2})s_i^2\Delta\phi_{Si} = 0.0; \quad i=1,2,3
\end{aligned} \tag{2.17}$$

2.4.3 Vertical Forces Acting Through the Suspension Springs

The forces generated by the compression and extension of the suspension springs must satisfy the following equation in order to maintain equilibrium along the $\vec{k}_{U1}$ axis.

$$F_{i1} + F_{i2} = (WAXL_i - W_{Ui})\cos\phi_{Ui} + (WAXL_i - W_{Ui})a_y \sin\phi_{Ui} \tag{2.18}$$

By invoking the small angle assumption, Equation (2.18) can be expressed as:

$$(K_{i1}+K_{i2})\Delta z_{Ui} - (K_{i1}-K_{i2})s_i\Delta\phi_{Si} + (K_{i1}-K_{i2})s_i\Delta\phi_{ui}$$
$$- (WAXL_i-W_{Ui})\phi_{Ui}\Delta a_y - (WAXL_i-W_{Ui})a_y\Delta\phi_{Ui} = 0.0; \quad i=1,2,3 \qquad (2.19)$$

2.4.4 Vertical Forces Generated by the Tires

The vertical load carried by each composite axle is assumed to remain constant, while neglecting the influence of grade and vehicle pitch. The tire vertical forces are expressed as:

$$(F_{Z11}+F_{Z12}+F_{Z13}+F_{Z14}) = WAXL_i \qquad (2.20)$$

For small deviations about an equilibrium condition, Equation (2.20) is written as:

$$\Delta F_{Z11} + \Delta F_{Z12} + \Delta F_{Z13} + \Delta F_{Z14} = 0.0 \qquad (2.21)$$

Substituting Equation (2.15) into Equation (2.21), we obtain:

$$[(-KT_{i1}+KT_{i4})(T_i+A_i) + (-KT_{i2}+KT_{i3})T_i - (KT_{i3}+KT_{i4})y_i]\Delta\phi_{Ui}$$
$$+ (KT_{i1}+KT_{i2}+KT_{i3}+KT_{i4})\Delta H_{Ui}$$
$$- (KT_{i3}+KT_{i4})\phi_{Ui}\Delta y_i = 0.0; \quad i = 1,2,3 \qquad (2.22)$$

2.4.5 Lateral Forces Acting on the Outside Tires

When the lateral acceleration approaches the rollover limit of the vehicle, the tires on the outside of the turn carry almost the entire

axle load. Thus a lateral translation of the centroid of the normal pressure, acting between a tire and the road surface, is experienced. For a dual tire set, the lateral force experienced by axle i is expressed as:

$$F_{yi} = (KYT_{i3}+KYT_{i4})y_i \cos \phi_{Ui} \tag{2.23}$$

where KYT_{i3} and KYT_{i4} are the linear spring rates of tires 3 and 4 on axle i, oriented along the $\vec{j}_{Ui}$ axis. F_{yi} is the total lateral force acting on the tires given by:

$$F_{yi} = WAXL_i a_y \tag{2.24}$$

Invoking the small roll angles assumption and considering small deviations about an equilibrium condition, the lateral forces acting on the tires are expressed as:

$$WAXL_i \Delta a_y = (KYT_{i3}+KYT_{i4})\Delta y_i \tag{2.25}$$

2.5 SOLUTION PROCEDURE

Equations (2.3) through (2.25) constitute the fifteen equations needed to compute the vehicle roll response during a steady turning maneuver. When written in the matrix form, these equations are expressed as:

$$[A]\{\Delta x\} = \{b\}\Delta\phi_{S3} \tag{2.26}$$

where [A] and {b} are (15x15) and (15x1) matrices, respectively containing vehicle parameters, and {Δx} is the vector of vehicle response variables given by:

$$\{\Delta x\}^T = (\Delta a_y,\ \Delta\phi_{S1},\ \Delta\phi_{S2},\ \Delta\phi_{Ui},\ \Delta z_{Ui},\ \Delta H_{Ui},\ \Delta y_i);\quad i=1,2,3 \qquad (2.27)$$

where 'T' designates the transpose. Initially, the vehicle is assumed to be upright ($\phi_{S1}=\phi_{Ui}=0$). Equation (2.26) is solved for a small increment in the roll angle of the semitrailer sprung mass ($\Delta\phi_{S3}$). The response vector, {Δx} is computed for a series of increments in $\Delta\phi_{S3}$, and the corresponding variations in the lateral acceleration and roll angles of the sprung and unsprung masses are computed for the series of equilibrium positions. The computations are terminated when the deflections of the trailer and tractor rear axle tires on the inside of the turn approach zero. The highest lateral acceleration achieved during the computation process is termed as the steady turning rollover threshold of the vehicle.

2.6 DETERMINATION OF PARAMETERS RELATED TO ONSET OF VEHICLE ROLLOVER DURING STEADY TURNING

The mechanics of vehicle rollover reveals that the roll instability during steady turning can be directly related to the normal load on the inside tires of the semitrailer and tractor rear axles. When the normal load acting on these tires approaches zero, the tires lose contact with the ground indicating the onset of potential rollover. However, measurement of tire loads on a moving vehicle is quite complex and thus

such a parameter may be considered infeasible to detect the onset of vehicle instability.

Alternatively, vehicle rollover during steady turning has been related to the rollover threshold (lateral acceleration) experienced by the vehicle during steady turning. The lateral acceleration of the sprung mass can be conveniently measured in order to determine the onset of roll instability. The rollover threshold of a vehicle is however strongly dependent upon various loading and vehicle design parameters: sprung mass center of gravity height, tire track width, torque-deflection properties of the articulation mechanism, axle loads, force-deflection properties of the tires, cornering properties of the tires, etc. Of these parameters, the sprung mass center of gravity height and the tire track width affect the rollover threshold most significantly. Variations in the tire track width of most heavy vehicle configurations may be considered insignificant due to regulations on maximum vehicle width. Most vehicle configurations, currently in use, are limited to 2.44-meter (96 inches) width. The recently proposed 2.59-meter (102 inches) wide vehicle combinations are slowly gaining popularity in view of their increased freight volume and stability limits.

The rollover threshold limits of a five-axle tractor-semitrailer are investigated for various loading and vehicle design parameters to determine the variance of rollover threshold value. A parameter, as a function of lateral acceleration and the compliance characteristics of the vehicle, is derived to detect the onset of vehicle rollover.

2.6.1 Vehicle Parameters

The static roll model contains a comprehensive description of suspension and tire properties, such that the steady turning rollover threshold can be accurately predicted. In view of the dependency of the rollover threshold limit on various vehicle parameters, a comprehensive database on currently used suspension, tires and axle loads was compiled. The rollover thresholds of twenty-four different vehicle configurations with three different trailer center of gravity heights were computed. The tires, suspensions and physical dimensions used in the simulation are listed as follows:

Tire:	Michelin XZA Radial 11:00R22.50
Tractor front suspension:	International Harvester; 53000 N (12000 lbs) rating
Tractor rear suspension:	Hendrickson RTE380; 84000 N (19000 lbs) rating
	Hendrickson RTE440; 97000 N (22000 lbs) rating
	Neway ARD244 16K; 71000 N (16000 lbs) rating
	Mack Camel Back SS38C; 84000 N (19000 lbs) rating
Trailer suspension:	Neway AR95.17 24K; 106000 N (24000 lbs) rating
	Neway AR95.17 16K; 71000 N (16000 lbs) rating
	Reyco 21B; 93000 N (21000 lbs) rating
Overall vehicle width:	2.44 meters (96 in) 2.59 meters (102 in)
Center of gravity height:	1.52 meter (60 in) 1.78 meter (70 in) 2.03 meters (80 in)

The load-deflection curves of the various suspension springs are shown in Figures 2.6 to 2.13. The Neway suspensions use air springs, and are considerably softer than the leaf-spring suspensions especially in the zero-deflection region, as shown in Figures 2.9 and 2.12. The leaf spring suspension however are usually stiffer and possess lash except for the Mack SS38C suspension which is considerably softer than the other leaf spring suspension due to its camel back configuration. The various vehicle configurations used in the simulation are presented in Table 2.1 and the parameters of the baseline vehicle are listed in Table 2.2.

2.6 2 Rollover Threshold of Vehicle Combination

Equation (2.26) is solved via Gaussian elimination method for various vehicle configurations listed in the previous section. The lateral acceleration and the roll angle response corresponding to vehicle rollover are evaluated for three different values of sprung mass center of gravity height and two different values of vehicle width. Figures 2.14 to 2.19 show the lateral acceleration and the roll angle experienced by the semitrailer when the vehicle rollover is attained. The different types of semitrailer suspensions are indicated on the abscissa, while the suspension systems employed at the tractor's rear axle are presented with an increasing order of linear stiffness.

Figure 2.14 illustrates the roll angle and lateral acceleration response of the 2.44-meter wide vehicle, with semitrailer's center of gravity height of 1.52 meter. The figure illustrates the rollover threshold is around 5 m/s^2, and varies slightly for different suspension systems at the tractor's rear and semitrailer axles. The roll angle,

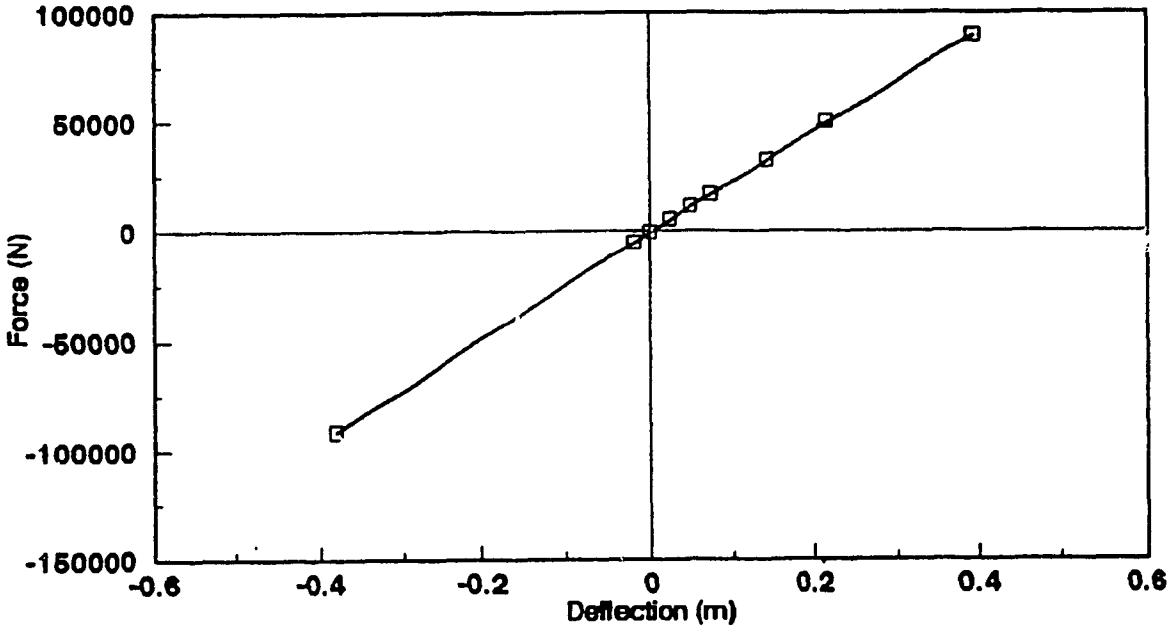

FIGURE 2.6: Force-Displacement Characteristic of the International Harvester Suspension Spring

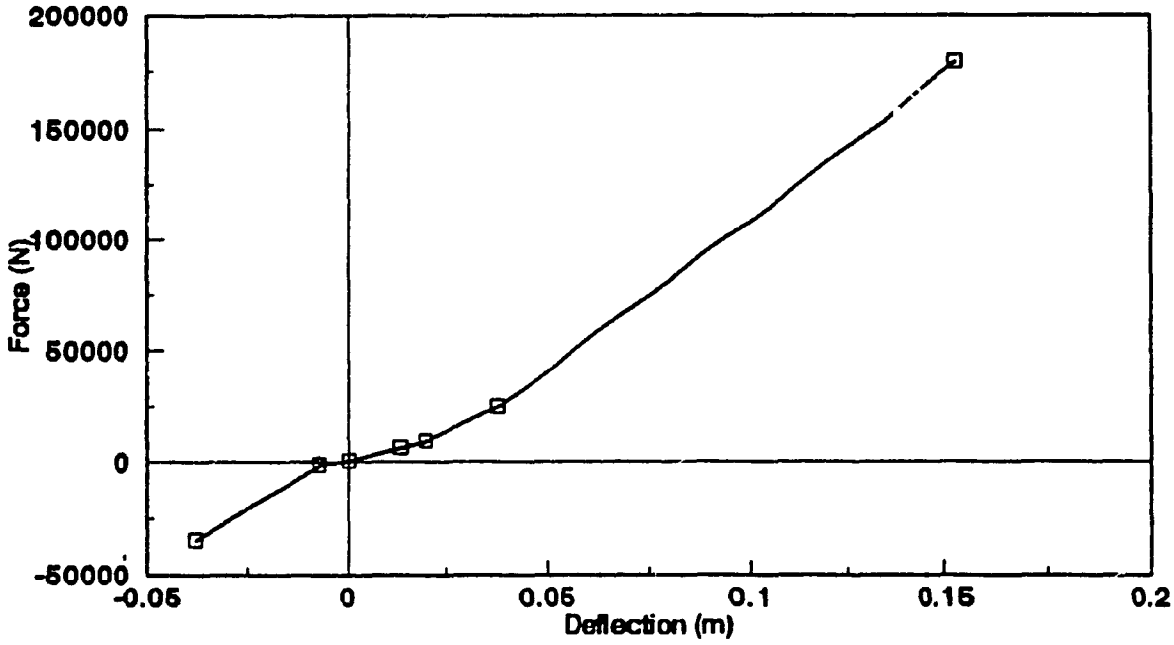

FIGURE 2.7: Force-Displacement Characteristic of the Hendrickson RTE380 Suspension Spring

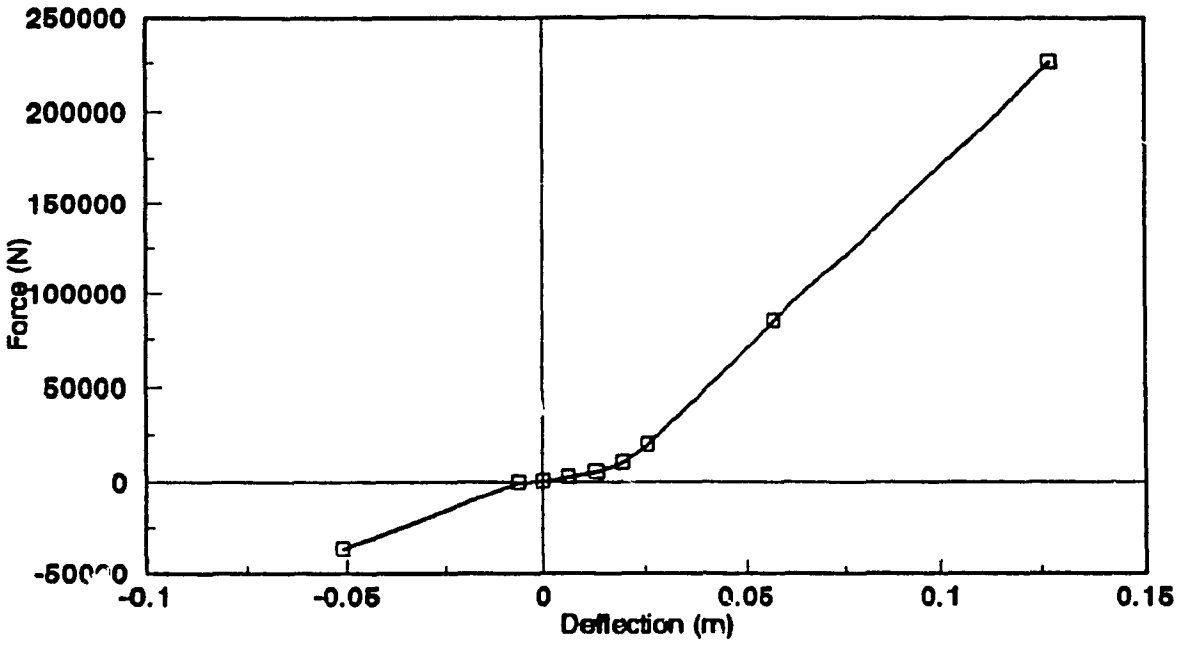

FIGURE 2.8: Force-Displacement Characteristic of the Hendrickson RTE440 Suspension Spring

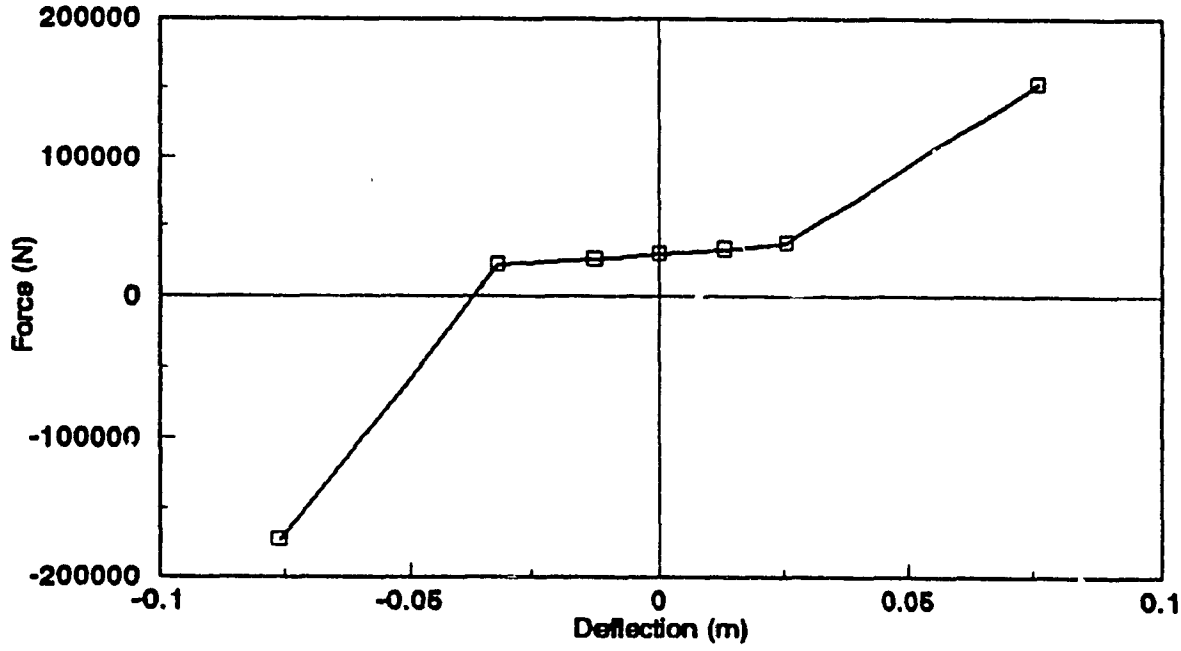

FIGURE 2.9: Force-Displacement Characteristic of the Neway ARD244 16K Suspension Spring

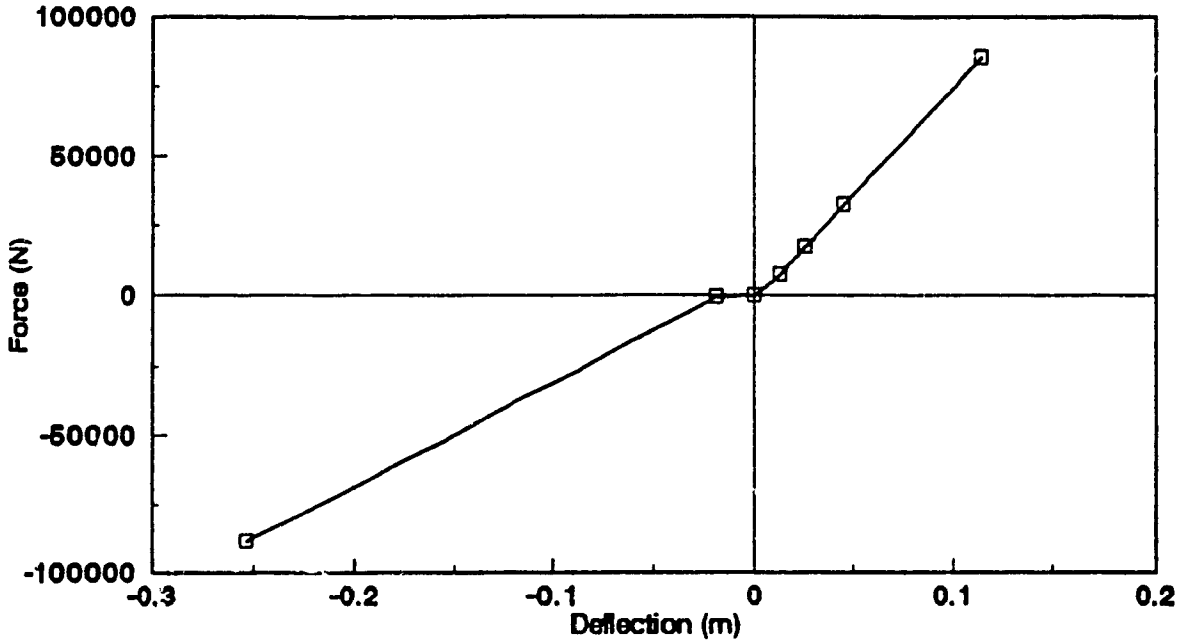

FIGURE 2.10: Force-Displacement Characteristic of the Mack Camel Back SS38C Suspension Spring

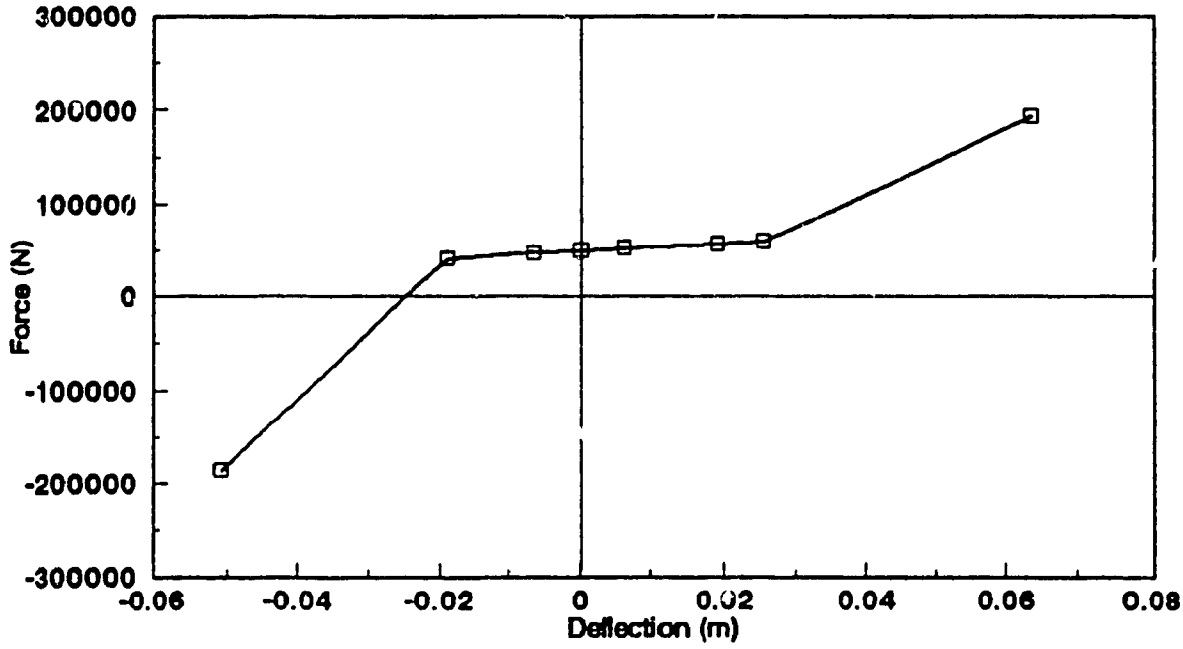

FIGURE 2.11: Force-Displacement Characteristic of the Neway AR95.17 24K Suspension Spring

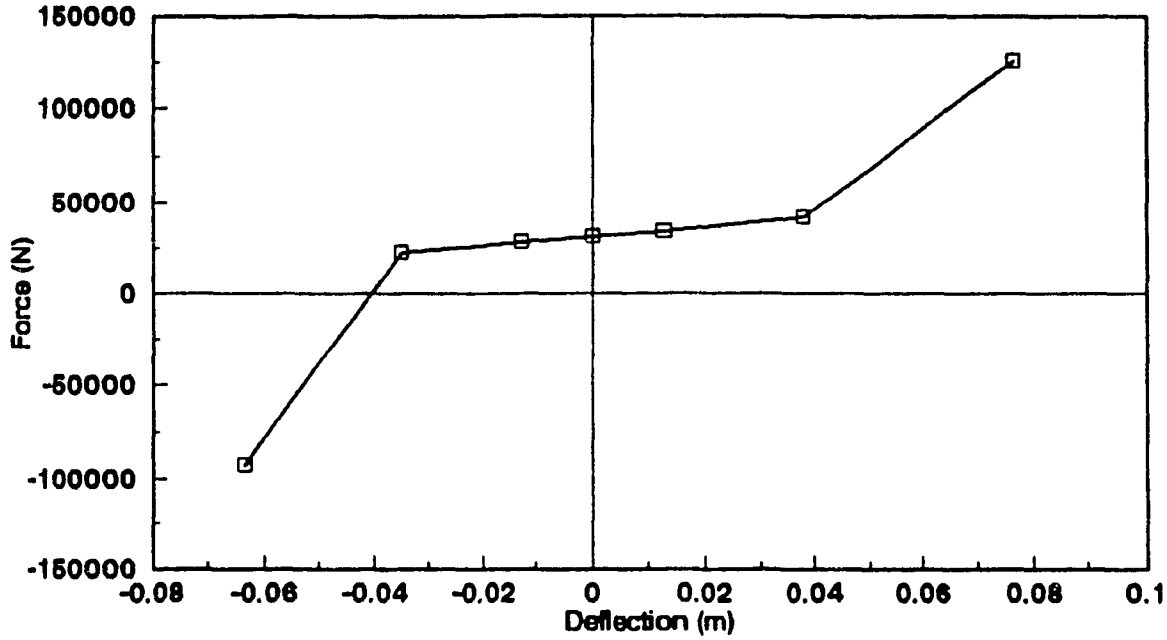

FIGURE 2.12: Force-Displacement Characteristic of the Neway AR95.17 16K Suspension Spring

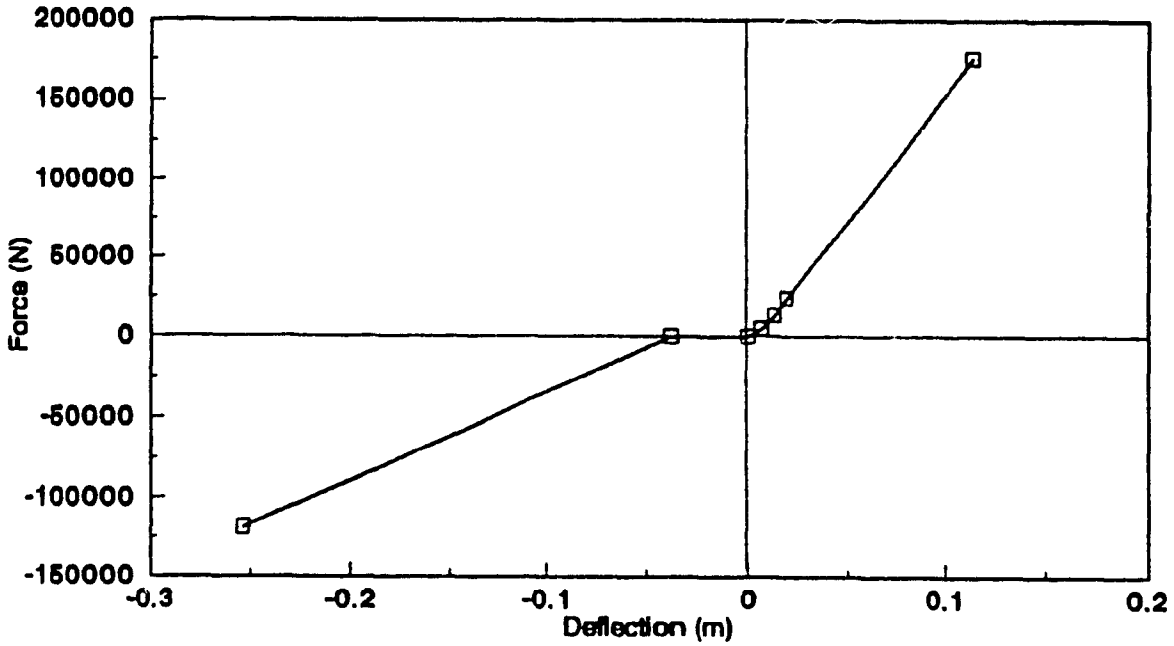

FIGURE 2.13: Force-Displacement Characteristic of the Reyco 21B Suspension Spring

TABLE 2.1
VEHICLE CONFIGURATIONS

Vehicle Configuration	Sprung Mass C.G. Height (m)	Vehicle Width (m)	Suspensions						
			Tractor Rear Axle				Semitrailer Axle		
			Neway ARD244 16K	Mack SS38C	Hendr. RTE 380	Hendr. RTE 440	Neway AR9517 16K	Neway AR9517 24K	Reyco 21B
1	1.52	2.44	X				X		
2	1.52	2.44		X			X		
3	1.52	2.44			X		X		
4	1.52	2.44				X	X		
5	1.52	2.44	X					X	
6	1.52	2.44		X				X	
7	1.52	2.44			X			X	
8	1.52	2.44				X		X	
9	1.52	2.44	X						X
10	1.52	2.44		X					X
11	1.52	2.44			X				X
12	1.52	2.44				X			X
13	1.78	2.44	X				X		
14	1.78	2.44		X			X		
15	1.78	2.44			X		X		
16	1.78	2.44				X	X		
17	1.78	2.44	X					X	
18	1.78	2.44		X				X	
19	1.78	2.44			X			X	
20	1.78	2.44				X		X	
21	1.78	2.44	X						X
22	1.78	2.44		X					X
23	1.78	2.44			X				X
24	1.78	2.44				X			X
25	2.03	2.44	X				X		
26	2.03	2.44		X			X		
27	2.03	2.44			X		X		
28	2.03	2.44				X	X		
29	2.03	2.44	X					X	
30	2.03	2.44		X				X	
31	2.03	2.44			X			X	
32	2.03	2.44				X		X	
33	2.03	2.44	X						X
34	2.03	2.44		X					X
35	2.03	2.44			X				X
36	2.03	2.44				X			X

TABLE 2.1 (Continued)
VEHICLE CONFIGURATIONS

Vehicle Configuration	Sprung Mass C.G. Height (m)	Vehicle Width (m)	Suspensions						
			Tractor Rear Axle				Semitrailer Axle		
			Neway ARD244 16K	Mack SS38C	Hendr. RTE 380	Hendr. RTE 440	Neway AR9517 16K	Neway AR9517 24K	Reyco 21B
37	1.52	2.59	X				X		
38	1.52	2.59		X			X		
39	1.52	2.59			X		X		
40	1.52	2.59				X	X		
41	1.52	2.59	X					X	
42	1.52	2.59		X				X	
43	1.52	2.59			X			X	
44	1.52	2.59				X		X	
45	1.52	2.59	X						X
46	1.52	2.59		X					X
47	1.52	2.59			X				X
48	1.52	2.59				X			X
49	1.78	2.59	X				X		
50	1.78	2.59		X			X		
51	1.78	2.59			X		X		
52	1.78	2.59				X	X		
53	1.78	2.59	X					X	
54	1.78	2.59		X				X	
55	1.78	2.59			X			X	
56	1.78	2.59				X		X	
57	1.78	2.59	X						X
58	1.78	2.59		X					X
59	1.78	2.59			X				X
60	1.78	2.59				X			X
61	2.03	2.59	X				X		
62	2.03	2.59		X			X		
63	2.03	2.59			X		X		
64	2.03	2.59				X	X		
65	2.03	2.59	X					X	
66	2.03	2.59		X				X	
67	2.03	2.59			X			X	
68	2.03	2.59				X		X	
69	2.03	2.59	X						X
70	2.03	2.59		X					X
71	2.03	2.59			X				X
72	2.03	2.59				X			X

TABLE 2.2
PARAMETERS OF THE BASELINE VEHICLE

Parameter	Tractor Front Axle	Tractor Rear Axle	Semi-trailer Axle
Axle Load (N), $WAXL_i$	53000	142000	142000
Dual Tire Spacing (m), A_i	0.0	0.33	0.33
Rolling Radius (m), R_i	0.5	0.5	0.5
Tire Vertical Stiffness (N/m), KT_{ij}	788000		
Tire Lateral Stiffness (N/m), KYT_{ij}	876000		
Tire Overturning Stiffness (N·m/deg), $KOVT_{ij}$	40		
Fifth Wheel Height (m), z_5	1.27		
Tractor Frame Height (m), z_{FR}	0.97		
Tractor Frame Stiffness (N·m/deg), K_{FR}	78.9		
Tractor Frame Coulomb Friction (N), C_{FR}	445		
Fifth wheel stiffness (N·m/deg), K_5	1972		
Fifth wheel load (N), W_5	138000		
Weight of Tractor Rear Section (N), W_{S2}	4290		

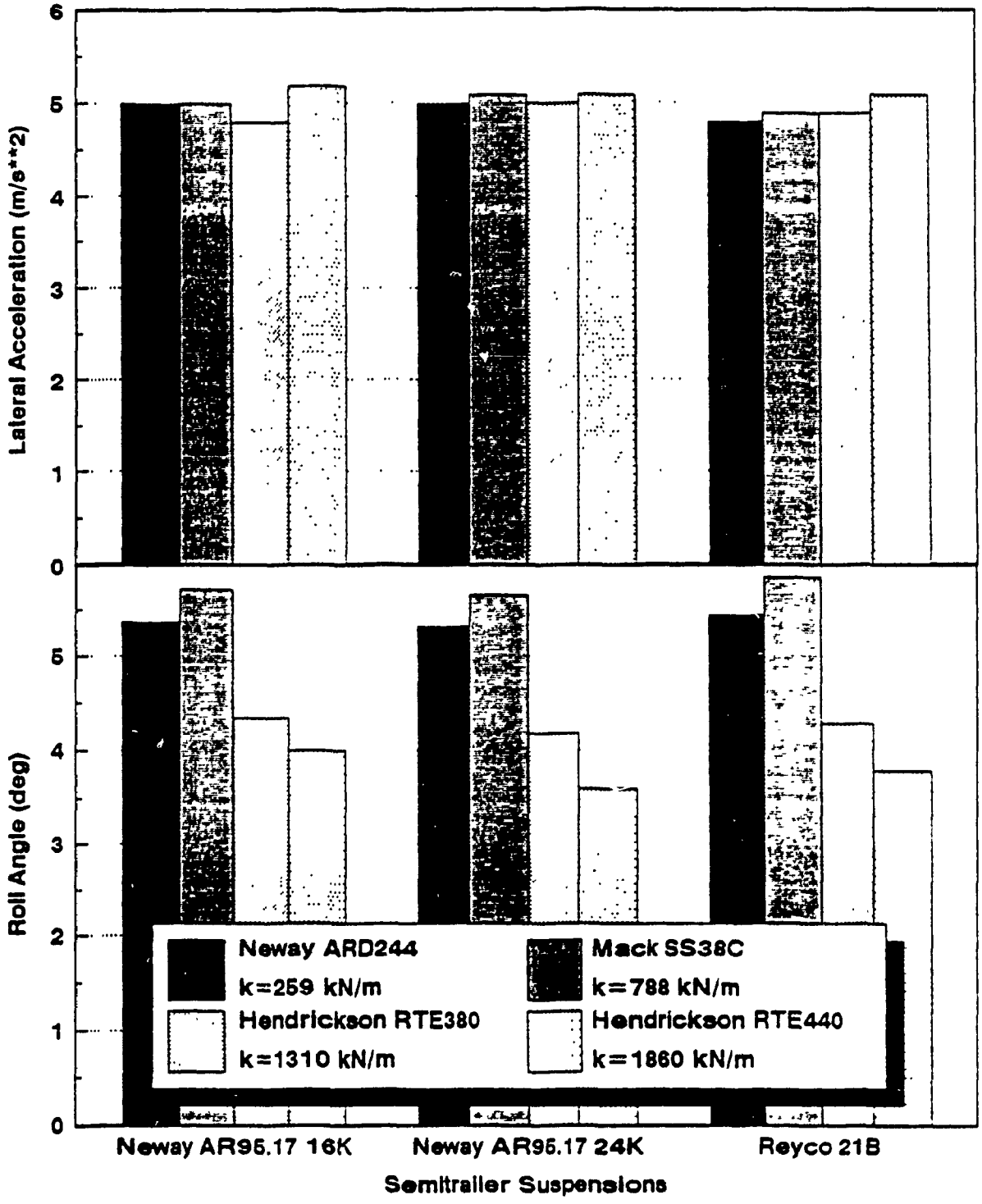

FIGURE 2.14: The Semitrailer Roll Angle and Lateral Acceleration at Rollover (Vehicle Width = 2.44 m; C.G. Height = 1.52 m)

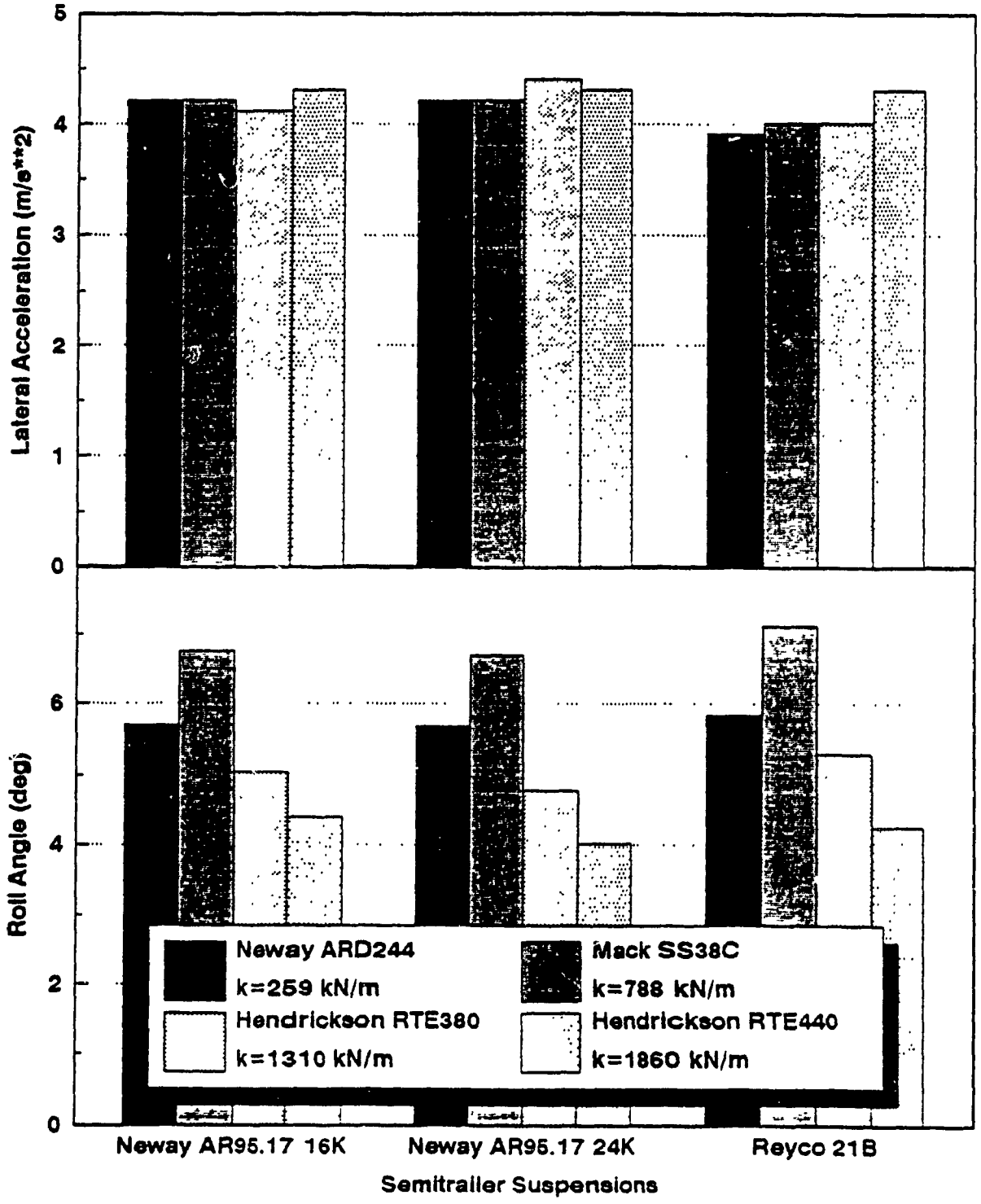

FIGURE 2.15: The Semitrailer Roll Angle and Lateral Acceleration at Rollover (Vehicle Width = 2.44 m; C.G. Height = 1.78 m)

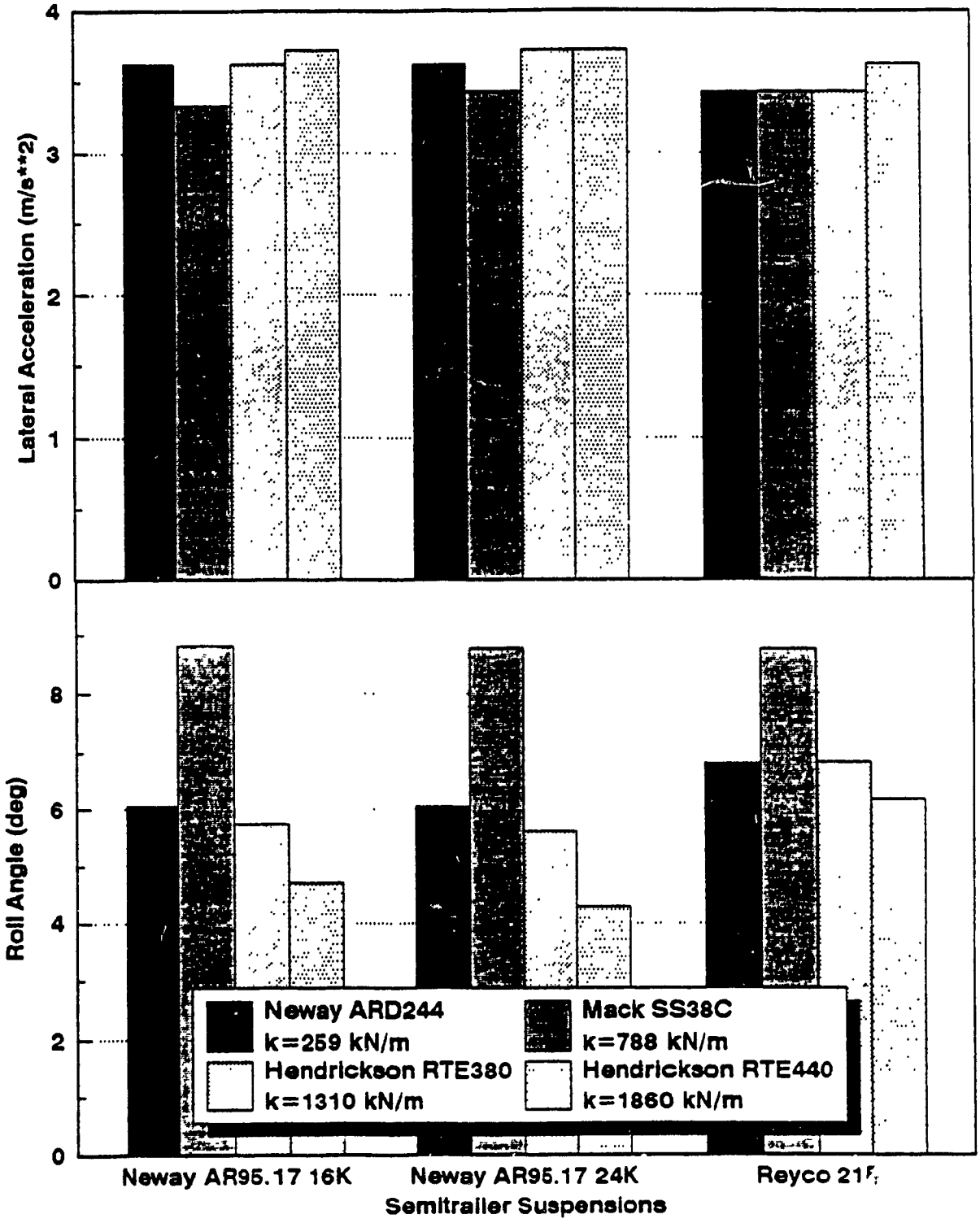

FIGURE 2.16: The Semitrailer Roll Angle and Lateral Acceleration at Rollover (Vehicle Width = 2.44 m; C.G. Height = 2.03 m)

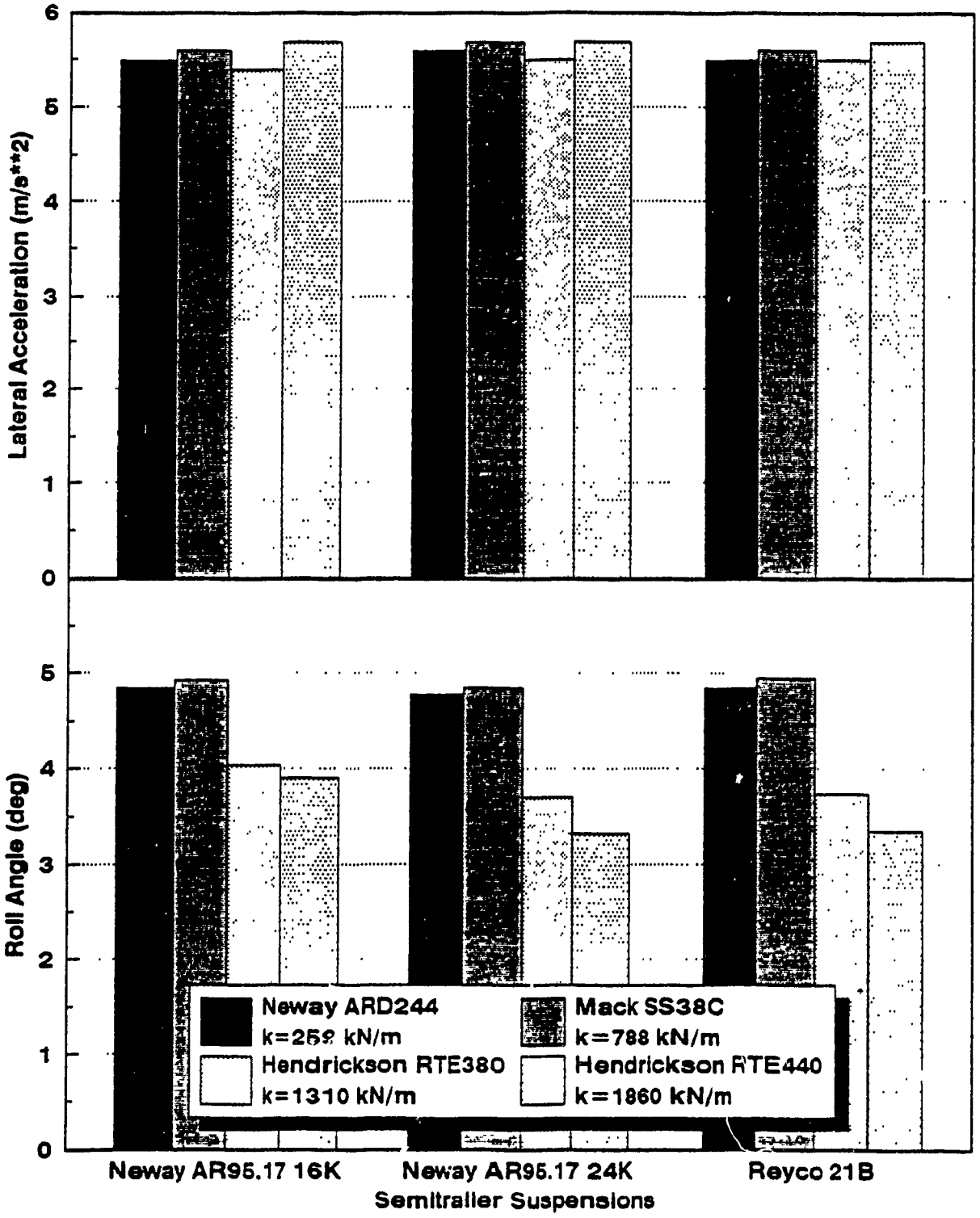

FIGURE 2.17: The Semitrailer Roll Angle and Lateral Acceleration at Rollover (Vehicle width = 2.59 m; C.G. Height = 1.52 m)

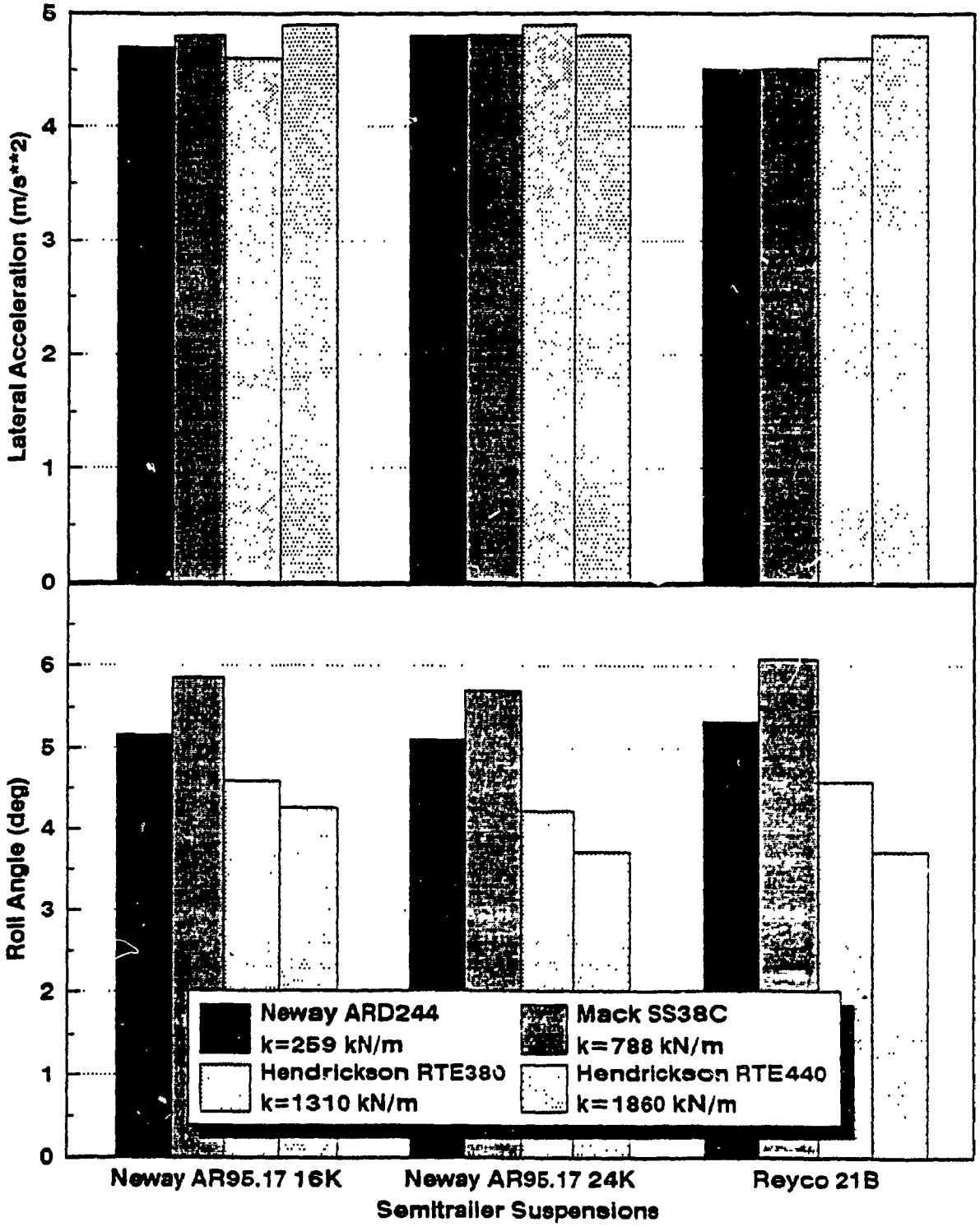

FIGURE 2.18: The Semitrailer Roll Angle and Lateral Acceleration at Rollover (Vehicle Width = 2.59 m; C.G. Height = 1.78 m)

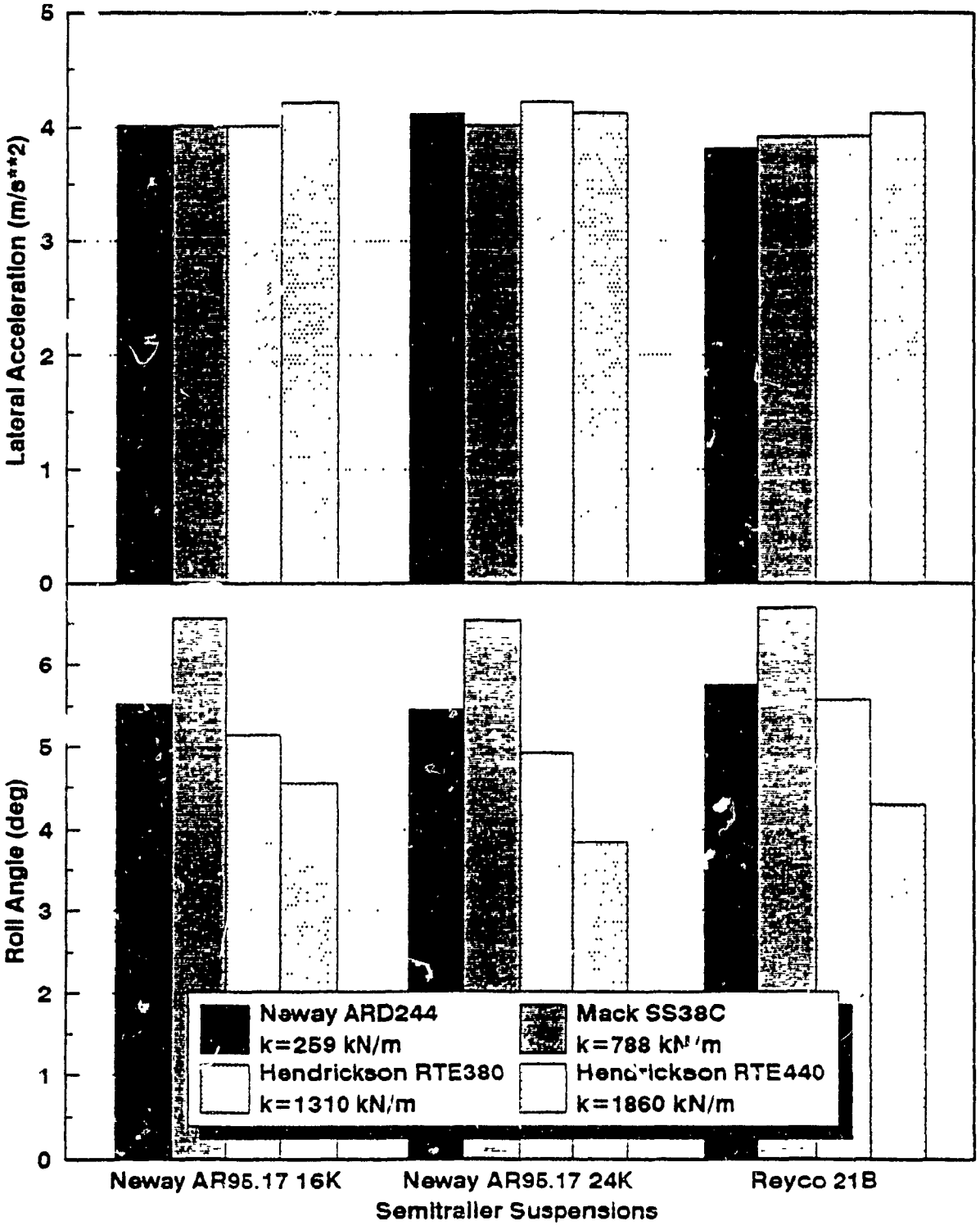

FIGURE 2.19: The Semitrailer Roll Angle and Lateral Acceleration at Rollover (Vehicle Width = 2.59 m; C.G. Height = 2.03 m)

corresponding to vehicle rollover ranges from 3.6 to 5.8 degrees. The response characteristics further reveal that the roll angle decreases as the suspension stiffness is increased. However, the Mack SS38C suspension (linear spring rate, K = 788 kN/m) exhibits slightly larger roll than the softer Neway air suspension (linear spring rate, K = 259 kN/m). The smaller roll angle response of the air suspension can be attributed to the progressively hardening nature of the air spring.

The roll angle and lateral acceleration response of the vehicle is presented in Figure 2.15, when the center of gravity height is increased to 1.78 meter. The magnitude of lateral acceleration corresponding to the vehicle rollover (rollover threshold) reduces to around 4 m/s^2 due to the increased center of gravity height. The corresponding roll angle response ranges from 4.0 to 6.8 degrees, as shown in Figure 2.15.

Figure 2.16 illustrates the vehicle's response during turning, when the semitrailer's sprung mass center of gravity height is further raised to 2.03 meters. The rollover threshold lateral acceleration value is further reduced to around 3.4 m/s^2, while the roll angle response ranges from 4.2 to 8.4 degrees.

Figures 2.17 to 2.19 illustrates the roll angle and lateral acceleration response corresponding to vehicle rollover for a 2.59-meter wide vehicle with three different values of semitrailer's sprung mass center of gravity height. The lateral acceleration threshold increases to around 5.4 m/s^2 due to increased tire track width, when the sprung mass center of gravity height is selected as 1.52 meter. The lateral acceleration threshold reduces to around 4.6 m/s^2 and 4.0 m/s^2 when the center of gravity height is raised to 1.78 meter and 2.03 meters, respectively, as shown in Figures 2.18 and 2.19.

The steady turning response characteristics reveal that for a given loading condition and vehicle track width, the lateral acceleration corresponding to the rollover varies only slightly with variation in suspension properties. However, the roll angle response of the semitrailer sprung mass varies considerably with the suspension properties. Moreover, the lateral acceleration corresponding to vehicle rollover is relatively insensitive to the torsional stiffness characteristics of the tractor chassis (K_{FR}), and that of the articulation mechanism and trailer structure (K_S), as shown in Figures 2.20 and 2.21. Thus the vehicle's lateral acceleration can be directly related to the onset of vehicle rollover provided the sprung mass center of gravity height and the tire track width do not vary. In majority of the freight vehicle combinations, the tire track width is held constant due to limits imposed on the maximum vehicle width. However, the sprung mass center of gravity height and thus the roll stability limit vary with changing loading condition. Tables 2.3 and 2.4 summarize the roll stability limits in terms of lateral acceleration of various vehicle and loading configurations.

Tables 2.3 and 2.4 clearly demonstrate that onset of roll instability can be directly related to the lateral acceleration response of the vehicle. In view of the dependency of vehicle's lateral acceleration rollover threshold on the semitrailer's sprung mass center of gravity height, the following two schemes are proposed to detect the onset of roll instability during steady turning:

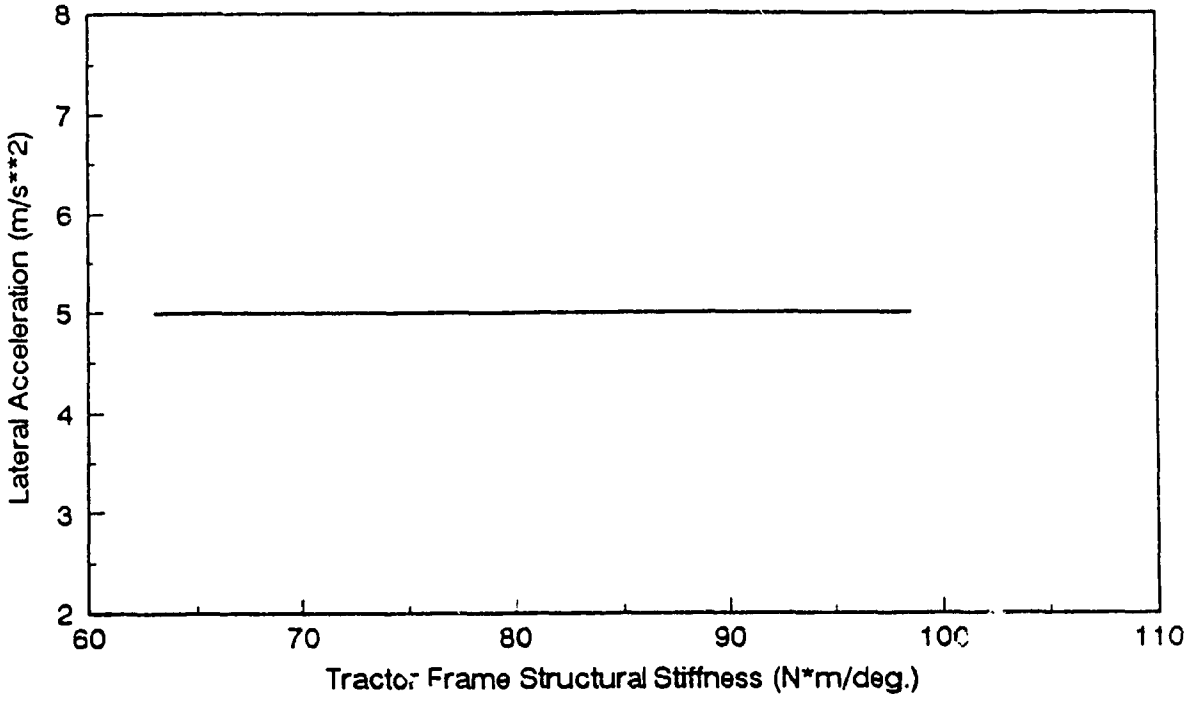

FIGURE 2.20: Rollover Threshold versus Torsional Stiffness of the Tractor Chassis

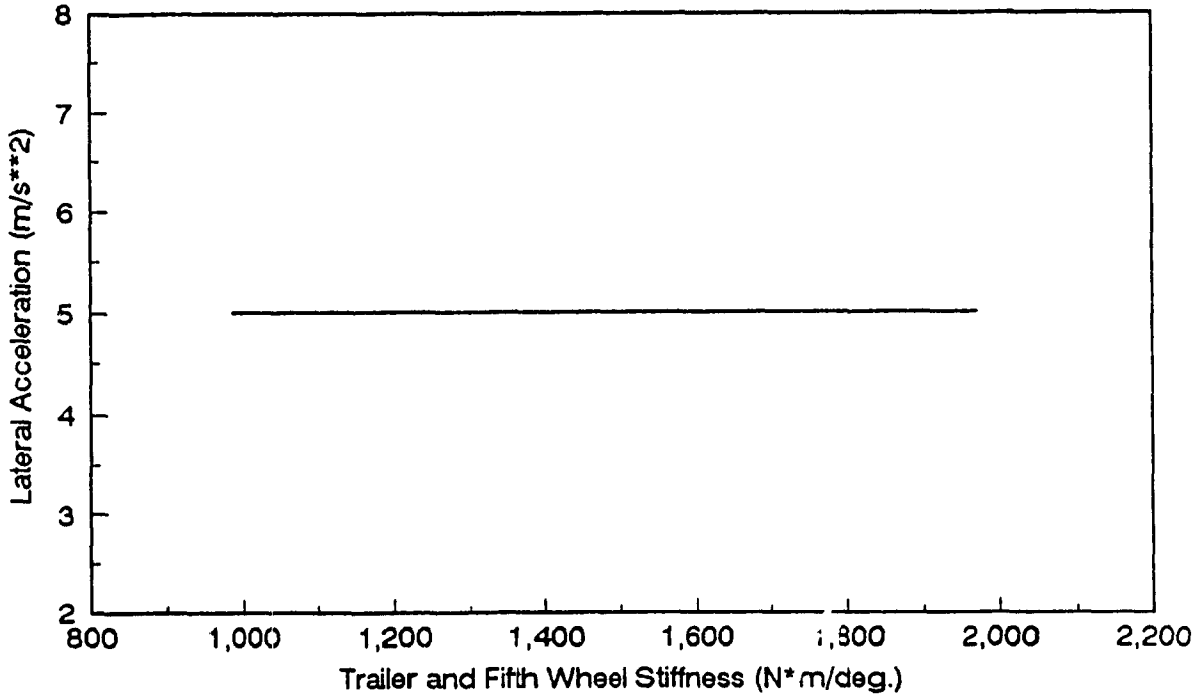

FIGURE 2.21: Rollover Threshold versus Torsional Stiffness of the Fifth Wheel and Trailer Structure

TABLE 2.3
ROLLOVER THRESHOLD LATERAL ACCELERATION
OF 2.44-METER WIDE VEHICLE

Vehicle Configuration Suspension at the three composite axles	Rollover Threshold		
	Center of Gravity Height		
	1.52 m	1.78 m	2.03 m
Rigid	7 0 m/s^2	6.0	5.2
I-H, Hendrickson RTE380, Neway AR95.17 24K	5.0	4.4	3.7
I-H, Hendrickson RTE380, Neway AR95.17 16K	4.8	4.1	3.6
I-H, Hendrickson RTE380, Reyco 21B	4.9	4.0	3.4
I-H, Hendrickson RTE440, Neway AR95.17 24K	5.1	4.3	3.7
I-H, Hendrickson RTE440, Neway AR95.17 16K	5.2	4.3	3.7
I-H, Hendrickson RTE440, Reyco 21B	5.1	4.3	3.6
I-H, Neway ARD244 16K, Neway AR95.17 24K	5.0	4.2	3.6
I-H, Neway ARD244 16K, Neway AR95.17 16K	5.0	4.2	3.6
I-H, Neway ARD244 16K, Reyco 21B	4.8	3.9	3.4
I-H, Mack Camel Back SS38C, Neway AR95.17 24K	5.1	4.2	3.4
I-H, Mack Camel Back SS38C, Neway AR95.17 16K	5.0	4.2	3.3
I-H, Mack Camel Back SS38C, Reyco 21B	4.9	4.0	3.4

TABLE 2.4
ROLLOVER THRESHOLD LATERAL ACCELERATION
OF 2.59-METER WIDE VEHICLE

Vehicle Configuration Suspension at the three composite axles	Rollover Threshold		
	Center of Gravity Height		
	1.52 m	1.78 m	2.03 m
Rigid	7.5 m/s^2	6.4	5.6
I-H, Hendrickson RTE380, Neway AR95.17 24K	5.5	4.9	4.2
I-H, Hendrickson RTE380, Neway AR95.17 16K	5.4	4.6	4.0
I-H, Hendrickson RTE380, Reyco 21B	5.5	4.6	3.9
I-H, Hendrickson RTE440, Neway AR95.17 24K	5.7	4.8	4.1
I-H, Hendrickson RTE440, Neway AR95.17 16K	5.7	4.9	4.2
I-H, Hendrickson RTE440, Reyco 21B	5.7	4.8	4.1
I-H, Neway ARD244 16K, Neway AR95.17 24K	5.6	4.8	4.1
I-H, Neway ARD244 16K, Neway AR95.17 16K	5.5	4.7	4.0
I-H, Neway ARD244 16K, Reyco 21B	5.5	4.5	3.8
I-H, Mack Camel Back SS38C, Neway AR95.17 24K	5.7	4.8	4.0
I-H, Mack Camel Back SS38C, Neway AR95.17 16K	5.6	4.8	4.0
I-H, Mack Camel Back SS38C, Reyco 21B	5.6	4.5	3.9

1. Detection of Roll Instability when the Center of Gravity Height is Unknown

Studies conducted by Miller and Barter [32] revealed that the center of gravity of the sprung mass of a fully laden trailer lies around 2 meters. Thus the onset of roll instability of the vehicle can be directly related to the lateral acceleration listed in Tables 2.3 and 2.4 corresponding to the 2.03-meter center of gravity height. A safe value of lateral acceleration can then be established as:

$$\bar{a}_y = \frac{a_y}{\alpha} \tag{2.28}$$

where a_y is the lower limit of the rollover threshold and α is the safety factor. This scheme will provide a conservative estimate of the impending roll instability, when the semitrailer is partly laden.

2. Detection of Roll Instability with Known Center of Gravity Height

The onset of roll instability can be detected quite precisely when the center of gravity height is known. The rollover threshold of the compliant five-axle tractor-semitrailer vehicle can be related to that of a rigid vehicle:

$$a_y = C \cdot a_y^* \tag{2.29}$$

where a_y and a_y^* are the rollover thresholds of the compliant and rigid vehicles, respectively. C is a compliance factor, determined from the elastic properties of the suspension, tires and articulation mechanism. The compliance factor is always less than 1 and can be expressed as the

ratio of rollover threshold of the compliant vehicle to that of the rigid vehicle:

$$C = \frac{a_y}{a_y^*} \tag{2.30}$$

The compliance factors and the corresponding lateral acceleration responses of the selected vehicle configurations are presented in Figures 2.22 and 2.23. Tables 2.5 and 2.6 present the vehicle suspension configurations and the corresponding compliance factors for 2.44-meter and 2.59-meter wide vehicles, respectively. Tables 2.5 and 2.6 show that the compliance factors of all the vehicle configurations analyzed are quite similar irrespective of the suspension type and center of gravity height. The mean compliance factor is obtained as 0.72 with a standard deviation of 0.03. The roll stability of the vehicle can thus be related to the compliance factor. The threshold value of compliance factor, C^* is obtained as:

$$C^* = \frac{1}{\alpha}(\bar{C}-3\sigma) \tag{2.31}$$

where α is the safety factor, $\bar{C}$ is the mean value of compliance factor and σ is the standard deviation. Assuming a safety factor of 1.1, the threshold value of compliance factor is achieved as 0.57.

For known values of trailer track width and center of gravity height, the rollover threshold of a rigid vehicle, a_y^* can be computed using Equation (2.2). A safe value of vehicle lateral acceleration is then obtained as:

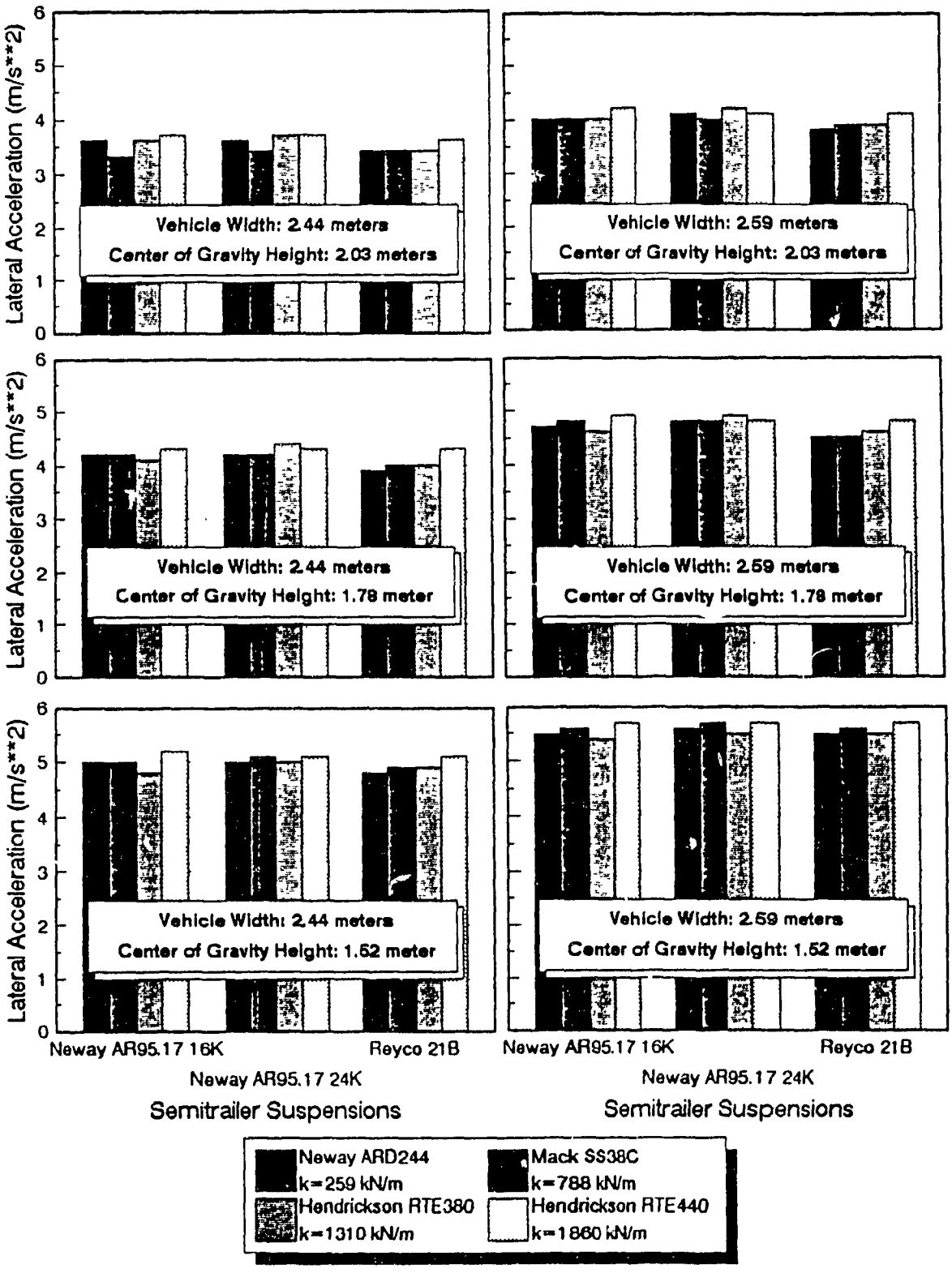

FIGURE 2.22: Rollover Threshold of the Vehicles Analyzed

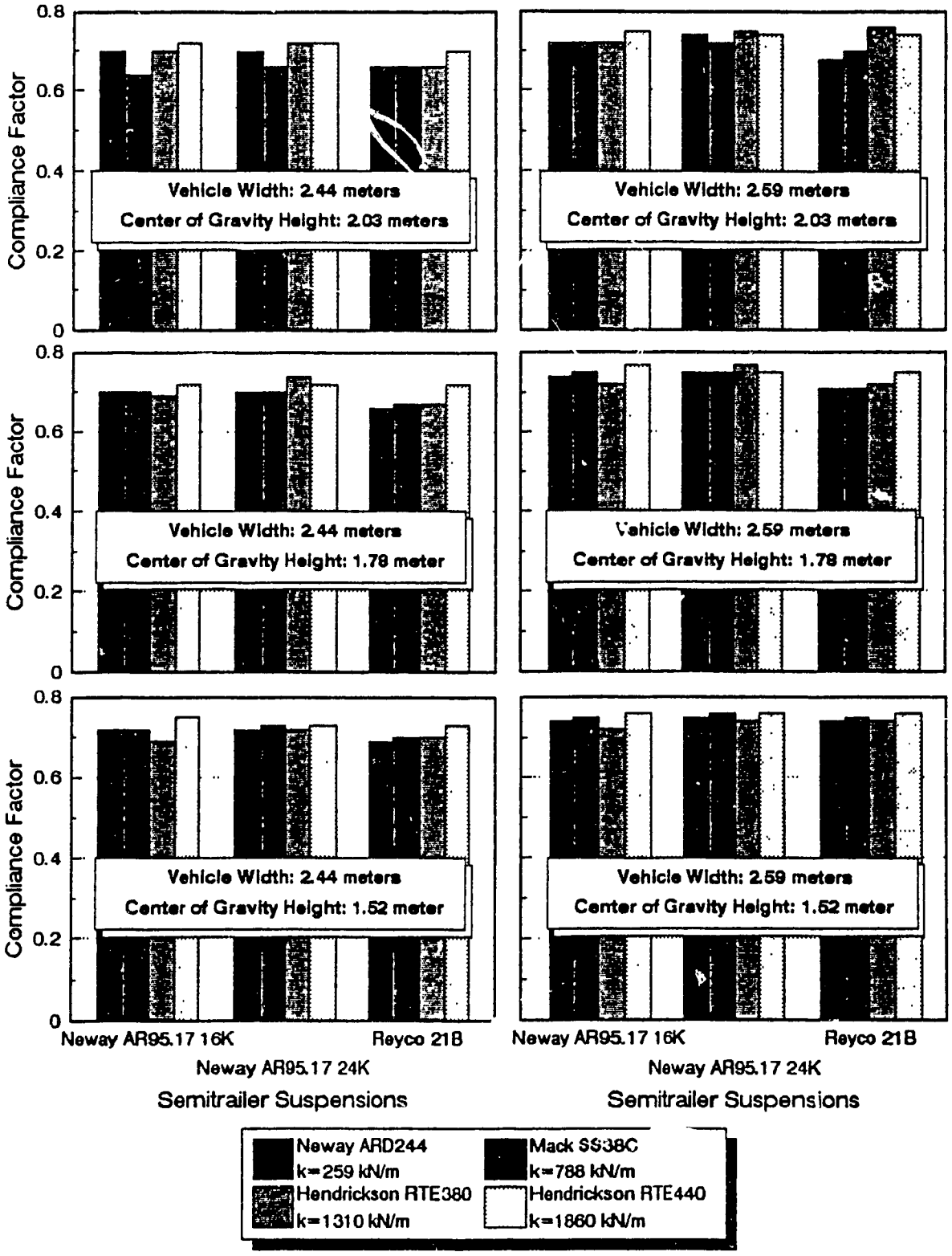

FIGURE 2.23: Compliance Factors of the Vehicles Analyzed

TABLE 2.5
COMPLIANCE FACTORS
OF 2.44-METER WIDE VEHICLE

Vehicle Configuration Suspension at the three composite axles	Compliance Factor		
	Center of Gravity Height 1.52 m	1.78 m	2.03 m
I-H, Hendrickson RTE380, Neway AR95.17 24K	0.72	0.74	0.72
I-H, Hendrickson RTE380, Neway AR95.17 16K	0.69	0.69	0.70
I-H, Hendrickson RTE380, Reyco 21B	0.70	0.67	0.66
I-H, Hendrickson RTE440, Neway AR95.17 24K	0.73	0.72	0.72
I-H, Hendrickson RTE440, Neway AR95.17 16K	0.75	0.72	0.72
I-H, Hendrickson RTE440, Reyco 21B	0.73	0.72	0.70
I-H, Neway ARD244 16K, Neway AR95.17 24K	0.72	0.70	0.70
I-H, Neway ARD244 16K, Neway AR95.17 16K	0.72	0.70	0.70
I-H, Neway ARD244 16K, Reyco 21B	0.69	0.66	0.66
I-H, Mack Camel Back SS38C, Neway AR95.17 24K	0.73	0.70	0.66
I-H, Mack Camel Back SS38C, Neway AR95.17 16K	0.72	0.70	0.64
I-H, Mack Camel Back SS38C, Reyco 21B	0.70	0.67	0.66

TABLE 2.6
COMPLIANCE FACTORS
OF 2.59-METER WIDE VEHICLE

Vehicle Configuration Suspension at the three composite axles	Compliance Factor		
	Center of Gravity Height 1.52 m	1.78 m	2.03 m
I-H, Hendrickson RTE380, Neway AR95.17 24K	0.74	0.77	0.75
I-H, Hendrickson RTE380, Neway AR95.17 16K	0.72	0.72	0.72
I-H, Hendrickson RTE380, Reyco 21B	0.74	0.72	0.70
I-H, Hendrickson RTE440, Neway AR95.17 24K	0.76	0.75	0.74
I-H, Hendrickson RTE440, Neway AR95.17 16K	0.76	0.77	0.75
I-H, Hendrickson RTE440, Reyco 21B	0.76	0.75	0.74
I-H, Neway ARD244 16K, Neway AR95.17 24K	0.75	0.75	0.74
I-H, Neway ARD244 16K, Neway AR95.17 16K	0.74	0.74	0.72
I-H, Neway ARD244 16K, Reyco 21B	0.74	0.71	0.68
I-H, Mack Camel Back SS38C, Neway AR95.17 24K	0.76	0.75	0.72
I-H, Mack Camel Back SS38C, Neway AR95.17 16K	0.75	0.75	0.72
I-H, Mack Camel Back SS38C, Reyco 21B	0.75	0.71	0.70

$$\bar{a}_y = C^* a_y^* \tag{2.32}$$

where $\bar{a}_y$ is the safe value of lateral acceleration related to onset of roll instability during steady turning. The lateral acceleration of the vehicle during steady turning can be easily measured using a piezo-resistive accelerometer. The onset of vehicle rollover can be detected by comparing the measured value of lateral acceleration to the precalculated safe limit $\bar{a}_y$.

2.7 SUMMARY

A static roll plane model of the articulated vehicle combination is developed to investigate steady turning stability limits. The onset of roll instability during steady turning is described via the rollover threshold lateral acceleration. The sensitivity of rollover threshold to variations in vehicle's design parameters is investigated to determine a feasible parameter that can directly describe the onset of roll instability. Two criteria, based upon the vehicle's lateral acceleration response are proposed to detect the onset of roll instability during steady turning.

CHAPTER 3

DYNAMIC ROLL STABILITY ANALYSIS

3.1 GENERAL

The static roll plane model of the articulated vehicle combinations, presented in the previous chapter, describes the roll behavior of the vehicle during a steady turn. The dynamics associated with the vehicle motion in the roll and yaw planes are neglected and the steady turning stability of the vehicle is described by its static rollover threshold. Although the vehicle rollover during a steady turn is directly related to its rollover threshold lateral acceleration, the vehicle rollover during a severe directional maneuver at highway speeds may occur at lateral acceleration levels considerably lower than the rollover threshold. The design of a safety monitor will thus require the scanning of vehicle response parameters that describe the onset of dynamic roll instability of the vehicle.

The dynamic roll stability of a tractor-semitrailer combination is investigated through analysis of a three dimensional vehicle model. The three dimensional vehicle model, incorporating yaw and roll plane dynamics, analyzes the directional response of the vehicle assuming constant forward speed. The directional dynamics of the vehicle combination is investigated using the "Yaw-Roll Analysis" software, developed by the University of Michigan Transportation Research Institute (UMTRI) [26]. A parametric sensitivity analysis is conducted to derive the key response parameters related to onset of dynamic roll instability. The roll stability of the vehicle is investigated for

single lane change and evasive steering maneuvers at typical highway speeds.

3.2 YAW-ROLL ANALYSIS

The yaw-roll model is one of the simulation programs developed at UMTRI to study the directional response of multi-articulated vehicles to dynamic directional maneuvers. The model was originally conceived to simulate a road train of up to four units, with up to eleven axles distributed in any arbitrary configuration, except for a single tractor front axle. In order to investigate the directional dynamics of the tractor-semitrailer combinations, the yaw-roll analysis software is appropriately modified. The modified yaw-roll analysis software, limited to a minimum of two units and six axles, is then used to carry out the stability analysis of the tractor-semitrailer combination efficiently.

The highlights of the yaw-roll vehicle model include nonlinear cornering characteristics of the tires and nonlinear suspension characteristics. The nonlinear cornering forces and aligning moments of the tires are computed as functions of normal load and sideslip angles using look-up tables. The nonlinear suspension characteristics such as backlash are represented in the form of load-deflection tables. The leaf springs tend to twist in the roll plane and hence produce an additional roll resisting moment when a relative roll motion takes place between the sprung mass and the axles. This property of the leaf-spring suspension is represented by an auxiliary roll stiffness parameter. Simulations can be performed in either the closed-loop or open-loop steering modes. In the open-loop mode, the time history of the steering

input is provided as input to the model. In the closed-loop mode, the desired trajectory is specified and the necessary steering input at the front wheels is computed using a driver model incorporating preset preview time and time delays.

3.3 ASSUMPTIONS

In order to simplify the equations, it is assumed that the pitch angles of the sprung masses and the relative roll angles between the sprung and unsprung masses are small, such that the small angle assumption can hold. Further, the principal axes of inertia of the sprung and unsprung masses are assumed to coincide with their respective body fixed coordinate system.

The model further assumes that each unit consists of a rigid body sprung mass and a number of beam axles, represented by unsprung masses, connected to the sprung mass through a compliant suspension system. The vehicle is assumed to move at a constant forward speed on a horizontal surface with uniform frictional characteristic. The relative motion between the sprung and the unsprung masses are assumed to occur about the roll center of each axle. The roll center is assumed to be located directly underneath the sprung mass and free to move in the vertical axis of the unsprung mass. Each suspension is independent of other suspension, such that inter-axle load transfer or load-sharing is neglected. The fifth wheel coupling allows each unit to roll, pitch, and yaw with respect to one another.

3.4 EQUATIONS OF MOTION

The differential equations governing the yaw and roll motion of an articulated vehicle are derived. In the model, each sprung mass is treated as a rigid body with five degrees-of-freedom, namely: lateral, vertical, yaw, roll, and pitch. Since the tractor forward velocity is assumed constant, the longitudinal degree-of-freedom is neglected. Each axle is permitted to roll and bounce with respect to the sprung mass, each unsprung mass is thus modeled as a two-degrees-of-freedom system. The development of the yaw-roll model is organized under the following systematic stages:

- Axis Systems
- Suspension Forces
- Equations of Motion for the Sprung Masses
- Equations of Motion for the Unsprung Masses
- Constraint Force and Moment Equations
- Tire Forces

3.4.1 Axis Systems

Three types of axis systems are used in the process of developing the equations of motion: (i) an inertial axis system fixed in space, (ii) axis system fixed to each of the sprung masses, and (iii) axis system fixed to each of the axles. Figure 3.1 illustrates the three axis systems. Euler angles are used to define the orientation of the sprung and unsprung masses with respect to the inertial axis system. Since all sprung mass axis systems are defined alike, the transformation equations are given below for only one sprung mass. For the same

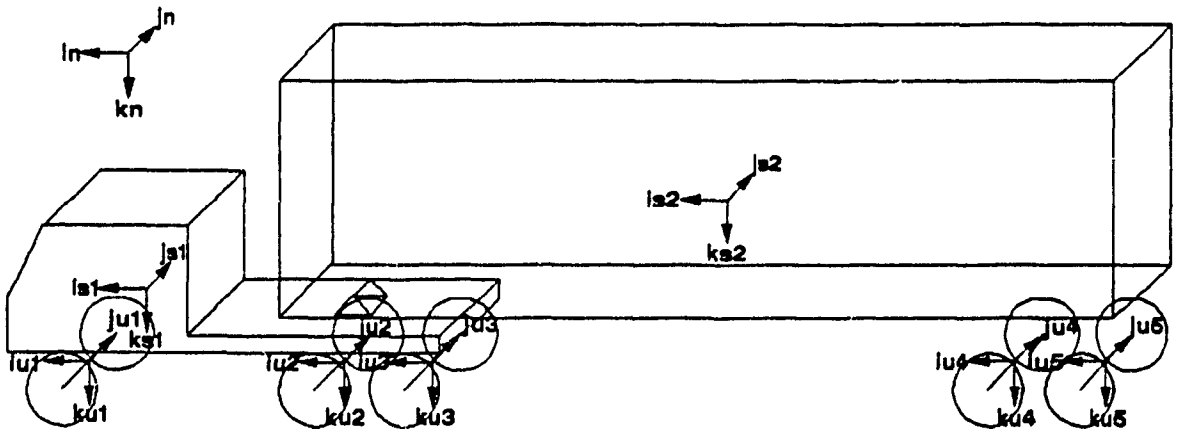

FIGURE 3.1: Axis Systems

reason, the transformation equations for the unsprung mass axis systems are derived for a single axle.

3.4.1.1 Sprung Mass Axis System

The three Euler angles, yaw (ψ_s), pitch (θ_s), and roll (ϕ_s), are needed to describe the orientation of each of the sprung mass axis system. The transformation equation between the inertial and sprung mass axis systems is derived using the Euler angles. For the yaw rotation, ψ_s:

$$\{\vec{i}_n,\ \vec{j}_n,\ \vec{k}_n\}^T = [a_{ij}]\{\vec{i}',\ \vec{j}',\ \vec{k}'\}^T \tag{3.1}$$

For the pitch rotation, θ_s:

$$\{\vec{i}',\ \vec{j}',\ \vec{k}'\}^T = [b_{ij}]\{\vec{i}'',\ \vec{j}'',\ \vec{k}''\}^T \tag{3.2}$$

Similarly, the roll rotation, ϕ_s:

$$\{\vec{i}'',\ \vec{j}'',\ \vec{k}''\}^T = [c_{ij}]\{\vec{i}_s,\ \vec{j}_s,\ \vec{k}_s\}^T \tag{3.3}$$

The transformation matrix needed to relate the sprung mass and the inertial axes systems are obtained by combining (3.1), (3.2), and (3.3):

$$\{\vec{i}_n,\ \vec{j}_n,\ \vec{k}_n\}^T = [A_{ij}]_k\{\vec{i}_s,\ \vec{j}_s,\ \vec{k}_s\}^T_k \tag{3.4}$$

where k = 1,2, designates the sprung weight due to the tractor and the

semitrailer, $[A_{ij}] = [a_{ij}][b_{ij}][c_{ij}]$ and the superscript 'T' denotes the transpose.

Sprung mass pitch angles are assumed to be small during directional maneuvers at constant forward speed, such that $\sin\theta_s = \theta_s$ and $\cos\theta_s = 1$. The transformation matrix $[A_{ij}]_k$ is thus expressed as:

$$[A_{ij}]_k = \begin{bmatrix} \cos\psi_s & -\sin\psi_s\cos\phi_s+\theta_s\cos\psi_s\sin\phi_s & \sin\psi_s\sin\phi_s+\theta_s\cos\psi_s\cos\phi_s \\ \sin\psi_s & \cos\psi_s\cos\phi_s+\theta_s\sin\psi_s\sin\phi_s & -\cos\psi_s\sin\phi_s+\theta_s\sin\psi_s\cos\phi_s \\ -\theta_s & \sin\phi_s & \cos\phi_s \end{bmatrix}_k \quad (3.5)$$

The body fixed sprung mass axis system is related to the inertial axis system by the following:

$$\{\vec{i}_s, \vec{j}_s, \vec{k}_s\}^T_k = [A_{ij}]^{-1}_k \{\vec{i}_n, \vec{j}_n, \vec{k}_n\}^T \quad (3.6)$$

where:

$$[A_{ij}]^{-1}_k = \begin{bmatrix} \cos\psi_s & \sin\psi_s & -\theta_s \\ -\sin\psi_s\cos\phi_s+\theta_s\cos\psi_s\sin\phi_s & \cos\psi_s\cos\phi_s+\theta_s\sin\psi_s\sin\phi_s & \sin\phi_s \\ \sin\psi_s\sin\phi_s+\theta_s\cos\psi_s\cos\phi_s & -\cos\psi_s\sin\phi_s+\theta_s\sin\psi_s\cos\phi_s & \cos\phi_s \end{bmatrix}_k \quad (3.7)$$

3.4.1.2 Unsprung Mass Axis System

Each axle is allowed to roll and bounce only with respect to the sprung mass to which it is attached. The orientation of the axle with respect to the inertial axis system is therefore defined by the yaw angle, ψ_s, and the roll angle, ϕ_u. The transformation equation relating the axis systems located on the sprung and unsprung masses, respectively is derived as follows:

$$\begin{Bmatrix} \vec{i}_U \\ \vec{j}_U \\ \vec{k}_U \end{Bmatrix}_i = \begin{bmatrix} 1 & \theta_{Sk}\sin\phi_{Sk} & \theta_{Sk}\cos\phi_{Sk} \\ -\theta_{Sk}\sin\phi_U & \cos(\phi_{Sk}-\phi_U) & -\sin(\phi_{Sk}-\phi_U) \\ -\theta_{Sk}\cos\phi_U & \sin(\phi_{Sk}-\phi_U) & \cos(\phi_{Sk}-\phi_U) \end{bmatrix}_i \begin{Bmatrix} \vec{i}_S \\ \vec{j}_S \\ \vec{k}_S \end{Bmatrix}_k \tag{3.8}$$

where i = 1,2,3 for k =1 and i = 4,5 for k = 2.

3.4.1.3 Angular Velocities of the Sprung Masses

The equations of motion of each sprung mass are written in terms of the body-fixed translational $(u_s, v_s, w_s)_k$ and angular velocities $(p_s, q_s, r_s)_k$ and their derivatives. The Euler angular velocities $(\dot{\phi}_s, \dot{\theta}_s, \dot{\psi}_s)_k$, calculated from the body-fixed angular velocities $(p_s, q_s, r_s)_k$, are integrated numerically to yield the Euler angles. The Euler angular velocities $(\dot{\phi}_s, \dot{\theta}_s, \dot{\psi}_s)_k$, defined along the $(\vec{i}_{Sk}, \vec{j}", \vec{k}_n)$ directions, are equated to the body-fixed velocities to yield:

$$p_{Sk}\vec{i}_{Sk} + q_{Sk}\vec{j}_{Sk} + r_{Sk}\vec{k}_{Sk} = \dot{\phi}_{Sk}\vec{i}_{Sk} + \dot{\theta}_{Sk}\vec{j}" + \dot{\psi}_{Sk}\vec{k}_n \tag{3.9}$$

From (3.3) and (3.5):

$$\vec{j}" = \cos\phi_{Sk}\vec{j}_{Sk} - \sin\phi_{Sk}\vec{k}_{Sk}$$

$$\vec{k}_n = -\theta_{Sk}\vec{i}_{Sk} + \sin\phi_{Sk}\vec{j}_{Sk} + \cos\phi_{Sk}\vec{k}_{Sk} \tag{3.10}$$

Upon substituting (3.10) into (3.9) we get:

$$p_{Sk}\vec{i}_{Sk} = (\dot{\phi}_{Sk} - \theta_{Sk}\dot{\psi}_{Sk})\vec{i}_{Sk} \tag{3.11}$$

$$q_{Sk}\vec{j}_{Sk} = (\dot{\theta}_{Sk}\cos\phi_{Sk} + \sin\phi_{Sk}\dot{\psi}_{Sk})\vec{j}_{Sk} \tag{3.12}$$

$$r_{Sk}\vec{k}_{Sk} = (-\dot{\theta}_{Sk}\sin\phi_{Sk} + \dot{\psi}_{Sk}\cos\phi_{Sk})\vec{k}_{Sk} \tag{3.13}$$

The above three equations can be solved to express the Euler angular velocities in terms of the body-fixed angular velocities, $(p_S, q_S, r_S)_k$.

$$\dot{\phi}_{Sk} = p_{Sk} + (q_{Sk}\sin\phi_{Sk} + r_{Sk}\cos\phi_{Sk})\theta_{Sk} \tag{3.14}$$

$$\dot{\theta}_{Sk} = q_{Sk}\cos\phi_{Sk} - r_{Sk}\sin\phi_{Sk} \tag{3.15}$$

$$\dot{\psi}_{Sk} = q_{Sk}\sin\phi_{Sk} + r_{Sk}\cos\phi_{Sk} \tag{3.16}$$

Equations (3.14) to (3.16) are numerically integrated to obtain the Euler angles.

3.4.2 Suspension Forces

Each suspension is assumed to consist of a pair of nonlinear springs and linkages providing a roll center. The suspension springs are assumed to remain parallel to the $\vec{k}_{Ui}$ axis of the unsprung mass, and are capable of transmitting either compressive or tensile forces only. All the roll plane forces perpendicular to the suspension springs are assumed to act through the roll center located at a fixed distance, z_{Ri}, beneath the sprung mass as shown in Figure 3.2. The roll center is allowed to slide along the $\vec{k}_{Ui}$ axis of the unsprung mass. The suspension forces transmitted to the sprung mass from any given axle, i, are therefore:

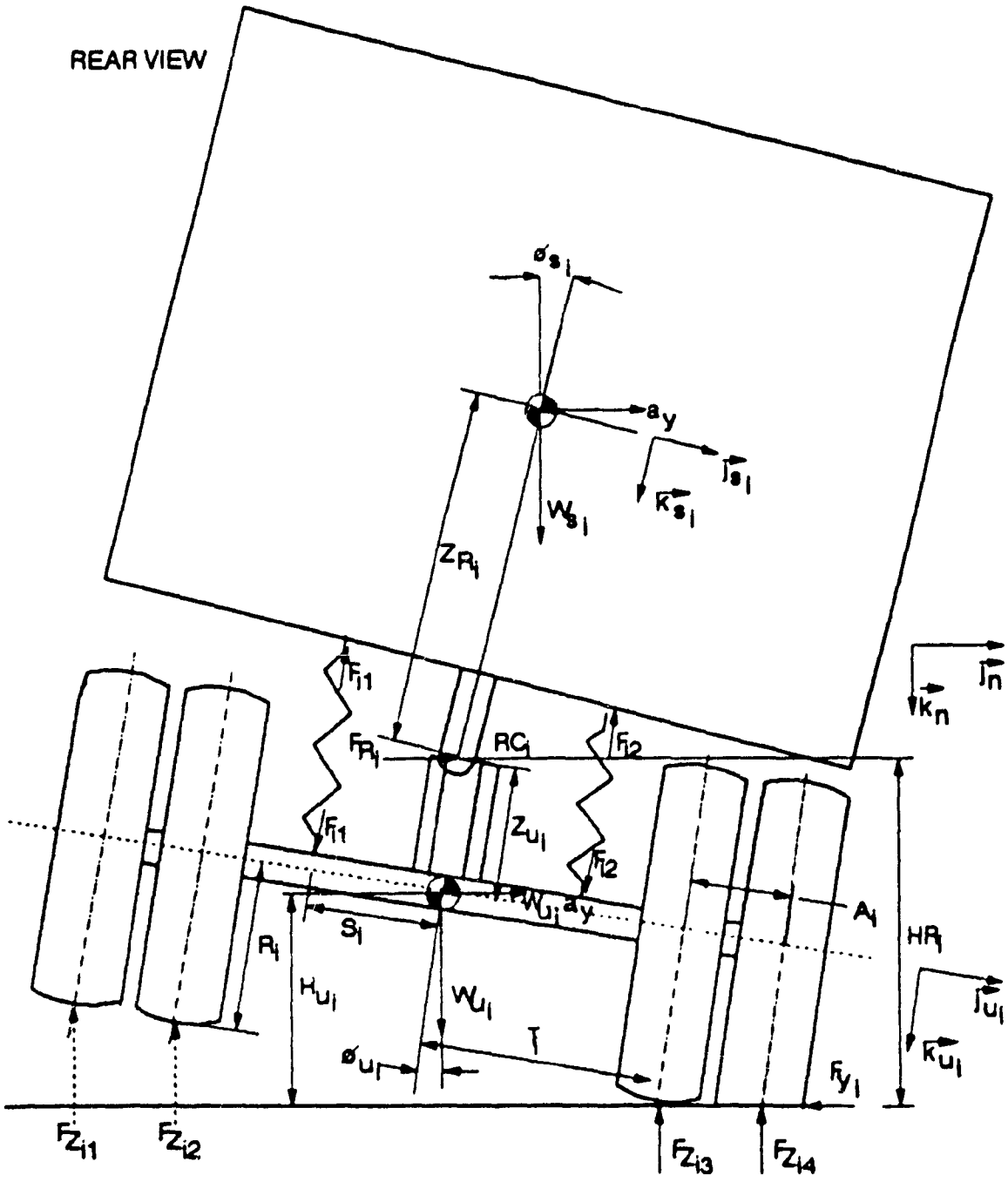

FIGURE 3.2: Forces and Moments Acting in the Roll Plane of the Vehicle

$$F_{si} = F_{Ri}\vec{j}_{Ui} - (F_{i1}+F_{i2})\vec{k}_{Ui} \tag{3.17}$$

where F_{i1} and F_{i2} are the forces due to springs located on right and left side of axle i.

The suspension forces are defined in the sprung mass coordinate system by applying the coordinate transformation expressed by equations (3.8). Upon applying the transformation, we get:

$$\begin{aligned} F_{si} = {} & [-F_{Ri}\theta_{Sk}\sin\phi_{Ui} + (F_{i1}+F_{i2})\theta_{Sk}\cos\phi_{Ui}]\vec{i}_{Sk} \\ & + [F_{Ri}\cos(\phi_{Sk}-\phi_{Ui}) - (F_{i1}+F_{i2})\sin(\phi_{Sk}-\phi_{Ui})]\vec{j}_{Sk} \\ & - [F_{Ri}\sin(\phi_{Sk}-\phi_{Ui}) + (F_{i1}+F_{i2})\cos(\phi_{Sk}-\phi_{Ui})]\vec{k}_{Sk} \end{aligned} \tag{3.18}$$

The force, F_{Ri}, acting through the roll center is an internal force which is eliminated by inspecting the dynamic equilibrium of the axle in the $\vec{j}_{Ui}$ direction. The equation for the lateral equilibrium of the axle can be written as:

$$\begin{aligned} m_{Ui}[\vec{a}_{mUi}\cdot\vec{j}_{Ui}] = {} & -F_{Ri} + (F_{yi1}+F_{yi2}+F_{yi3}+F_{yi4})\cos\phi_{Ui} \\ & - (F_{Zi1}+F_{Zi2}+F_{Zi3}+F_{Zi4})\sin\phi_{Ui} + m_{Ui}g\sin\phi_{Ui} \end{aligned} \tag{3.19}$$

Equation (3.19) is rearranged as:

$$\begin{aligned} F_{Ri} = {} & -m_{Ui}[\vec{a}_{mUi}\cdot\vec{j}_{Ui}] + (F_{yi1}+F_{yi2}+F_{yi3}+F_{yi4})\cos\phi_{Ui} \\ & - (F_{Zi1}+F_{Zi2}+F_{Zi3}+F_{Zi4})\sin\phi_{Ui} + m_{Ui}g\sin\phi_{Ui} \end{aligned} \tag{3.20}$$

where F_{yij} and F_{Zij} are the lateral and vertical forces, respectively due to the tire j on axle i.

Of the terms on the right hand side of (3.20), the only unknown is the acceleration $\vec{a}_{mUi}$ of the unsprung mass. Since the position of the axle is defined relative to the sprung mass to which it is attached, the acceleration of the unsprung mass is given by:

$$\vec{a}_{mUi} = \vec{a}_{mSk} + \vec{a}_{Ri/mSk} + \vec{a}_{mUi/Ri} \tag{3.21}$$

where $\vec{a}_{mSk}$, $\vec{a}_{mUi/Ri}$ and $\vec{a}_{Ri/mSk}$ are the accelerations of the sprung mass k, the unsprung mass i with respect to the roll center and the roll center i with respect to the sprung mass k, respectively.

The sprung mass acceleration along the body-fixed coordinates $(\vec{i}_S, \vec{j}_S, \vec{k}_S)_k$ is given by:

$$\vec{a}_{mSk} = (\dot{u}_S + q_S w_S - r_S v_S)_k \vec{i}_{Sk} + (\dot{v}_S + u_S r_S - p_S w_S)_k \vec{j}_{Sk} + (\dot{w}_S + p_S v_S - q_S u_S)_k \vec{k}_{Sk} \tag{3.22}$$

Since the roll center is at a fixed distance from the sprung mass center of gravity, the position of the roll center with respect to the sprung mass center of gravity can be expressed in the following manner:

$$\vec{r}_{Ri/mSk} = x_{Ri} \vec{i}_{Sk} + z_{Ri} \vec{k}_{Sk} \tag{3.23}$$

The corresponding velocity and acceleration are derived as follows:

$$\vec{w}_{Ri/mSk} = (z_{Ri} q_S)_k \vec{i}_{Sk} + (-p_S z_{Ri} + x_{Ri} r_S)_k \vec{j}_{Sk} - x_{Ri} q_{Sk} \vec{k}_{Sk} \tag{3.24}$$

$$\vec{a}_{R1/mSk} = (\dot{q}_s z_{R1} - x_{R1} q_s^2 + p_s r_s z_{R1} - x_{R1} r_s^2)_k \vec{i}_{Sk}$$
$$+ (-\dot{p}_s z_{R1} + x_{R1} \dot{r}_s + z_{R1} q_s r_s + x_{R1} q_s p_s)_k \vec{j}_{Sk}$$
$$+ (-p_s^2 z_{R1} + x_{R1} r_s p_s - z_{R1} q_s^2 - x_{R1} \dot{q}_s)_k \vec{k}_{Sk} \qquad (3.25)$$

Similarly, the unsprung mass acceleration with respect to the roll center is described as:

$$\vec{a}_{mU1/R1} = p_{U1} r_{U1} z_{U1} \vec{i}_{U1} - (\dot{p}_{U1} z_{U1} + 2p_{U1} \dot{z}_{U1}) \vec{j}_{U1} - (p_{U1}^2 z_{U1} - \ddot{z}_{U1}) \vec{k}_{U1} \qquad (3.26)$$

Hence, combining (3.22), (3.25) and (3.26), and transforming the acceleration defined in the sprung mass coordinate system to the unsprung mass coordinates system, we get:

$$\vec{a}_{mU1} \cdot \vec{j}_{U1} = -(\dot{u}_s + q_s w_s - r_s v_s + \dot{q}_s z_{R1} - x_{R1} q_s^2 + p_s r_s z_{R1} - x_{R1} r_s^2)_k \theta_{Sk} \sin \phi_{U1}$$
$$+ (\dot{v}_s + u_s r_s - p_s w_s - \dot{p}_s z_{R1} + x_{R1} \dot{r}_s + z_{R1} q_s r_s + x_{R1} q_s p_s)_k \cos(\phi_{Sk} - \phi_{U1})$$
$$- (\dot{w}_s + p_s v_s - q_s u_s - p_s^2 z_{R1} + x_{R1} r_s p_s - z_{R1} q_s^2 - x_{R1} \dot{q}_s)_k \sin(\phi_{Sk} - \phi_{U1})$$
$$- \dot{p}_{U1} z_{U1} - 2p_{U1} \dot{z}_{U1} \qquad (3.27)$$

From (3.20) and (3.27), the roll center force is obtained as:

$$F_{R1} = -m_{U1} \Big[- (\dot{u}_s + q_s w_s - r_s v_s + \dot{q}_s z_{R1} - x_{R1} q_s^2 + p_s r_s z_{R1} - x_{R1} r_s^2)_k \theta_{Sk} \sin \phi_{U1}$$
$$+ (\dot{v}_s + u_s r_s - p_s w_s - \dot{p}_s z_{R1} + x_{R1} \dot{r}_s + z_{R1} q_s r_s + x_{R1} q_s p_s)_k \cos(\phi_{Sk} - \phi_{U1})$$
$$- (\dot{w}_s + p_s v_s - q_s u_s - p_s^2 z_{R1} + x_{R1} r_s p_s - z_{R1} q_s^2 - x_{R1} q_s^2)_k \sin(\phi_{Sk} - \phi_{U1})$$
$$- \dot{p}_{U1} z_{U1} - 2p_{U1} \dot{z}_{U1} \Big] + (F_{y11} + F_{y12} + F_{y13} + F_{y14}) \cos \phi_{U1}$$
$$- (F_{z11} + F_{z12} + F_{z13} + F_{z14}) \sin \phi_{U1} + m_{U1} g \sin \phi_{U1} \qquad (3.28)$$

3.4.3 Equations of Motion of the Sprung Masses

Figures 3.1 and 3.2 present the pitch plane and roll plane of the articulated vehicle model. The five second-order differential equations derived for each of the sprung masses are presented in the following manner

Equations of Lateral Motion

$$m_{Sk}\dot{v}_{Sk} - m_{Sk}(p_S w_S - r_S u_S)_k$$
$$= \sum \vec{j}_{Sk} \text{ component of the constraint forces}$$
$$+ \sum_{i=j1}^{j2} [F_{Ri}\cos(\phi_{Sk}-\phi_{Ui}) - (F_{i1}+F_{i2})\sin(\phi_{Sk}-\phi_{Ui})]$$
$$+ m_{Sk} g \sin\phi_{Sk}, \quad k=1,2 \text{ and } i=1, \quad ,5 \qquad (3.29)$$

where $j1$ and $j2$ designate the axles attached to the sprung mass.

For tractor's sprung mass (k=1); $j1$ = 1 and $j2$ = 3

For trailer's sprung mass (k=2), $j1$ = 4 and $j2$ = 5

Equations of Vertical Motion

$$m_{Sk}\dot{w}_{Sk} - m_{Sk}(q_S u_S - p_S v_S)_k$$
$$= \sum \vec{k}_{Sk} \text{ component of constraint the forces}$$
$$+ \sum_{i=j1}^{j2} [F_{Ri}\sin(\phi_{Sk}-\phi_{Ui}) + (F_{i1}+F_{i2})\cos(\phi_{Sk}-\phi_{Ui})]$$
$$+ m_{Sk} g \cos\phi_{Sk} \qquad (3.30)$$

Equations of Roll Motion

$$I_{XXSk}\dot{p}_{Sk} - (I_{YYS}-I_{ZZS})_k q_{Sk} r_{Sk}$$
$$= \sum \text{roll moments from the constraints}$$
$$- \sum_{i=j1}^{j2} F_{Ri}\cos(\phi_{Sk}-\phi_{Ui})z_{Ri} + \sum_{i=j1}^{j2}(F_{i1}+F_{i2})s_i$$
$$+ \sum_{i=j1}^{j2}(F_{i1}+F_{i2})\sin(\phi_{Sk}-\phi_{Ui})z_{Ri} + \sum_{i=j1}^{j2} KRS_i(\phi_{Sk}-\phi_{Ui}) \qquad (3.31)$$

Equations of Pitch Motion

$$I_{YYSk}\dot{q}_{Sk} - (I_{ZZS}-I_{XXS})_k p_{Sk} r_{Sk}$$
$$= \sum \text{pitching moments from the constraints}$$
$$+ \sum_{i=j1}^{j2}[F_{Ri}\sin(\phi_{Sk}-\phi_{Ui}) + (F_{i1}+F_{i2})\cos(\phi_{Sk}-\phi_{Ui})]x_{Ui} \qquad (3.32)$$

Equations of the Yaw Motion

Since, the axles experience the yaw motion together with the sprung mass, the yaw moments of inertia of the axles are combined with the yaw moment of inertia of the sprung mass to obtain an equation applicable to the combined rigid body:

$$\left[\sum_{i=j1}^{j2} I_{ZZUi} + I_{ZZSk}\right]\dot{r}_{Sk} - (I_{XXS}-I_{YYS})_k p_{Sk} q_{Sk}$$
$$= \sum \text{yaw moments due to the constraints}$$
$$+ \sum_{i=j1}^{j2}\Big([F_{Ri}\cos(\phi_{Sk}-\phi_{Ui}) - (F_{i1}+F_{i2})\sin(\phi_{Sk}-\phi_{Ui})]x_{Ui}$$
$$+ (AT_{i1}+AT_{i2}+AT_{i3}+AT_{i4})\cos\phi_{Sk}\Big) \qquad (3.33)$$

Equations (3.29) to (3.33) constitute the governing differential equations of motion of the sprung masses. The equation needed to evaluate the unknown constraint forces and tire forces are developed in subsequent sections.

3.4.4 Equations of Motion of the Unsprung Masses

The equations of roll and bounce motion of each of the unsprung masses are given below.

Equations of Roll Motion

$$\begin{aligned} I_{xxUi}\dot{p}_{Ui} &= -(F_{i1}-F_{i2})s_i - F_{Ri}z_{Ui} \\ &- \Big[(F_{yi1}+F_{yi2}+F_{yi3}+F_{yi4})\cos\phi_{Ui} \\ &+ (F_{Zi1}+F_{Zi2}+F_{Zi3}+F_{Zi4})\sin\phi_{Ui}\Big](HR_i\cos\phi_{Ui}-z_{Ui}) \\ &+ (F_{Zi2}-F_{Zi4})(T_i+A_i)\cos\phi_{Ui} + (F_{Zi2}-F_{Zi3})T_i\cos\phi_{Ui} \\ &+ KRS_i(\phi_{Sk}-\phi_{Ui}) \end{aligned} \tag{3.34}$$

Equations of Vertical Motion

$$\begin{aligned} m_{Ui}\dot{\vec{a}}_{mUi}\cdot\vec{k}_{Ui} &= m_{Ui}g\cos\phi_{Ui} + F_{i1} + F_{i2} \\ &- (F_{Zi1}+F_{Zi2}+F_{Zi3}+F_{Zi4})\cos\phi_{Ui} \\ &- (F_{yi1}+F_{yi2}+F_{yi3}+F_{yi4})\sin\phi_{Ui} \end{aligned} \tag{3.35}$$

The acceleration $\vec{a}_{mUi}\cdot\vec{k}_{Ui}$ is evaluated in a manner similar to the one employed for evaluation of $\vec{a}_{mUi}\cdot\vec{j}_{Ui}$ in Equation (3.27).

$$\vec{a}_{mUi} \cdot \vec{k}_{Ui} = -(\dot{u}_s + q_s w_s - r_s v_s + \dot{q}_s z_{Ri} - x_{Ri} q_s^2 + p_s r_s z_{Ri} - x_{Ri} r_s^2)_k \theta_{Sk} \cos \phi_{Ui}$$
$$+ (\dot{v}_s + u_s r_s - p_s w_s - \dot{p}_s z_{Ri} + x_{Ri} \dot{r}_s + z_{Ri} q_s r_s + x_{Ri} q_s p_s)_k \sin(\phi_{Sk} - \phi_{Ui})$$
$$+ (\dot{w}_s + p_s v_s - q_s u_s - p_s^2 z_{Ri} + x_{Ri} r_s p_s - z_{Ri} q_s^2 - x_{Ri} \dot{q}_s)_k \cos(\phi_{Sk} - \phi_{Ui})$$
$$+ (\ddot{z}_{Ui} - p_{Ui}^2 z_{Ui}) \qquad (3.36)$$

3.4.5 Constraint Equation

The differential equations governing the motion of the sprung masses (Equations (3.29) to (3.33)) contain terms related to the constraint forces and moments. These constraint forces and moments, arising at the fifth wheel coupling, are derived using the kinematic equations defining the constraint. A vehicle combination model comprising of n sprung masses and m unsprung masses yields k second-order differential equations to describe the motion of the vehicle, where $k = 5n + 2m$. The set of k differential equations of motion of the vehicle model are written in the matrix form:

$$M\ddot{\vec{x}} = \vec{y} + N\vec{f}_c \qquad (3.37)$$

where M is the $[k \times k]$ inertia matrix, $\vec{y}$ is a vector of size k comprising of gravitational, suspension, and roll center forces, N is the $[k \times j]$ matrix of vehicle dimensions, $\vec{f}_c$ is a vector of length j containing unknown constraint forces, and $\ddot{\vec{x}}$ is the acceleration vector of length k.

The kinematic constraints existing at the fifth wheel, when written as a set of acceleration constraint equations, are of the form:

$$C\ddot{\vec{x}} = \vec{d} \qquad (3.38)$$

where:

C = a matrix of size $j \times k$, function of the vehicle dimensions and $\vec{x}$.

$\vec{d}$ = a vector of size j, function of $\vec{x}$, $\dot{\vec{x}}$ and the vehicle dimensions.

The constraint force vector, $\vec{f}_c$, is obtained via solving equations (3.37) and (3.38). Equation (3.37) is solved to yield:

$$\ddot{\vec{x}} = M^{-1}\vec{y} + M^{-1}N\vec{f}_c \tag{3.39}$$

Upon substituting (3.39) in (3.38), we get:

$$CM^{-1}\vec{y} + CM^{-1}N\vec{f}_c = \vec{d} \tag{3.40}$$

The vector of constraint forces is thus obtained as:

$$\vec{f}_c = [CM^{-1}N]^{-1}\{\vec{d}-CM^{-1}\vec{y}\} \tag{3.41}$$

The acceleration vector $\ddot{\vec{x}}$ is then obtained by substituting $\vec{f}_c$ from Equation (3.41) into Equation (3.39):

$$\ddot{\vec{x}} = M^{-1}\vec{y} + M^{-1}N[CM^{-1}N]^{-1}\{\vec{d}-CM^{-1}\vec{y}\} \tag{3.42}$$

Since all the terms in the right-hand side of (3.42) are known, Equations (3.42) are integrated using numerical integration techniques to obtain directional response characteristics of the vehicle.

The fifth wheel arrangement allows the tractor and the semitrailer to yaw and pitch with respect to one another, but is quite stiff in roll. The roll and pitch moments transmitted through the fifth wheel are easily evaluated in terms of the relative roll and pitch displacements between the adjacent units. Therefore, the acceleration constraint approach is not adopted to solve the roll and pitch moments. In the following section, the acceleration constraint equations needed to determine the lateral and vertical forces at the fifth wheel are developed.

3.4.5.1 Lateral and Vertical Constraint Forces

The fifth wheel is a single point constraint where the articulation takes place. The constraint acceleration equations, needed to solve for the lateral and vertical forces, are therefore formulated by equating the lateral and vertical accelerations of the constraint point on the tractor to the accelerations of the same point on the semitrailer. The acceleration of the constraint point on the tractor is given by the expression:

$$\begin{aligned}\vec{a}_c &= (\dot{u}_{S1}+q_{S1}w_{S1}-r_{S1}v_{S1}+\dot{q}_{S1}z_{c1}-x_{c1}q_{S1}^2+p_{S1}r_{S1}z_{c1}-x_{c1}r_{S1}^2)\vec{i}_{S1} \\ &+ (\dot{v}_{S1}+u_{S1}r_{S1}-p_{S1}w_{S1}-\dot{p}_{S1}z_{c1}+x_{c1}\dot{r}_{S1}+z_{c1}q_{S1}r_{S1}+x_{c1}q_{S1}p_{S1})\vec{j}_{S1} \\ &+ (\dot{w}_{S1}+p_{S1}v_{S1}-q_{S1}u_{S1}-x_{c1}\dot{q}_{S1}-p_{S1}^2z_{c1}+x_{c1}r_{S1}p_{S1}-z_{c1}q_{S1}^2)\vec{k}_{S1} \\ &= a_1\vec{i}_{S1} + b_1\vec{j}_{S1} + c_1\vec{k}_{S1} \end{aligned} \tag{3.43}$$

The acceleration of the same point in terms of the semitrailer motion variables is expressed as:

$$\vec{a}_c = (\dot{u}_{s2}+q_{s2}w_{s2}-r_{s2}v_{s2}+\dot{q}_{s2}z_{c2}-x_{c2}q_{s2}^2+p_{s2}r_{s2}z_{c2}-x_{c2}r_{s2}^2)\vec{i}_{s2}$$
$$+ (\dot{v}_{s2}+u_{s2}r_{s2}-p_{s2}w_{s2}-\dot{p}_{s2}z_{c2}+x_{c2}\dot{r}_{s2}+z_{c2}q_{s2}r_{s2}+x_{c2}q_{s2}p_{s2})\vec{j}_{s2}$$
$$+ (\dot{w}_{s2}+p_{s2}v_{s2}-q_{s2}u_{s2}-x_{c2}\dot{q}_{s2}-p_{s2}^2z_{c2}+x_{c2}r_{s2}p_{s2}-z_{c2}q_{s2}^2)\vec{k}_{s2}$$
$$= a_2\vec{i}_{s2} + b_2\vec{j}_{s2} + c_2\vec{k}_{s2} \qquad (3.44)$$

The tractor coordinate system is transformed to the semitrailer coordinate system, in order to equate the accelerations at the constraint point.

Referring to Equation (3.4), we note that:

$$\begin{Bmatrix}\vec{i}_n\\ \vec{j}_n\\ \vec{k}_n\end{Bmatrix} = [A_{ij}]_1\{\vec{i}_{s1},\ \vec{j}_{s1},\ \vec{k}_{s1}\}^T \qquad (3.45)$$

and

$$\begin{Bmatrix}\vec{i}_{s2}\\ \vec{j}_{s2}\\ \vec{k}_{s2}\end{Bmatrix} = [A_{ij}]_2^{-1}\{\vec{i}_n,\ \vec{j}_n,\ \vec{k}_n\}^T \qquad (3.46)$$

Upon eliminating the inertial axis system, $\{\vec{i}_n,\ \vec{j}_n,\ \vec{k}_n\}$ from (3.45) and (3.46), we get:

$$\begin{Bmatrix}\vec{i}_{s2}\\ \vec{j}_{s2}\\ \vec{k}_{s2}\end{Bmatrix} = [A_{ij}]_2^{-1}[A_{ij}]_1\{\vec{i}_{s1},\ \vec{j}_{s1},\ \vec{k}_{s1}\}^T = [T_{ij}]\{\vec{i}_{s1},\ \vec{j}_{s1},\ \vec{k}_{s1}\}^T \qquad (3.47)$$

Elements of the matrix $[T_{ij}]$, derived using the transformation matrices in Equations (3.5) and (3.7), are expressed as follows:

$$
\begin{aligned}
T_{11} &= \cos(\psi_{S2}-\psi_{S1}) + \theta_{S1}\theta_{S2} \\
T_{12} &= \sin(\psi_{S2}-\psi_{S1})\cos\phi_{S1} - \theta_{S2}\sin\phi_{S1} \\
&\quad + \sin\phi_{S1}\theta_{S1}\cos(\psi_{S2}-\psi_{S1}) \\
T_{13} &= -\sin(\psi_{S2}-\psi_{S1})\sin\phi_{S1} - \theta_{S2}\cos\phi_{S1} \\
&\quad + \cos\phi_{S1}\theta_{S1}\cos(\psi_{S2}-\psi_{S1}) \\
T_{21} &= -\cos\phi_{S2}\sin(\psi_{S2}-\psi_{S1}) - \theta_{S1}\sin\phi_{S2} \\
&\quad + \sin\phi_{S2}\theta_{S2}\cos(\psi_{S2}-\psi_{S1}) \\
T_{22} &= \cos\phi_{S1}\cos\phi_{S2}\cos(\psi_{S2}-\psi_{S1}) + \sin\phi_{S1}\sin\phi_{S2} \\
&\quad - \sin\phi_{S1}\theta_{S1}\cos\phi_{S2}\sin(\psi_{S2}-\psi_{S1}) \\
&\quad + \sin\phi_{S2}\theta_{S2}\cos\phi_{S1}\sin(\psi_{S2}-\psi_{S1}) \\
T_{23} &= -\sin\phi_{S1}\cos\phi_{S2}\cos(\psi_{S2}-\psi_{S1}) + \cos\phi_{S1}\sin\phi_{S2} \\
&\quad - \cos\phi_{S1}\cos\phi_{S2}\theta_{S1}\sin(\psi_{S2}-\psi_{S1}) \\
&\quad - \sin\phi_{S1}\sin\phi_{S2}\theta_{S2}\sin(\psi_{S2}-\psi_{S1}) \\
T_{31} &= \sin\phi_{S2}\sin(\psi_{S2}-\psi_{S1}) - \cos\phi_{S2}\theta_{S1} \\
&\quad + \cos\phi_{S2}\theta_{S2}\cos(\psi_{S2}-\psi_{S1}) \\
T_{32} &= -\cos\phi_{S1}\sin\phi_{S2}\cos(\psi_{S2}-\psi_{S1}) + \cos\phi_{S2}\sin\phi_{S1} \\
&\quad + \sin\phi_{S1}\sin\phi_{S2}\theta_{S1}\sin(\psi_{S2}-\psi_{S1}) \\
&\quad + \cos\phi_{S1}\cos\phi_{S2}\theta_{S2}\sin(\psi_{S2}-\psi_{S1}) \\
T_{33} &= \sin\phi_{S1}\sin\phi_{S2}\cos(\psi_{S2}-\psi_{S1}) + \cos\phi_{S1}\cos\phi_{S2} \\
&\quad + \cos\phi_{S1}\sin\phi_{S2}\theta_{S1}\sin(\psi_{S2}-\psi_{S1}) \\
&\quad - \sin\phi_{S1}\cos\phi_{S2}\theta_{S2}\sin(\psi_{S2}-\psi_{S1})
\end{aligned}
\tag{3.48}
$$

The constraint equations needed to evaluate the lateral and vertical constraint forces are thus derived as:

$$b_2\vec{j}_{S2} = (a_1T_{21}+b_1T_{22}+c_1T_{23})\vec{j}_{S2} \tag{3.49}$$

$$c_2\vec{k}_{S2} = (a_1T_{31}+b_1T_{32}+c_1T_{33})\vec{k}_{S2} \tag{3.50}$$

3.4.5.2 Roll and Pitch Moments due to a Fifth Wheel Connection

The roll moments due to the torsional compliance of the articulation mechanism are evaluated from the relative angular displacement between the sprung weights of the tractor and the semitrailer. The roll moment acting on the tractor, M_{X1}, is computed from the product of the constraint stiffness K_s and relative angular displacement resolved about the $\vec{i}_{S1}$ coordinate, as shown in Figure 3.3. The roll and pitch moments acting on the sprung weight of the semitrailer, M_{X2} and M_{Y2} respectively, are determined by the coordinate transformation:

$$M_{X1} = K_s\left[\phi_{S2}\cos(\psi_{S2}-\psi_{S1}) - \theta_{S2}\sin(\psi_{S2}-\psi_{S1}) - \phi_{S1}\right] \tag{3.51}$$

$$M_{X2} = -M_{X1}\left[\cos(\psi_{S2}-\psi_{S1}) + \theta_{S1}\theta_{S2}\right] \tag{3.52}$$

$$M_{Y2} = -M_{X1}\left[\theta_{S2}\cos(\psi_{S2}-\psi_{S1})\sin\phi_{S2} - \theta_{S1}\sin\phi_{S2} - \sin(\psi_{S2}-\psi_{S1})\cos\phi_{S2}\right] \tag{3.53}$$

3.4.6 Forces and Moments at the Tire-Road Interface

The measured tire data are used to compute the lateral forces and aligning moments generated at the tire-road interface. The sideslip angle and the vertical load acting on a tire are computed at every integration step, and the corresponding lateral forces and aligning moments are established from the tabulated tire data using linear interpolation. Expressions for the sideslip angle and the vertical load at the tire-road interface are derived in terms of the velocities and displacements of the sprung and unsprung masses.

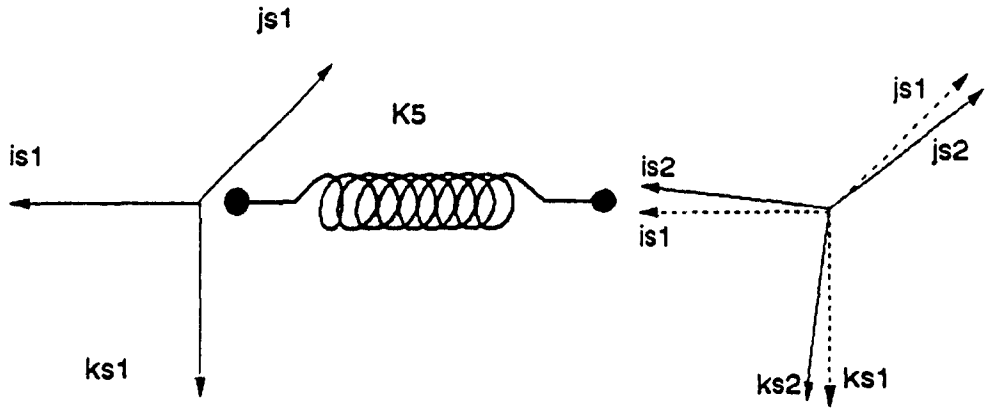

FIGURE 3.3: Representation of the Axes Systems at the Fifth Wheel Constraint

The sideslip angle at the tire-road interface is expressed in terms of the body-fixed velocities of the sprung masses and the axles. The sideslip angle of the tire j on axle i is expressed as:

$$\alpha_{ij} = \tan^{-1}\left(\frac{v_{axle_i}}{u_{tire_{ij}}}\right) - \delta_i; \quad i=1,\ldots,5 \text{ and } j=1,\ldots,4 \tag{3.54}$$

where:

$$\begin{aligned}
v_{axle_i} &= (v_s - z_{R1} p_s)_k \cos\phi_{Sk} + \frac{x_{U1} r_{Sk}}{\cos\phi_{Sk}} - p_{U1} HR_i \cos\phi_{U1} \\
u_{tire_{i1}} &= u_{Sk} + (T_i + A_i) r_{Sk} \\
u_{tire_{i2}} &= u_{Sk} + T_i r_{Sk} \\
u_{tire_{i3}} &= u_{Sk} - T_i r_{Sk} \\
u_{tire_{i4}} &= u_{Sk} - (T_i + A_i) r_{Sk}
\end{aligned} \tag{3.55}$$

and δ_1 is the front wheel steer angle and $\delta_i = 0$; $i = 2,\ldots,5$.

The vertical load acting on the tire j on axle i, F_{Zij} is computed from the linear compliance of the tire KT_{ij} and the vertical deflection Δ_{ij}:

$$F_{Zij} = KT_{ij}\Delta_{ij} \tag{3.56}$$

The vertical deflection of the tire is expressed in terms of the deflection of the sprung and unsprung masses. The deflection of the outer left tire on axle i is given by the equation:

$$\Delta_{i1} = \Delta_{oi} + \Delta z_{Sk} - z_{Ri}(1-\cos\phi_{Sk}) + z_{Ui}\cos\phi_{Ui} - z_{Uoi} - (T_i+A_i)\sin\phi_{Ui} - x_{Ui}\theta_{Sk} \quad (3.57)$$

where:

Δz_{Sk} = the vertical deflection of the center of gravity of sprung mass k along the inertial axis $\vec{k}_n$, $\Delta z_{Sk} = 0.0$ at time $t = 0.0$

z_{Uoi} = the vertical distance between the roll center and the axle center of gravity at time $t = 0.0$

Δ_{oi} = the static deflection of the tires.

The deflection of the other three tires on axle i are:

$$\begin{aligned} \Delta_{i2} &= \Delta_{i1} + A_i\sin\phi_{Ui} \\ \Delta_{i3} &= \Delta_{i2} + 2T_i\sin\phi_{Ui} \\ \Delta_{i4} &= \Delta_{i3} + A_i\sin\phi_{Ui} \end{aligned} \quad (3.58)$$

3.5 METHOD OF SOLUTION

The set of differential equations, (3.29) to (3.35) represent the equations of motion of a five-axle tractor-semitrailer vehicle subject to a directional maneuver at highway speeds. For a given steer maneuver, the lateral forces and aligning moments developed at the tire-road interface are computed using Equations (3.54) to (3.58) and the look-up tables. The spring forces and the constraint forces and moments are computed using the Equations (3.17) to (3.28) and (3.43) to (3.53), respectively. The equations of motion are then solved to

determine the directional response of the vehicle using numerical integration based upon a predictor-corrector method.

3.6 VEHICLE PARAMETERS

The parameters of the simulation vehicle, such as vehicle dimensions, inertial properties and axles loads, are given in Table 3.1. The nonlinear force-deflection properties of various vehicle suspension used in the simulation have been presented in Chapter 2. The cornering properties of the tires are shown in Figure 3.4, as function of the normal load and the sideslip angle. The dynamic roll stability of the vehicle combination is investigated for typical lane change and evasive maneuvers executed at typical highway speed of 100 km/h. The trajectories of the lane change and evasive maneuvers are presented in Figures 3.5 and 3.6, respectively.

3.7 DIRECTIONAL STABILITY OF ARTICULATED VEHICLE COMBINATION

The yaw-roll vehicle model contains comprehensive description of suspension and tire properties, the directional dynamics and stability characteristics of the vehicle can thus be predicted quite accurately. The yaw-roll analysis program has been extensively validated by UMTRI [1]. The directional dynamics of the vehicle combination is investigated for typical lane change and evasive maneuvers to determine the response parameters that can describe the onset of dynamic roll instability.

Lift-off of tires at the rearmost axles is often considered as the first noticeable phenomenon prior to vehicle rollover. Since tire loads are very intricate to measure, a measure of dynamic suspension loads is

TABLE 3.1
SIMULATION VEHICLE PARAMETERS

	Tractor	Semitrailer	
Sprung Weight (kN)	45.40	251.80	
Roll Mass Moment of Inertia ($kg \cdot m^2$)	2900	25000	
Pitch Mass Moment of Inertia ($kg \cdot m^2$)	19200	679000	
Yaw Mass Moment of Inertia ($kg \cdot m^2$)	19200	679000	
Center of Gravity Height (m)	1.11	1.52, 1.78, 2.03	
	Axle 1	Axle 2	Axle 3
Axle Load (kN)	53.30	71.20	71.20
Longitudinal Position from C.G. (m)*	1.4	-2.8	-4.0
Axle Center of Gravity Height (m)	0.5	0.5	0.5
Dual Tire Spacing (m)	0.0	0.33	0.33
		Axle 4	Axle 5
Axle Load (kN)		71.20	71.20
Longitudinal Position from C.G. (m)		-5.33	-6.55
Axle Center of Gravity Height (m)		0.5	0.5
Dual Tire Spacing (m)		0.33	0.33
Fifth Wheel			
Longitudinal Position from Tractor C.G. (m)			3.0
Longitudinal Position from Semitrailer C.G. (m)			-6.6
Roll Stiffness (kN·m/deg)			1130
Tires			
Vertical Stiffness (kN/m)			788
Aligning Torque (N·m/deg)			148

* Longitudinal location of axles located behind the center of gravity is specified by negative distance

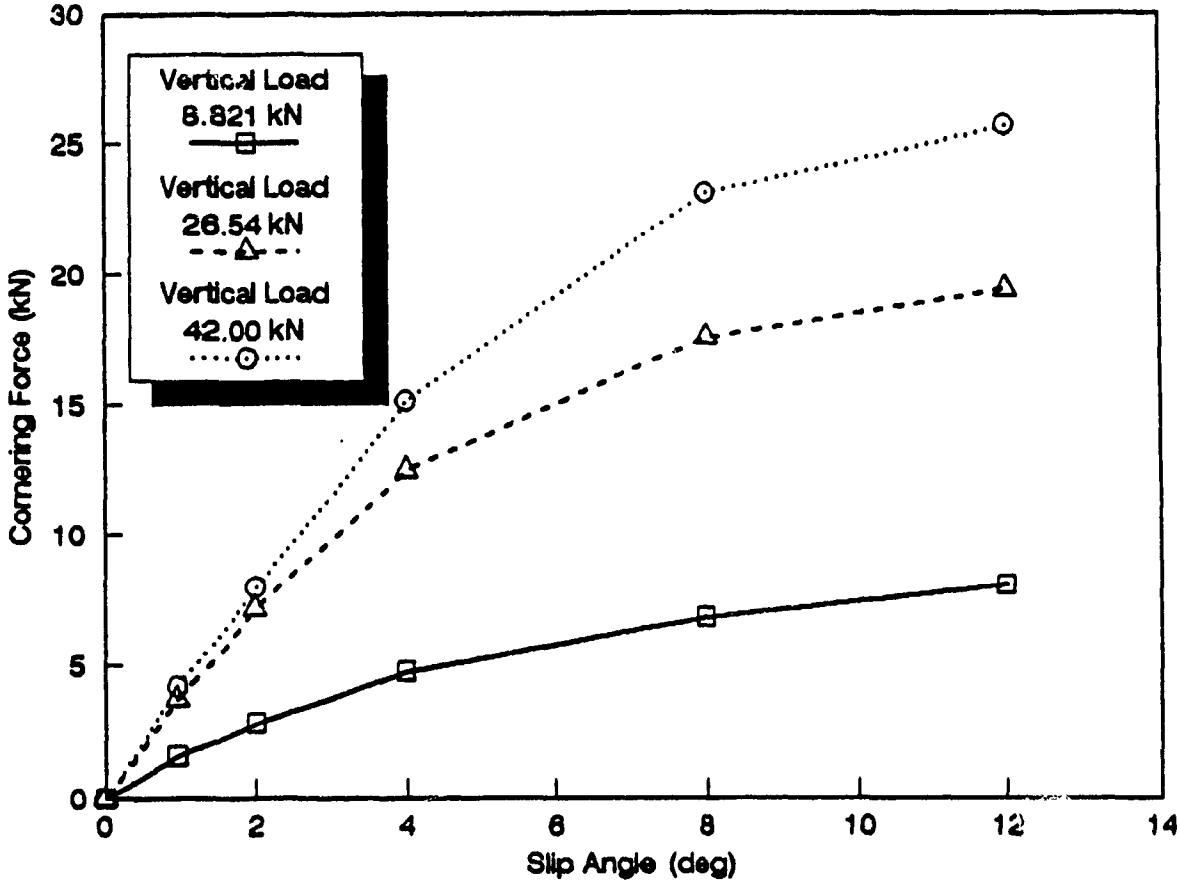

FIGURE 3.4: Cornering Properties of Michelin XZA Radial Tires

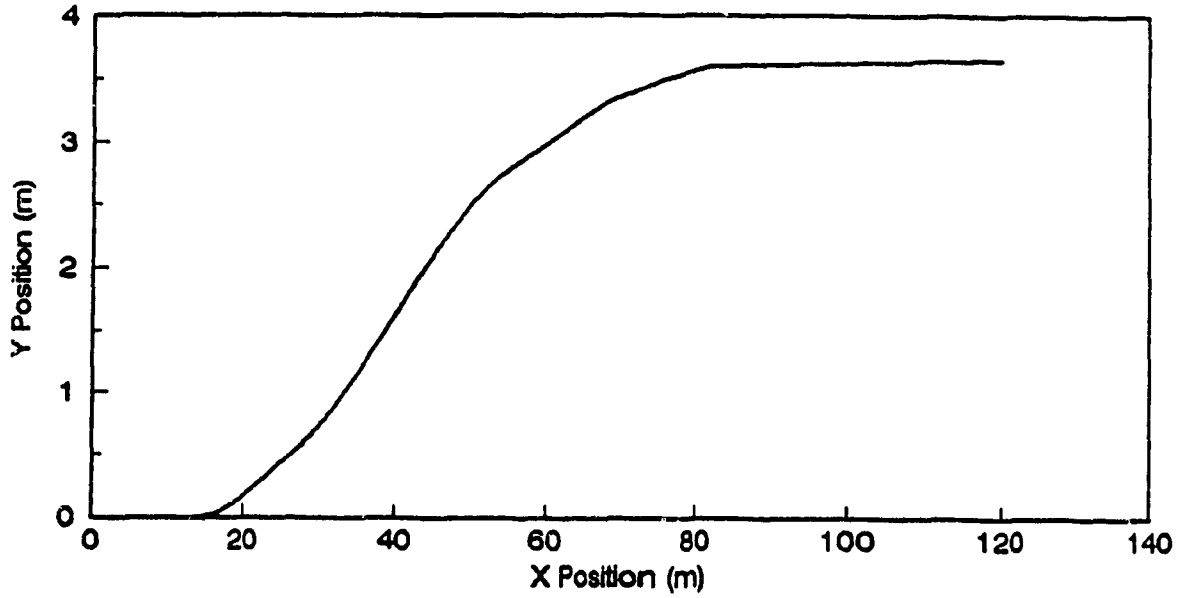

FIGURE 3.5: Trajectory of the Vehicle During a Typical Lane Change Maneuver

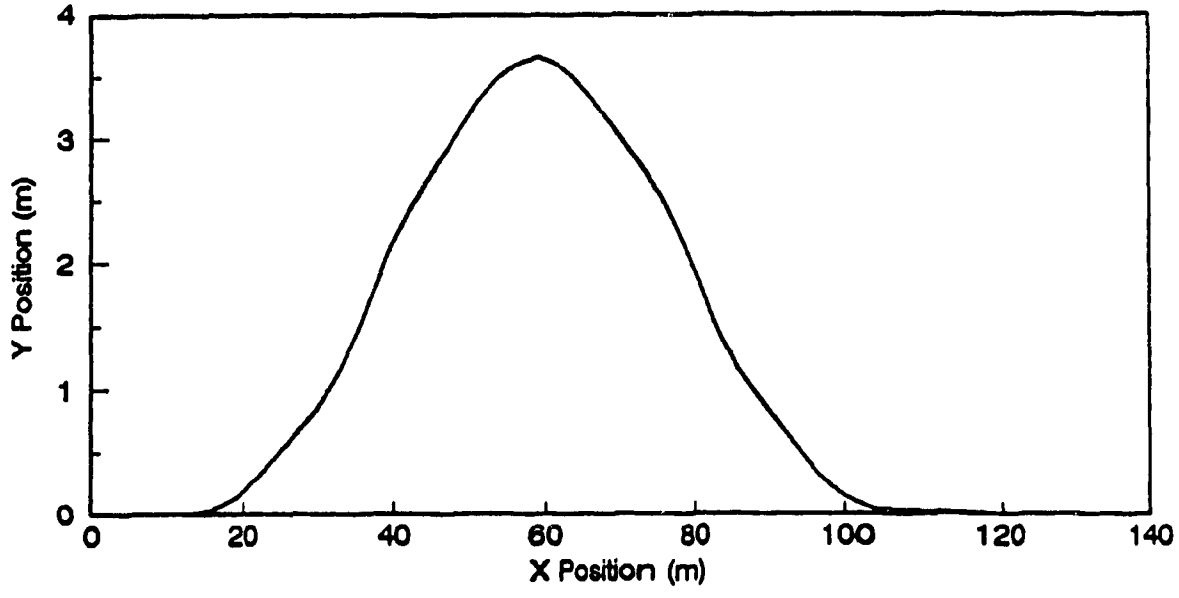

FIGURE 3.6: Trajectory of the Vehicle During a Typical Evasive Maneuver

considered to detect the onset of tire lift-off and thus the vehicle rollover. The directional response of the vehicle subject to an evasive maneuver is investigated to determine the relationship between the dynamic suspension forces and the wheel loads. Computer simulations are carried out for different types of suspension at the semitrailer axles, and the center of gravity of the semitrailer is selected as 2.03 meters.

The dynamic wheel and suspension loads are expressed in terms of dynamic wheel load ratio (ratio of the vertical load to the static load on tires) and dynamic spring force ratio (ratio of dynamic spring force to the static suspension force), respectively. The dynamic wheel and spring ratio response characteristics of the semitrailer axles, equipped with a leaf-spring suspension (Reyco 21B) are presented in Figure 3.7, for an evasive maneuver. The wheel load and spring force ratio response of the trailing axle is quite similar to that of the leading axle, as shown in Figure 3.7. The dynamic wheel load ratio increases during the initial steering maneuver and approaches a peak value of approximately 1.75. The dynamic wheel load ratio decreases when the steering direction is reversed as shown in Figure 3.7. The dynamic wheel load ratio approaches zero around t = 2.85 s indicating a wheel lift-off and thus the vehicle rollover.

The dynamic suspension force ratio increases in a manner similar to the wheel load ratio during the initial steering maneuver. The dynamic suspension force ratio approaches a peak value of approximately 2.0 and then decreases as the steering direction is reversed. The suspension force begins to increase after a wheel lift-off is encountered as shown in Figure 3.7. The dynamic spring force ratio approaches a negative

value corresponding to the wheel lift-off, indicating that the springs on one side of the axle are under tension. Thus the negative suspension force ratio may be considered as an indicator of wheel lift-off and the impending vehicle rollover.

This indicator of wheel lift-off is further investigated for different types of semitrailer axle suspension. Figure 3.8 presents the dynamic wheel and suspension force ratio response of the semitrailer axles, equipped with an air-spring suspension (Neway AR95.17 16K). The dynamic wheel load ratio approaches zero near t = 2.7 s indicating the vehicle rollover. The suspension force ratio, corresponding to wheel lift-off, however remains positive ($\cong$ 0.55). Since the air springs are precharged and usually do not go into tension, the variations in dynamic spring force of the air suspension are quite different than those in the leaf-spring type suspension. A measure of suspension loads thus does not provide a reliable indication of the wheel lift-off and thus the onset of vehicle rollover.

Alternatively, the detection of tire lift-off is attempted via measuring the axle roll angle. Owing to the dynamic load transfer, the lift-off of tires on the inside of the turn occurs at a certain roll angle of the axles. The relationship between the tire lift-off and axle roll angle is investigated via computer simulation. Figures 3.9 to 3.12 present the dynamic wheel load ratio and the roll angle response of the leading and trailing semitrailer axles for typical lane change and evasive maneuvers. These figures clearly demonstrate that the dynamic load ratio and thus the tire lift-off can be directly related to the axle's roll angle. Since the axle roll angle can be directly measured

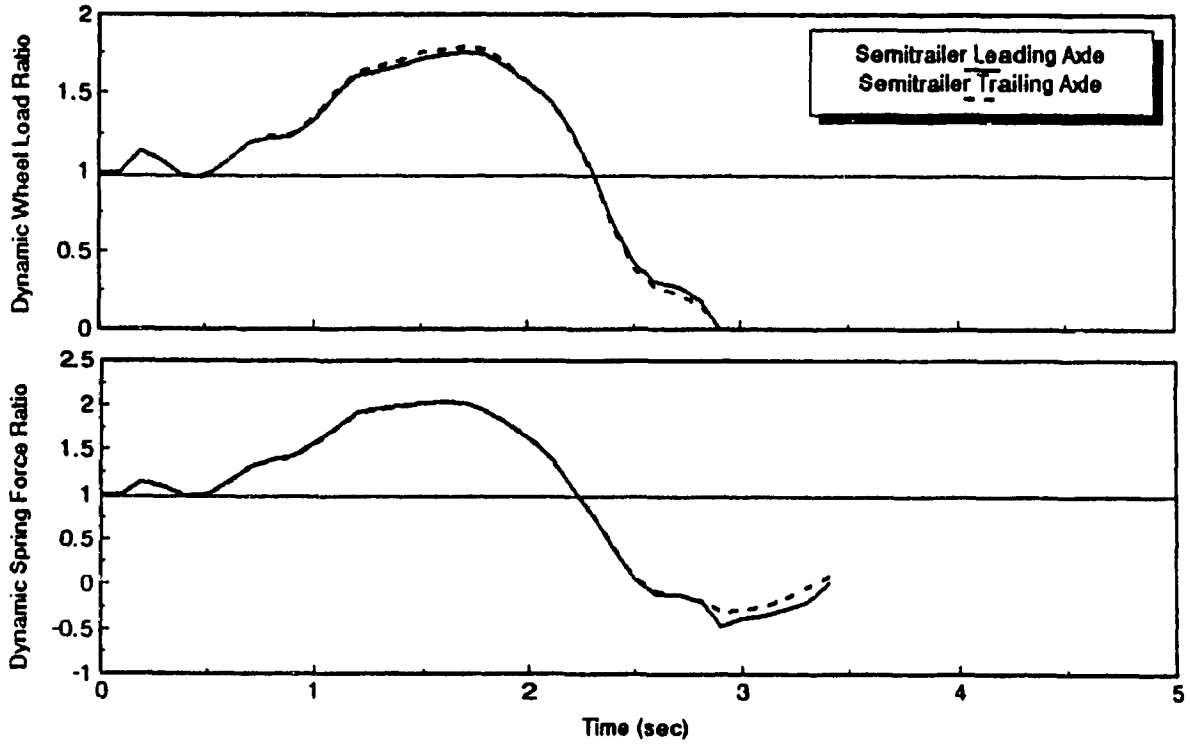

FIGURE 3.7: Dynamic Response of the Semitrailer Axles with Leaf-Spring Suspension

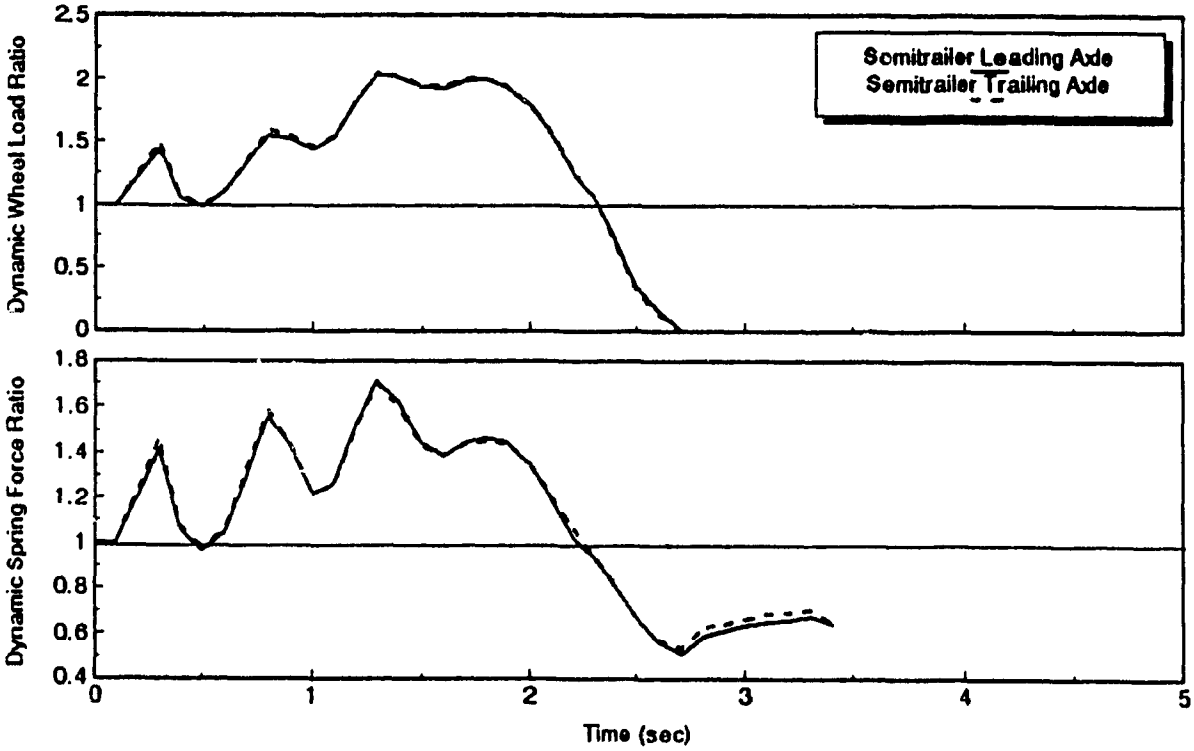

FIGURE 3.8: Dynamic Response of the Semitrailer Axles with Air-Spring Suspension

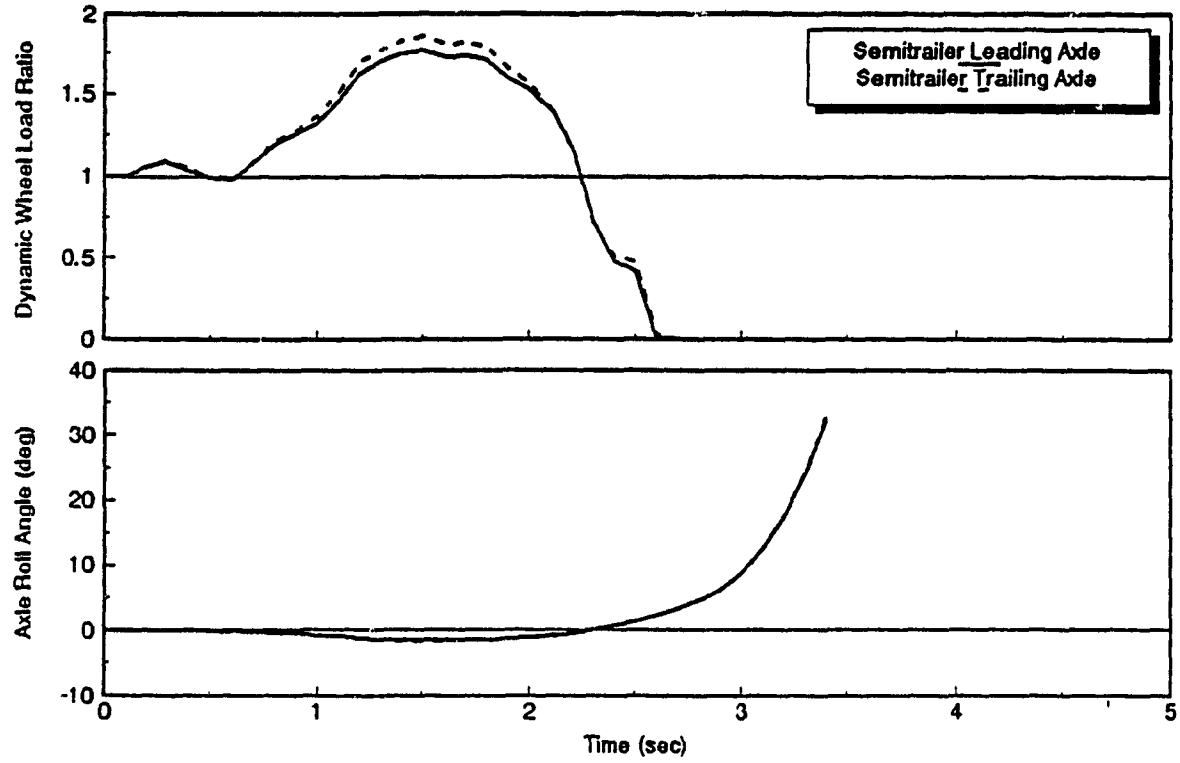

FIGURE 3.9: Dynamic Wheel Load Ratio ($F_{dyn.}/F_{sta.}$) and Axle Roll Angle of the Semitrailer Axles for an Evasive Maneuver. (Vehicle Width = 2.44 m, Center of Gravity Height = 2.03 m)

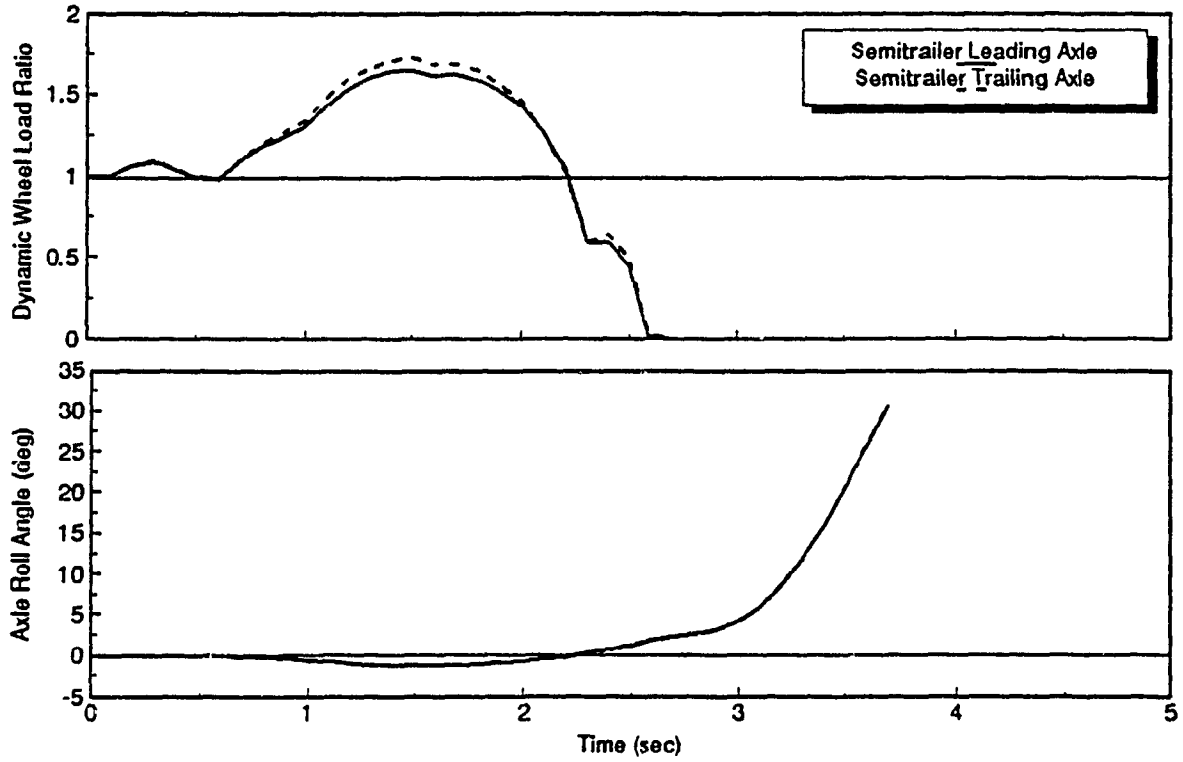

FIGURE 3.10: Dynamic Wheel Load Ratio ($F_{dyn.}/F_{sta.}$) and Axle Roll Angle of the Semitrailer Axles for an Evasive Maneuver. (Vehicle Width = 2.59 m, Center of Gravity Height = 2.03 m)

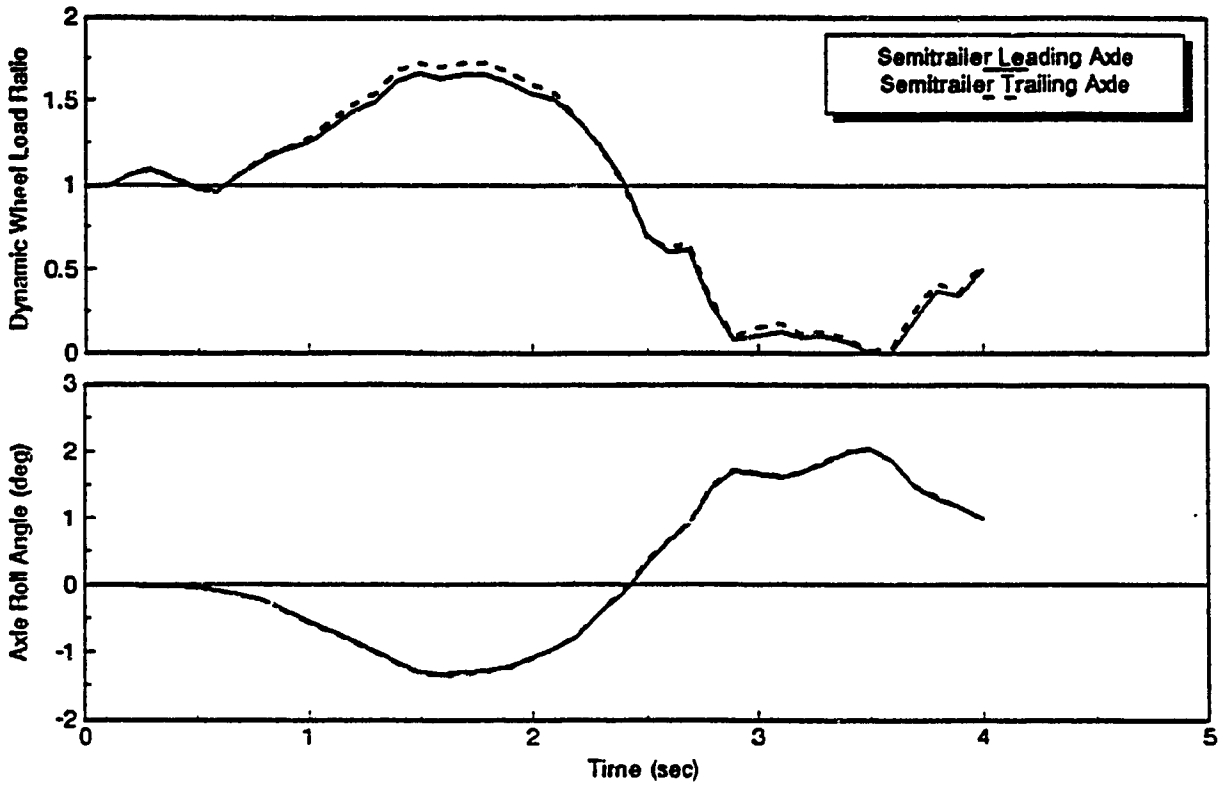

FIGURE 3.11: Dynamic Wheel Load Ratio ($F_{dyn.}/F_{sta.}$) and Axle Roll Angle of the Semitrailer Axles for an Evasive Maneuver. (Vehicle Width = 2.44 m, Center of Gravity Height = 1.52 m)

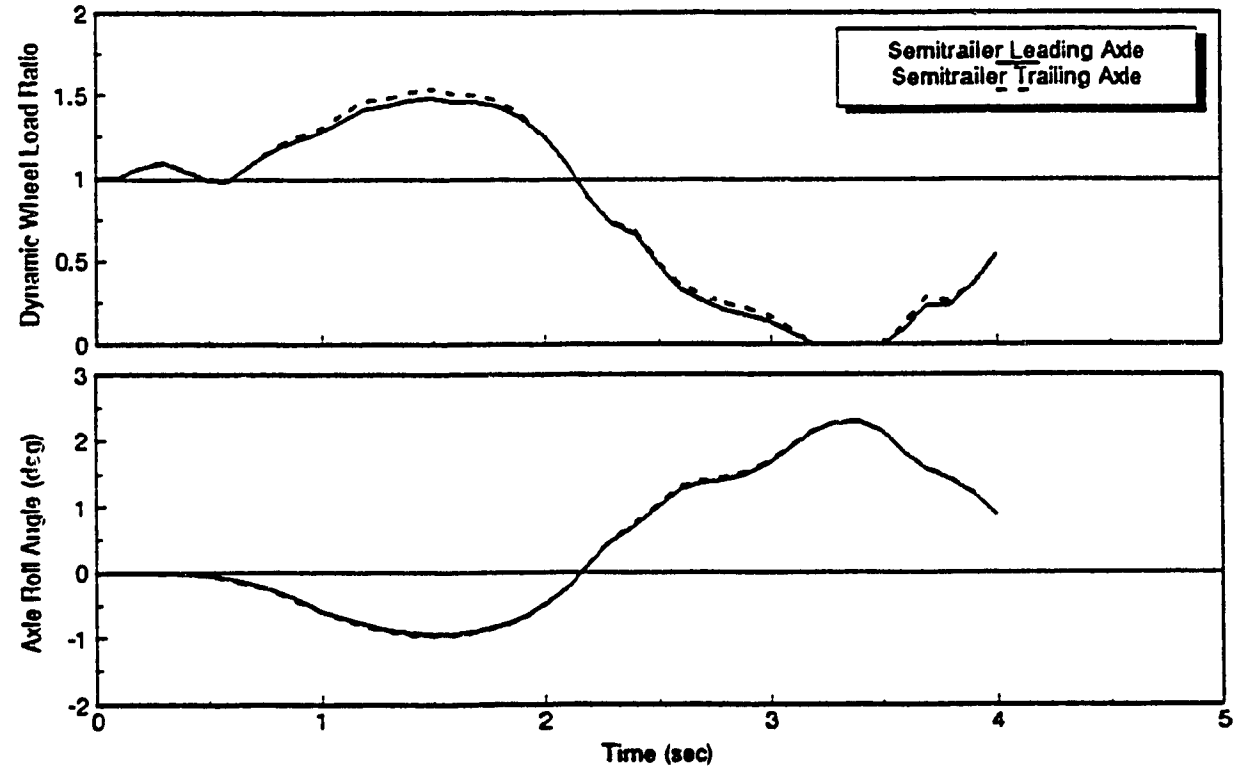

FIGURE 3.12: Dynamic Wheel Load Ratio ($F_{dyn.}/F_{sta.}$) and Axle Roll Angle of the Semitrailer Axles for a Lane Change Maneuver. (Vehicle Width = 2.44 m, center of gravity height = 2.03 m)

during the vehicle operation, the detection of onset of vehicle roll instability via axle roll angle merits further investigations.

The semitrailer's wheel load ratio and axle roll angle response characteristics are evaluated for various values of center of gravity height (1.52 meter and 2.03 meters) when the vehicle is subject to an evasive maneuver, as shown in Figures 3.9, 3.10 and 3.11. Figures 3.9 and 3.10 present the dynamic wheel load ratio and roll angle response characteristics of the semitrailer's axles of 2.44- and 2.59-meter wide vehicles for a constant value of center of gravity height (2.03 meters). Figures 3.9 and 3.10 clearly demonstrate that as the dynamic load ratio approaches zero the axle roll angle grows rapidly leading to vehicle rollover. However, it is also possible that the tires which experience a lift-off during the initial steering input may return to the road under the corrective steering action, as demonstrated in Figure 3.11. The dynamic wheel load ratio approaches zero, indicating the wheel lift-off at $t \cong 3.6$ s, and then continues to increase indicating that the wheel has returned to the road. The axle roll angle response also demonstrates the stable characteristics of the vehicle, as shown in Figure 3.11. In this case, the vehicle is considered to be marginally stable. The vehicle's response to a lane change maneuver, also reveals similar phenomenon as shown in Figure 3.12. The tires on the outside of the turn carry the entire axle load momentarily and the corresponding cornering forces generated at the tire-road interface are considerably small. The vehicle may experience rollover in the presence of an external sideways disturbance of extremely low magnitude. Thus in order to ensure an early warning of the impending rollover, it is vital to

consider the wheel lift-off, even though the vehicle may be marginally stable.

Figures 3.13 to 3.16 show the peak axle roll angles corresponding to the onset of wheel lift-off. The onset of wheel lift-off is assumed when the dynamic vertical load on a tire is less than one percent than its static load. The peak roll angle and the dynamic wheel load ratio response characteristics of the semitrailer axles are evaluated for various suspension configurations. The response characteristics are evaluated for lane change and evasive maneuvers executed at 100 km/h, the maximum legal speed on highways. All the vehicle configurations with a semitrailer's center of gravity height at 2.03 meters, considered in the study, experience rollover when subject to an evasive maneuver, as shown in Figure 3.13. The peak roll angles experienced at the semitrailer trailing axle before wheel lift-off range from 1.55 to 2.34 degrees.

During a lane change maneuver, only three of the vehicle configurations exhibit rollover, as shown in Figure 3.14. However, a wheel lift-off is encountered in the remaining vehicle configurations. The peak roll angles experienced at the semitrailer trailing axle before wheel lift-off range from 1.83 to 2.05 degrees. It can be also noticed that the combinations that rolled over used a relatively softer Mack SS38C suspension on the rear tractor axles.

The directional response characteristics of the vehicle are further investigated for different values of semitrailer's center of gravity height. Figure 3.15 shows the peak axle roll angle response of the semitrailer axle when the vehicle is subject to an evasive maneuver. The height of the center of gravity of the semitrailer is selected as

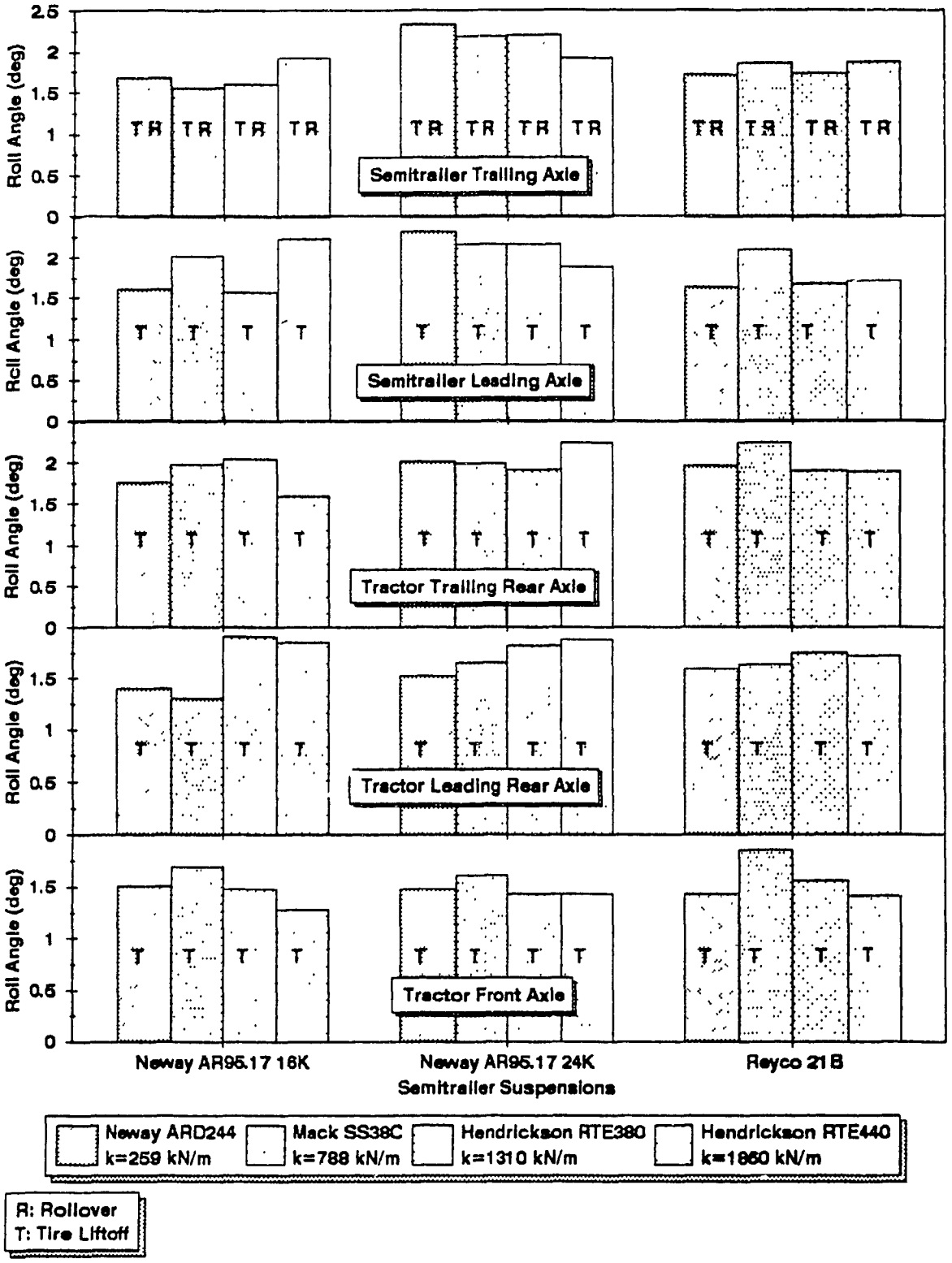

FIGURE 3.13: Axle Roll Angles for 2.44-Meter Wide Vehicles with a Semitrailer Center of Gravity Height of 2.03 Meters for Different Tractor Rear Suspensions and Semitrailer Suspensions During an Evasive Maneuver.

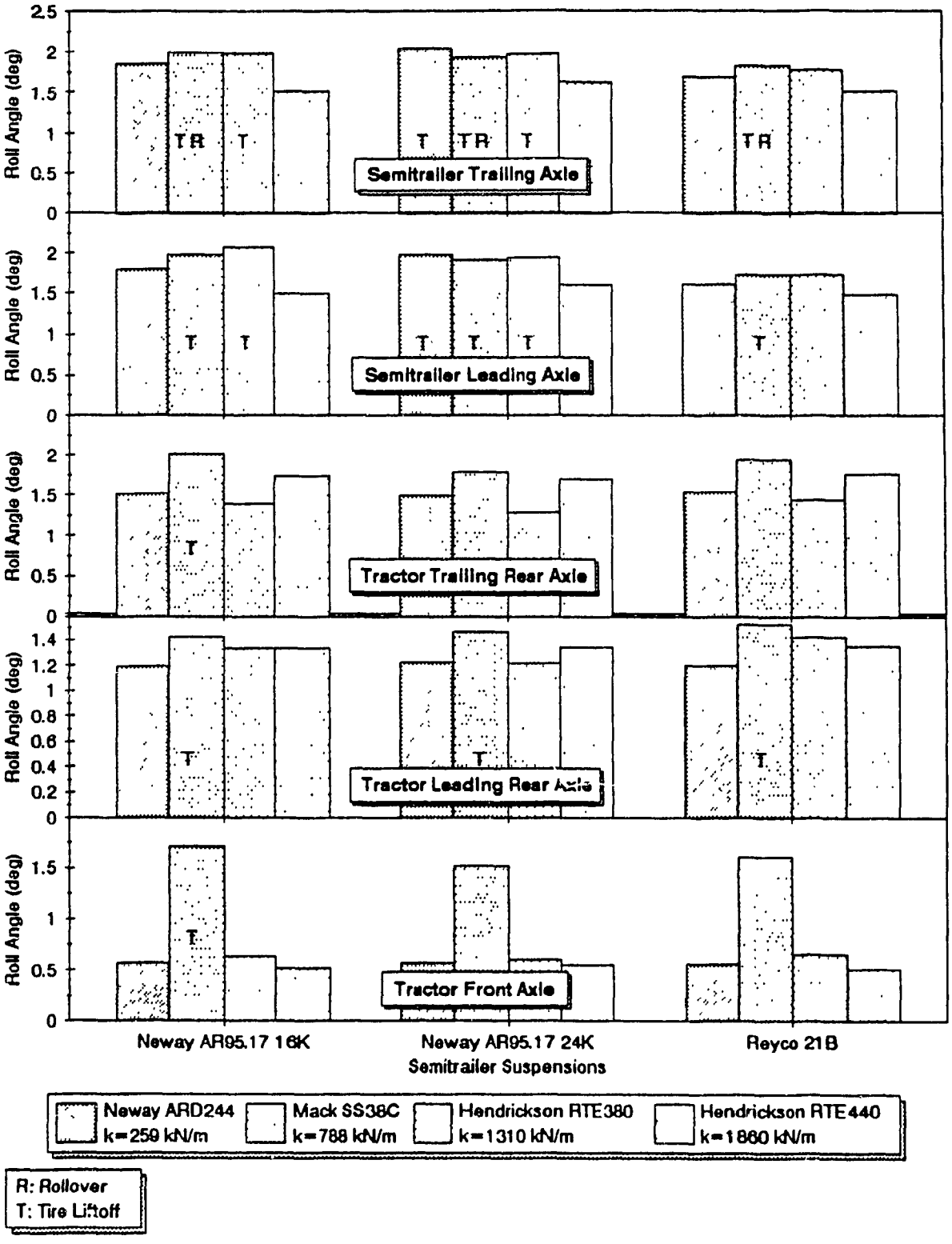

FIGURE 3.14: Axle Roll Angles for 2.44-Meter Wide Vehicles with a Semitrailer Center of Gravity Height of 2.03 Meters for Different Tractor Rear Suspensions and Semitrailer Suspensions During a Lane Change Maneuver.

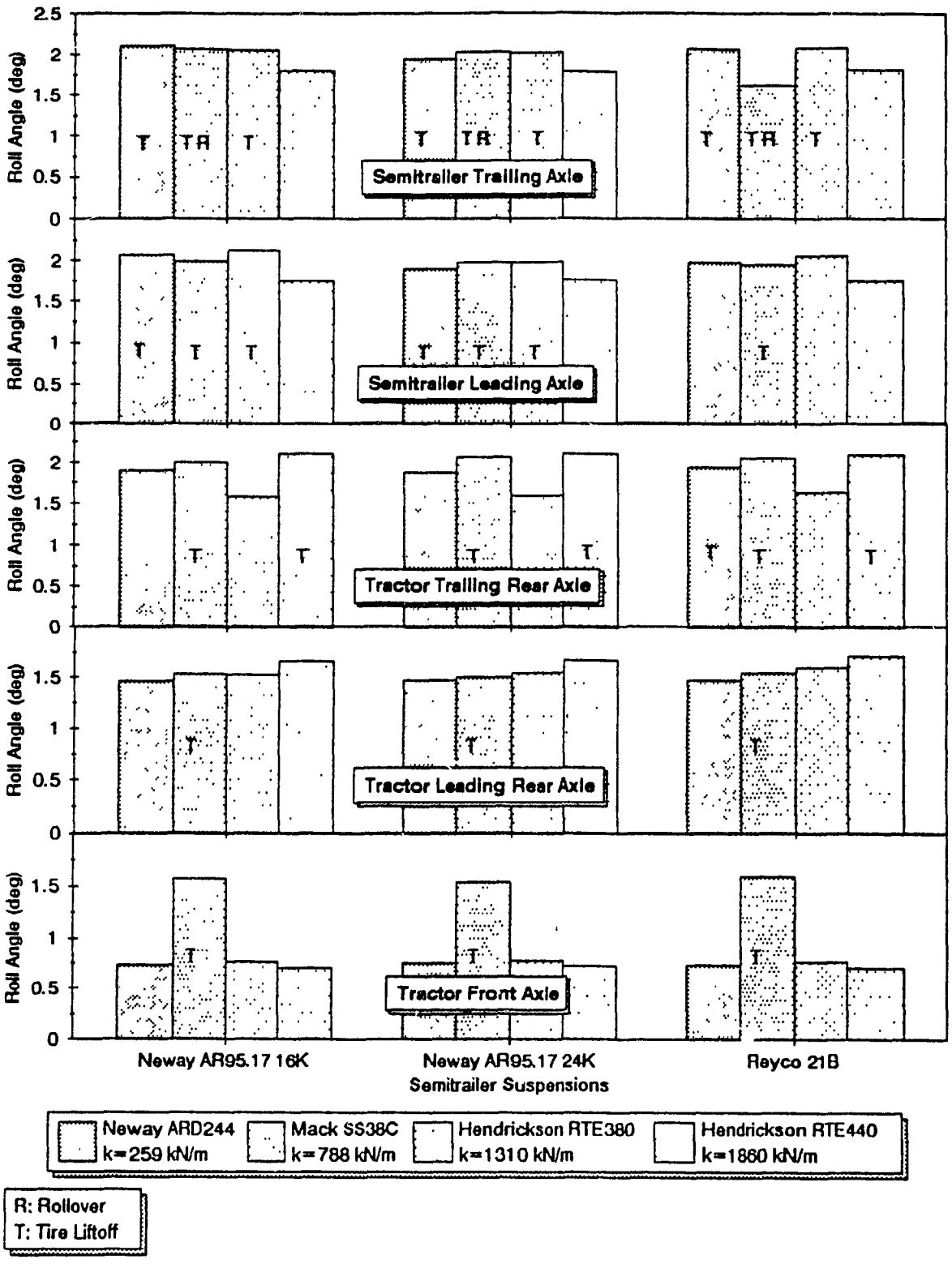

FIGURE 3.15: Axle Roll Angles for 2.44-Meter Wide Vehicles with a Semitrailer Center of Gravity Height of 1.52 Meter for Different Tractor Rear Suspensions and Semitrailer Suspensions During an Evasive Maneuver.

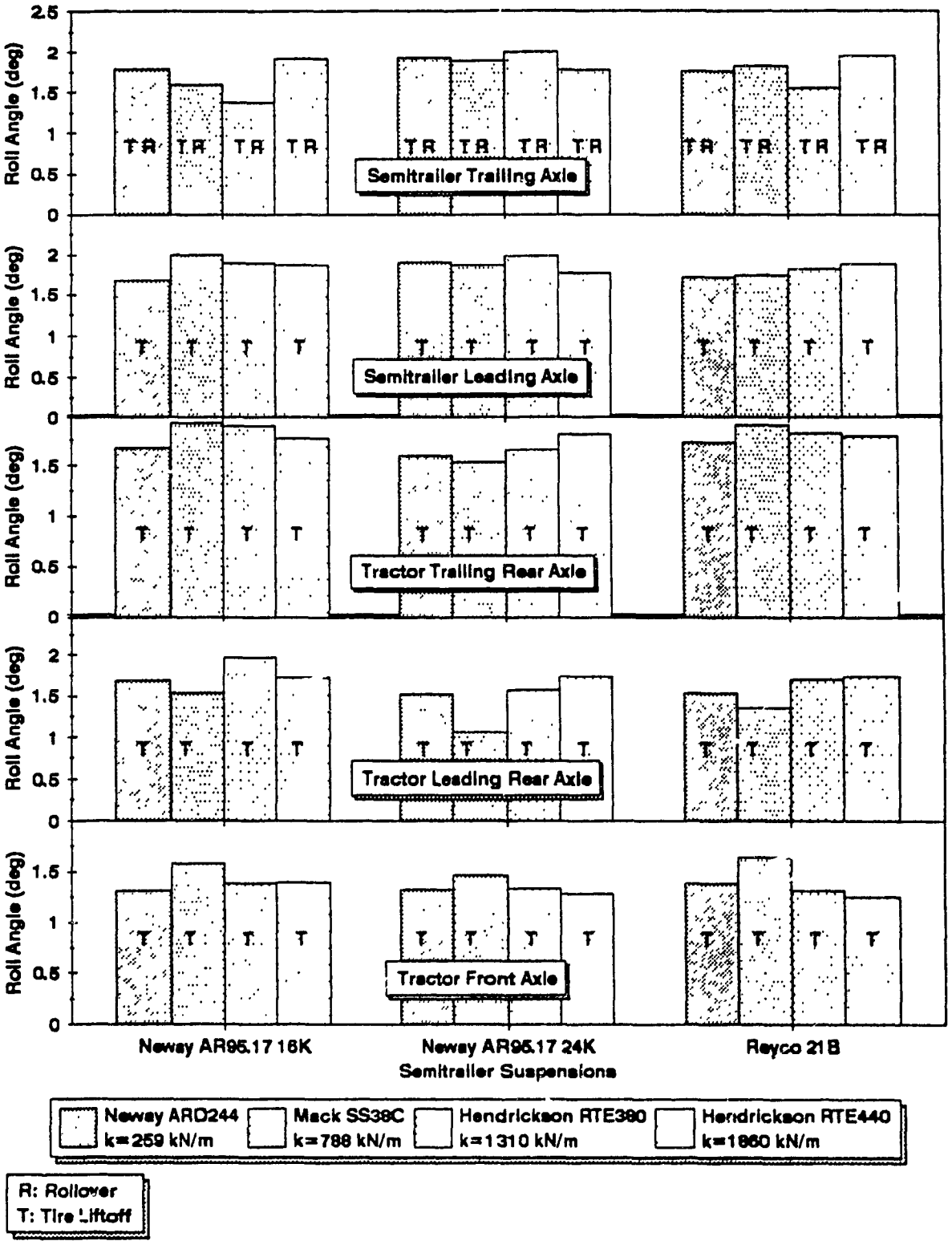

FIGURE 3.16: Axle Roll Angles for 2.59-Meter Wide Vehicles with a Semitrailer Center of Gravity Height of 2.03 Meters for Different Tractor Rear Suspensions and Semitrailer Suspensions During an Evasive Maneuver

1.52 meter. In this case also, only three vehicle configurations equipped with Mack SS38C suspension exhibit rollover. The range of roll angles of the semitrailer trailing axle at wheel lift-off is obtained as 1.62 to 2.11 degrees.

The dynamic stability of a heavy vehicle is strongly influenced by the effective track width and suspension spread. The directional dynamics of the vehicle is thus further investigated for 2.59-meter wide vehicle. The center of gravity of the semitrailer's sprung weight is selected as 2.03 meters. Peak roll angle response of semitrailer's trailing axle is presented in Figure 3.16 for an evasive maneuver. All the vehicle configurations, considered in the study, exhibit vehicle rollover and peak axle roll angle ranges from 1.38 to 2.01 degrees. Low values of the peak roll angle are attributed to increased tire track width.

Computer simulation results reveal that the semitrailer trailing axle roll angle can describe the onset of wheel lift-off most efficiently. Moreover, the axle roll angle can be directly measured during the vehicle operation. The lowest roll angles of the semitrailer trailing axles are obtained as 1.55 degrees and 1.38 degrees for the 2.44- and the 2.59-meter wide vehicles, respectively. Applying a factor of safety of 1.1, safe values of axle roll angles before wheel lift-off can be attained. These safe values are 1.41 degrees for the 2.44-meter wide vehicle and 1.26 degrees for the 2.59-meter wide vehicle.

3.8 SUMMARY

A yaw-roll plane model of the articulated vehicle combination is developed to investigate the dynamic roll stability during highway

maneuvers. The onset of roll instability during highway maneuvers is described via the tire lift-off of the semitrailer trailing axle. The sensitivity of the lift-off of the tires on the semitrailer axles to variations in vehicle design parameters is investigated to determine a feasible parameter that can directly describe the onset of roll instability during highway maneuvers. Through computer simulations, it is shown that the unsprung mass roll angle response can best describe the onset of dynamic roll instability.

CHAPTER 4

STABILITY ANALYSIS DURING BRAKING AND STEERING MANEUVERS

4.1 GENERAL

Articulated vehicles exhibit jackknife and trailer swing under simultaneous application of severe braking and steering. Tractor jackknife is a mode of instability in which the ratio of the tractor yaw angle to the semitrailer yaw angle approaches a large value. This phenomenon is usually initiated when the tires on the tractor rear axles skid. Compared with other modes of instability, the tractor jackknife is the most dangerous, most rapid and least controllable by the driver. Thus an early warning on the impending jackknife offers considerable potentials to minimize the number of accidents involving such vehicles. However, the jackknife instability needs to be defined in a quantitative manner in order to construct an early warning algorithm.

Although antilock braking systems detect the onset of wheel lockup via vehicle and wheel speed sensors, however the detection of wheel lockup is not early enough to warn the driver of impending instability [13]. Vehicle jackknife can also be caused by excessive engine torque developed during gearing down or driving on an icy surface and since the antilock braking system operates from the air brake systems it will not prevent such a power jackknife [16]. Consequently, alternate directly measurable vehicle response parameters are sought to quantitatively describe the onset of jackknife instability.

4.2 THE PHASE IV MODEL

The three dimensional vehicle model, developed by UMTRI (University of Michigan Transportation Research Institute) [67] to simulate the braking and steering dynamics of freight vehicles, is used to investigate the jackknife instability arising in a tractor-semitrailer vehicle combination. The software package, referred to as *Phase IV Model*, is written in a generalized fashion to permit simulation of various vehicle combinations. The vehicle chosen for this study is a five-axle tractor-semitrailer comprising of a three-axle tractor and a two-axle semitrailer. The tractor consists of a single front axle with single tires that can be arbitrarily steered. All other axles on the tractor-semitrailer combination are represented as tandem axles with dual wheel sets.

The Phase IV software can simulate vehicle combinations up to 71 degrees-of-freedom. The total number of degrees-of-freedom is dependent upon the vehicle configuration. The tractor-semitrailer vehicle is modeled as a 29 degrees-of-freedom system, derived from the following:

- Six degrees-of-freedom (three translational and three rotational) associated with the sprung mass of the tractor.
- Three degrees-of-freedom for the semitrailer (the three other degrees-of-freedom of the semitrailer are effectively eliminated by dynamic constraints at the hitch).
- Two degrees-of-freedom (vertical and roll) for each of the five axles.
- A rotational degree-of-freedom for each of the ten wheel sets.

The motion of each of the sprung masses is determined from the summation of forces and moments arising from the tires (acting through the unsprung mass of the axle and suspension), suspension, gravity and the hitch point constraints. The vehicle model incorporates dynamics of the air brake and antilock wheel control systems, and comprehensive tire-road friction models. The vehicle model can be used to evaluate the stopping distance performance, effects of brake timing, dynamic behavior in braking, antilock wheel control logic, tire-road friction coupling, performance on split friction surfaces, brake proportioning and tandem axle effects on braking limits. The nonlinear lateral force-sideslip characteristics of the tires along with roll-off effects during combined braking and steering are also incorporated in the vehicle model. A closed path follower model, employing the driver view time and lag time, is also integrated in the model in order to simulate for closed-loop directional maneuvers.

The Phase IV model is uniquely applicable to investigation of the directional response of vehicle combinations where the influence of the following items are to be considered in detail [2].

1) Spring force-deflection characteristics (hysteresis and backlash)
2) Brake fade - brake temperature
3) Brake hysteresis
4) Load-leveler action in tandem suspensions
5) Brake proportioning algorithms
6) Steering system compliance
7) Torsional stiffness of the frame

4.3 MAJOR ASSUMPTIONS

Small angle assumptions are made in the process of development of equations of motion, thus the simulation software is applicable up to the maneuver limits at which a wheel lift-off is encountered. The other major assumptions are as follow:

1) The sprung and unsprung masses are assumed to move as one rigid body in yaw, however the sprung and unsprung masses experience independent roll motions.
2) The unsprung mass acceleration is assumed to be a function of the total vehicle acceleration.
3) The height of the fifth wheel is assumed to be at the same height as the roll center.

The Phase IV program has been validated via field tests conducted by Ervin and Yoram [1]. El-Gindy and Wong [68] compared the simulation results of Phase IV with those obtained from its predecessors (yaw-roll, TBS, linear yaw plane) and concluded that the Phase IV package is capable of predicting the vehicle performance quite accurately. In this study, the Phase IV model was employed in a limited capacity. The one special application involved evaluation of the dynamics associated with the tractor jackknife during braking-in-a-turn maneuver. The repetitive computer simulations were carried out with various braking arrangements, braking torques and steer angles to arrive at a set of directly measurable parameters that can describe the onset of vehicle jackknife.

4.4 EQUATIONS OF MOTION

The equations of motion of the complex vehicle system are conveniently described via the dynamics of several subsystems and their interconnections. The dynamics of these subsystems are described in orthogonal coordinate systems discussed in the following subsection.

4.4.1 The coordinate systems

In order to interpret the vehicle motion, it is necessary to define the coordinate systems used. Two coordinate systems are necessary to describe the motion of the vehicle combinations: an inertial axis system and a body fixed coordinate system, as shown in Figure 3.1.

The inertial coordinate system $(\vec{i}_n, \vec{j}_n, \vec{k}_n)$, a right-hand orthogonal system fixed in space, is used as a reference point from which vehicle motions and attitudes are defined. The origin is placed at the tractor sprung mass center of gravity at the beginning of the simulation. The inertial coordinate system is aligned with the gravity vector and the horizontal projection of the tractor longitudinal axis. The body fixed coordinate system $(\vec{i}_s, \vec{j}_s, \vec{k}_s)_k$ defines the vehicle location and attitude. Its origin is placed at the sprung mass center of gravity, as shown in Figure 3.1.

The transformation equation between the inertial and sprung mass axis systems can be derived using the three sequential steps of rotation presented in Chapter 3.

4.4.2 Equations of Motion of the Sprung Masses

Application of Newton's law of motion yields six equations for each of the sprung masses. The equations of translational motion of the

sprung masses are derived in the following general form:

$$m_{Sk}(\dot{u}_s - v_s r_s + w_s q_s)_k = \Sigma F_x \tag{4.1}$$

$$m_{Sk}(\dot{v}_s + u_s r_s - w_s p_s)_k = \Sigma F_y \tag{4.2}$$

$$m_{sk}(\dot{w}_s - u_s q_s + v_s p_s)_k = \Sigma F_z \tag{4.3}$$

where m_{Sk} is the sprung mass k, u_s, v_s, and w_s are the translational velocities along the body fixed coordinates $\vec{i}_{Sk}$, $\vec{j}_{Sk}$ and $\vec{k}_{Sk}$, respectively. p_s, q_s and r_s are the roll, pitch and yaw rates of the sprung mass. F_x, F_y and F_z are the $\vec{i}_{Sk}$, $\vec{j}_{Sk}$ and $\vec{k}_{Sk}$ components respectively of the forces acting on the sprung mass. The equations of rotational motion of the sprung mass are expressed in the following general form:

$$I_{XXSk}\dot{p}_{Sk} + q_{Sk}r_{Sk}(I_{ZZSk} - I_{YYSk}) = \Sigma M_x \tag{4.4}$$

$$I_{YYSk}\dot{q}_{Sk} + p_{Sk}r_{Sk}(I_{XXSk} - I_{ZZSk}) = \Sigma M_y \tag{4.5}$$

$$I_{ZZSk}\dot{r}_{Sk} + p_{Sk}q_{Sk}(I_{YYSk} - I_{XXSk}) = \Sigma M_z \tag{4.6}$$

where I_{XXSk}, I_{YYSk} and I_{ZZSk} are the mass moment of inertia of sprung mass k about the body fixed axis system. M_x, M_y and M_z are the moments acting on the sprung mass, rotated about the body fixed axis system.

The forces acting on the sprung masses include the forces due to suspension, tires, roll centers, gravity and fifth wheel constraint. The nonlinear force-deflection characteristics of typical suspension springs, shown in Figure 4.1, are linearized about the operating point, using a look-up table. The forces due to suspension springs on a single axle are evaluated as function of the suspension deflection and the

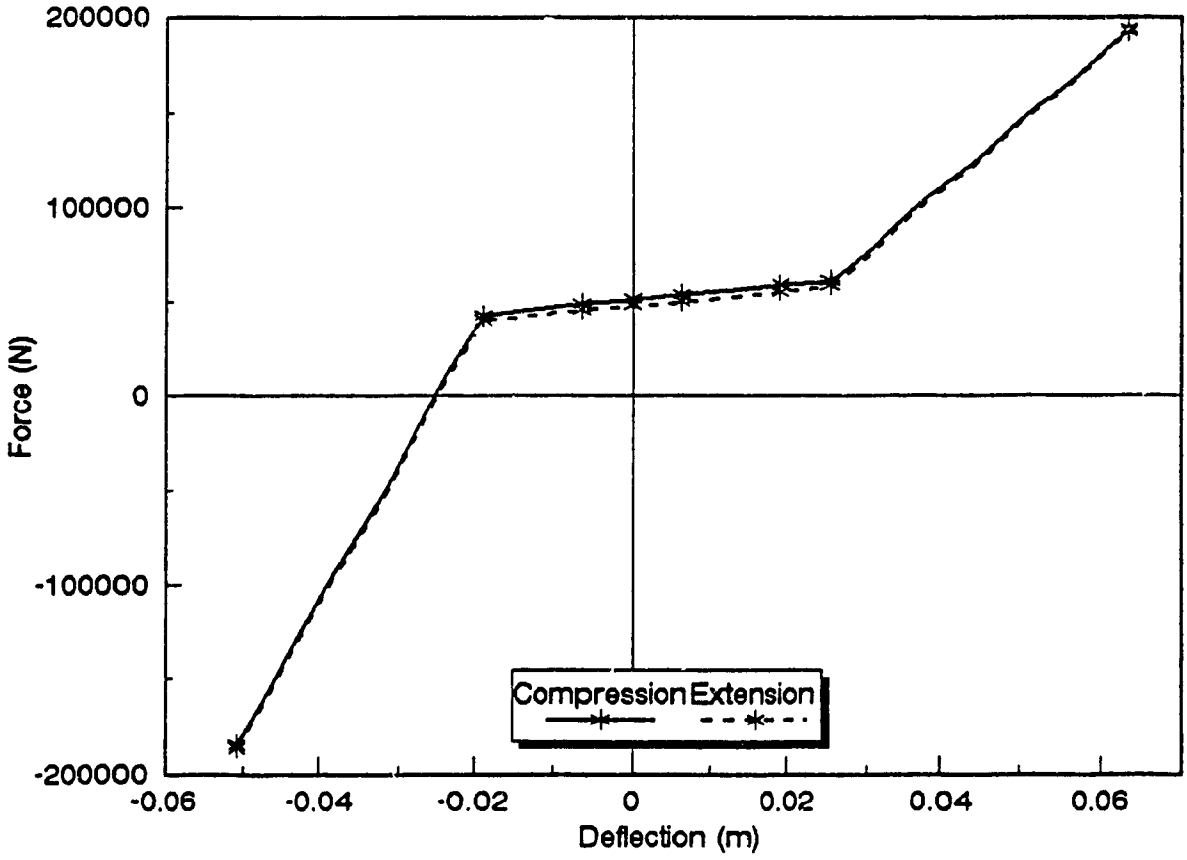

FIGURE 4.1: Force-Deflection Characteristics of Suspension Springs

linearized spring rate, as discussed in Chapter 3.

For tandem axle, the suspension force calculations use the same algorithms as the single axle. However when the braking occurs, the suspension forces at the leading and trailing axles are derived in view of the brake torque and load transfer:

$$\overline{SF}(LEAD) = SF(LEAD) + \frac{FSHIFT*BTORQ}{TD} \tag{4.7}$$

$$\overline{SF}(TRAIL) = SF(TRAIL) - \frac{FSHIFT*BTORQ}{TD} \tag{4.8}$$

where SF is the vertical suspension force in the absence of braking and $\overline{SF}$ is the total suspension force when braking occurs. BTORQ is the total brake torque due to all four brakes on the tandem set. FSHIFT is a factor related to the dynamic load transfer and TD is the tandem spread of the axles. The LEAD and TRAIL refer to leading and trailing axle, respectively.

The lateral forces due to the suspension may be viewed as the constraint forces holding sprung and unsprung masses together. To calculate these forces, the following procedure is used:

1) The sprung and unsprung masses are assumed to move as a rigid body in yawing but not in rolling or pitching. Thus the vehicle acceleration is calculated using the entire mass and the known forces at the tire-road interface.
2) The unsprung mass acceleration is assumed as a simple function of the gross vehicle acceleration calculated in (1). The yaw plane constraint forces are then computed from the known tire forces in the yaw plane.

3) These yaw plane constraint forces are then applied to the equations of motion for the sprung masses.

The Phase IV simulation uses a spring-dashpot model for the fifth wheel connection. This arrangement offers advantages in removing the dynamic coupling and in simulating the roll compliance at the coupling. At each integration time step the relative position of the tractor fifth wheel, a point located on the tractor with respect to the position of the trailer fifth wheel, a point on the trailer are calculated. A force is assumed to act along the line between these points. The magnitude of the force is computed from the linear spring rate, damping coefficient, and relative position and velocity of the two articulation points [67].

4.5 SIMULATION VEHICLE PARAMETERS

The computer simulations are carried out for only one vehicle configuration since the jackknife instability is mostly dependent on the tire properties, the selected vehicle configuration is described as follows:

Front Axle Suspension:	International Harvester
Drive Axle Suspension:	Neway ARD244 16K
Semitrailer Axle Suspension:	Neway AR95.17 24K
Center of Gravity Height:	1.52 m
Initial Velocity:	77 km/h
Tires:	Michelin XZA 11:00R22.50

The center of gravity height is selected as 1.52 meter in order to minimize the possibility of vehicle rollover, since the objective of this analysis is to investigate the onset of jackknife instability. The tire properties are of utmost importance when studying the braking or the jackknife stability performance of the vehicle. The cornering and longitudinal force coefficients of the selected tires, defined as the ratio of cornering and longitudinal force to the normal load, respectively, are taken from the measured data [1]. The cornering force coefficients in relation to the sideslip angles and the normal load of the selected tire are presented in Figure 4.2. The longitudinal force coefficients of the tire are presented in Figure 4.3 as functions of the normal load, deformation slip and the tire velocity. The maximum braking force is generated around a slip of 0.3 (30%).

The computer simulations are carried out for a braking-in-a-turn maneuver with a constant steer input of 1.7 degrees. The parameters used in the simulation such as vehicle dimensions, axle loads, inertial properties, etc... are listed in Table 4.1.

4.6 DETERMINATION OF PARAMETERS RELATED TO ONSET OF VEHICLE JACKKNIFE

Tractor jackknife is associated with saturation or limitation of the total side force produced by the drive axle tires. This saturation or limitation of the side force occurs when the magnitude of sideslip angle at either drive axle tire continues to grow and the rate of change of the side force generated by the tire approaches zero. This phenomenon can be demonstrated by the cornering force-sideslip relationship of a pneumatic tire, shown in Figure 4.4. As the sideslip angle grows, the cornering force generated by the tire approaches a

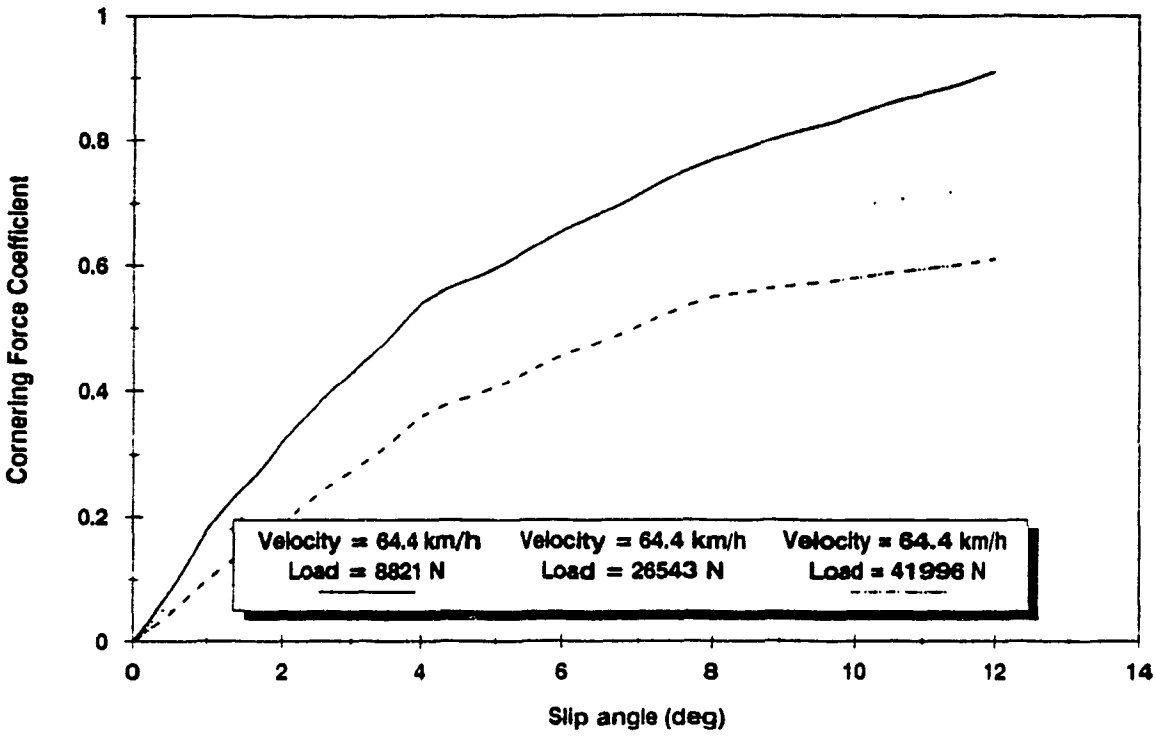

FIGURE 4.2: Cornering Force Coefficients of the Michelin XZA 11:00R22.50 Tires

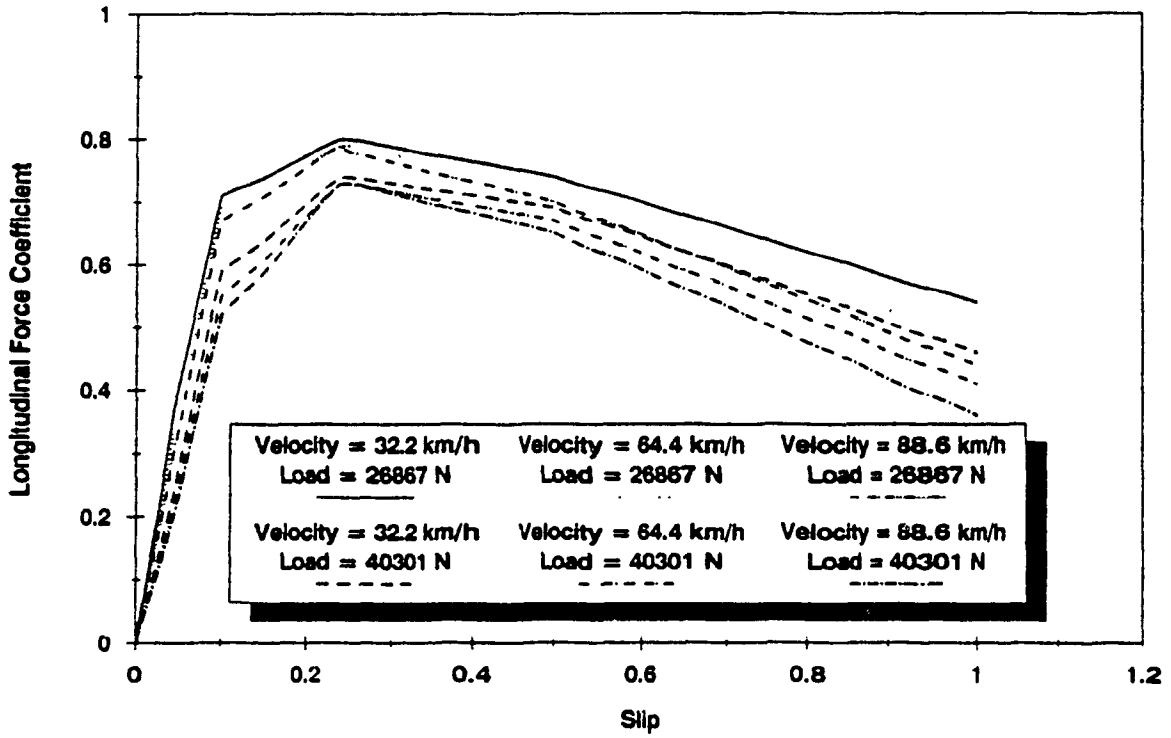

FIGURE 4.3: Longitudinal Force Coefficients of the Michelin XZA 11:00R22.50 Tires

TABLE 4.1
SIMULATION VEHICLE PARAMETERS

Tractor Parameters	
Wheelbase (m)	4.83
Base vehicle curb weight on front suspension (kN)	42.6
Base vehicle curb weight on rear suspension (kN)	37.4
Sprung mass center of gravity height (m)	1.12
Sprung mass roll moment of inertia ($kg \cdot m^2$)	2900
Sprung mass pitch moment of inertia ($kg \cdot m^2$)	38400
Sprung mass yaw moment of inertia ($kg \cdot m^2$)	38400
Fifth wheel location ahead of rear suspension center (m)	0.381
Fifth wheel height above ground (m)	1.22
Tractor frame stiffness (N·m/deg)	4520
Tractor frame torsional axis height above ground (m)	0.914
Semitrailer Parameters	
Wheelbase from kingpin to rear suspension center (m)	12.3
Base vehicle kingpin static load (kN)	23.1
Base vehicle curb weight on rear suspension (kN)	38.3
Sprung mass center of gravity height (m)	1.32
Sprung mass roll moment of inertia ($kg \cdot m^2$)	9040
Sprung mass pitch moment of inertia ($kg \cdot m^2$)	113000
Sprung mass yaw moment of inertia ($kg \cdot m^2$)	113000
Payload Parameters	
Payload (kN)	222
Payload distance ahead of rear suspension center (m)	5.94
Payload center of gravity height (m)	1.57
Payload roll moment of inertia ($kg \cdot m^2$)	11500
Payload pitch moment of inertia ($kg \cdot m^2$)	405000
Payload yaw moment of inertia ($kg \cdot m^2$)	416000

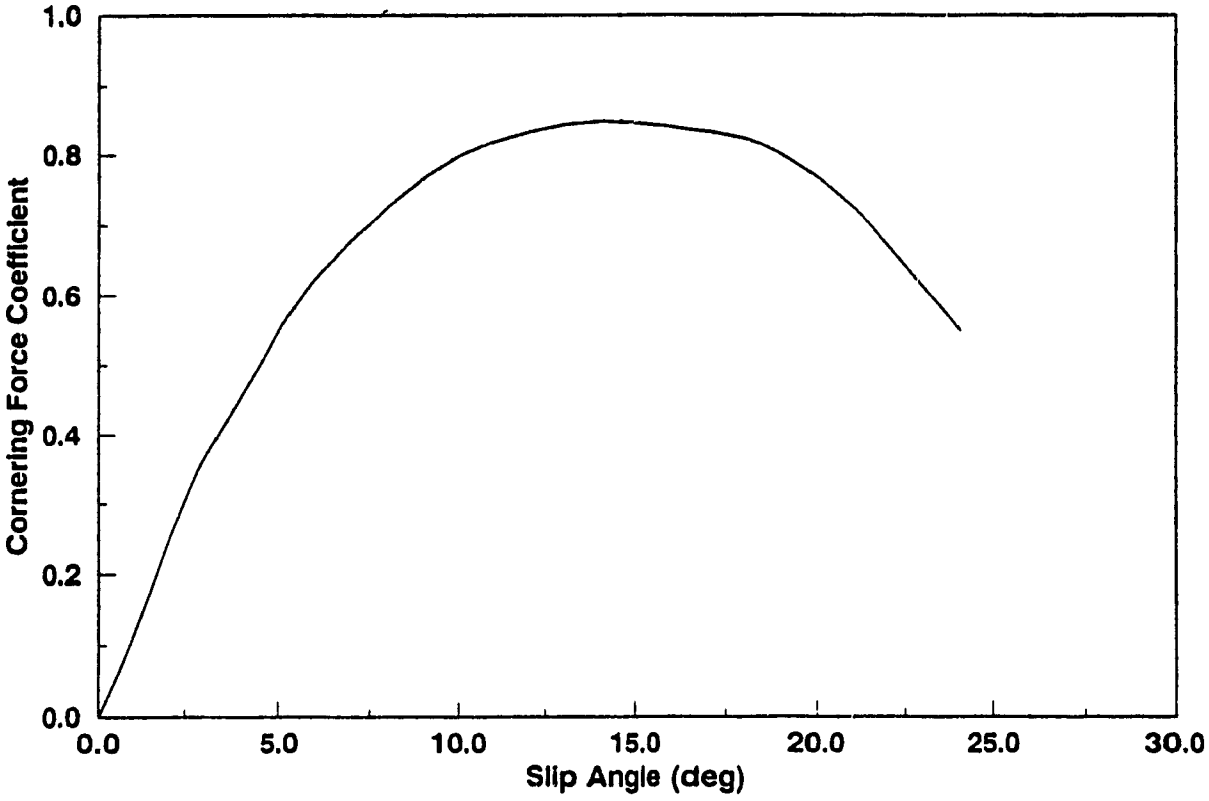

FIGURE 4.4: Cornering Properties of a Pneumatic Tire

maximum value. A further increase in the sideslip angle yields a rapid decrease in the cornering force until a wheel lockup is experienced. The rate of change of the cornering force approaches zero prior to the rapid decrease in the magnitude of the cornering force. The saturation or limitation of the side force can thus be detected when the sideslip angle grows and the rate of change of the cornering force approaches zero. This suggests that the side force-sideslip angle combination can be a useful indicator of the wheel lockup and thus the onset of vehicle jackknife.

The measurement of the total side force at the tractor rear axle is very intricate, an approximation of this force can be obtained by summing the yaw moments about the front axle. Figure 4.5 shows the yaw plane of the tractor, subject to lateral and yaw acceleration. An approximation of the cornering forces developed at the drive axles is represented by F_r and the lateral constraint force acting on the fifth wheel is represented by F_{5y}. The approximate force, F_r, required to maintain yaw equilibrium can be derived by summing the moments about the front axle, while assuming negligible vertical velocity:

$$F_r = \frac{m_1(\dot{v}_{S1}+r_{S1}u_{S1})x_{U1} - I_{ZZ1}\dot{r}_{S1} - F_{5y}(x_{U1}+x_5)}{x_{U1} + \frac{(x_{U2}+x_{U3})}{2}} \qquad (4.9)$$

where m_1 is the total mass of the tractor.

The approximate force, derived from Equation (4.9) is related to the total side force developed at the drive axle tires. It can be shown that the time derivative of the approximate force (F_r) and the time derivative of the total side force ($\sum_{j=1}^{4} F_{y2j}+F_{y3j}$) approach zero at the

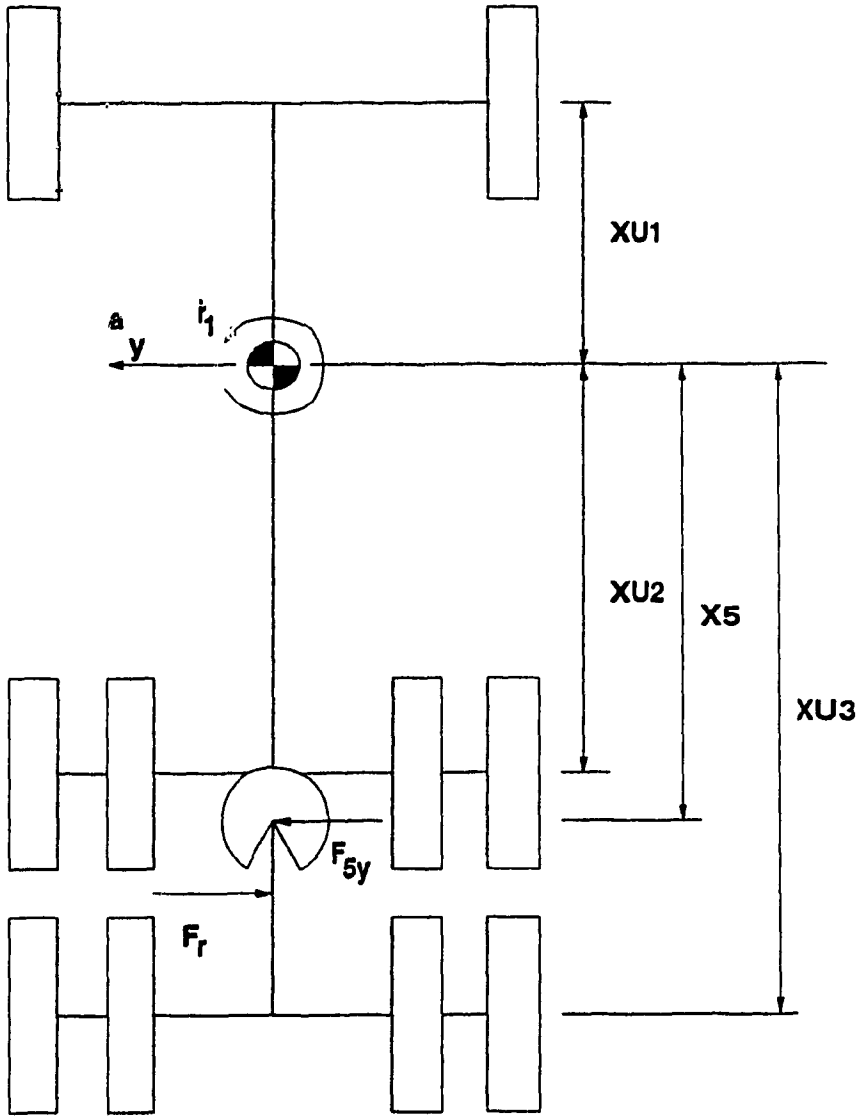

FIGURE 4.5: Yaw Plane Representation of the Tractor

same time. Equations (4.9) can then be used to determine the instant at which the derivative of the total side force becomes zero. The approximate force, F_r, is evaluated at each integration step using Equation (4.9). The total side force developed at the drive axle tires, is evaluated and compared with F_r for a constant steer input as shown in Figure 4.6. The presence of oscillations in the lateral force curves can be attributed to the Coulomb friction within the suspension springs. The Coulomb friction introduces variations in the normal load of the tires, leading to variations in the cornering forces. A comparison of the approximate side force and true lateral force generated at the drive axle tires reveal that both the lateral forces reach their maxima at the same time.

In the later sections, it will be shown that the approximate force F_r can be measured quite conveniently. However, the measurement of sideslip angle is quite complex. The corresponding drive axle sideslip and articulation angle response characteristics are also presented in Figure 4.6. It can be observed that the sideslip as well as the articulation angles follow a similar trend. The sideslip and articulation angles reach a peak value when the lateral forces approach their maximum values indicating that the jackknife will not occur. Figure 4.6 further reveals that the time derivatives of the magnitude of the sideslip and the articulation angles carry the same sign. Thus the articulation angle, which can be measured directly, can be used to detect the growing sideslip angle. The onset of tractor jackknife can thus be described by the following necessary conditions:

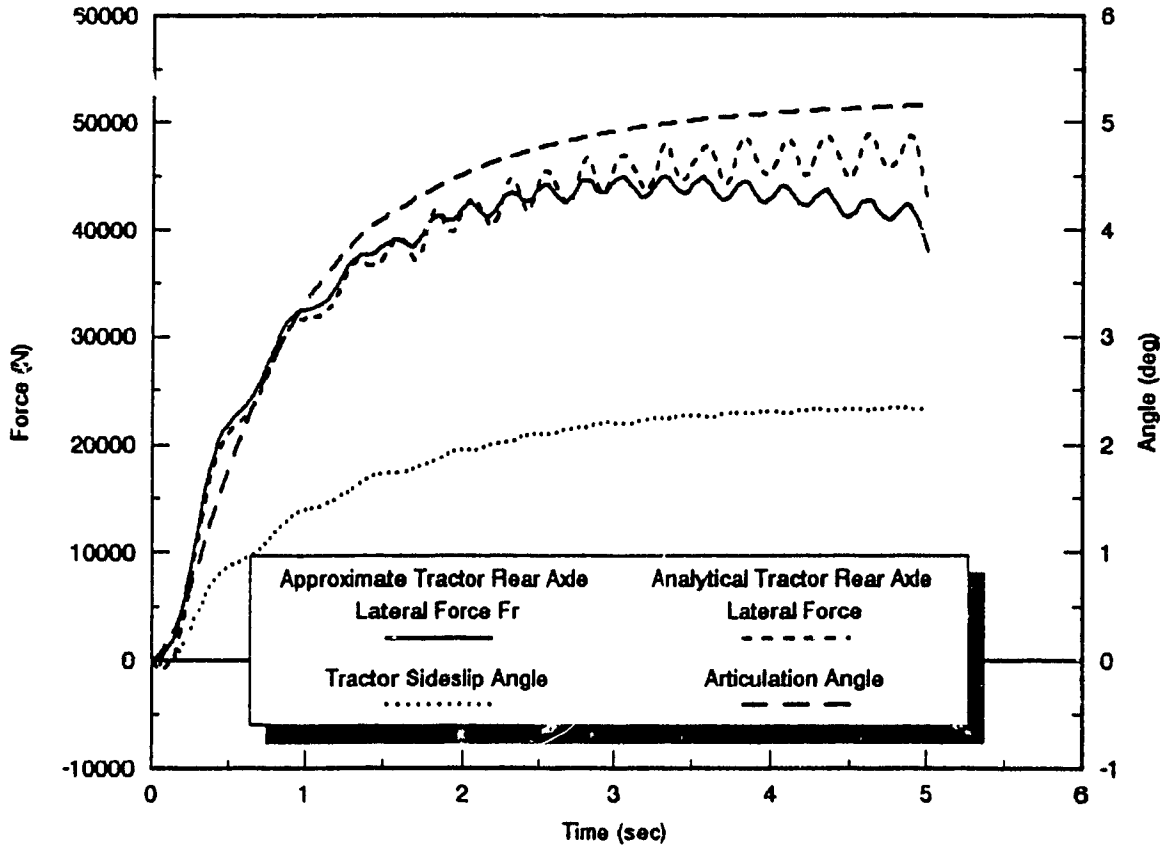

FIGURE 4.6: The Drive Axles Lateral Forces, Sideslip Angle and Articulation Angle Response Characteristics of the Tractor Subject to a Constant Steer Input (δ_1=1.7°)

$$(i)\quad \frac{d}{dt}(F_r) \cong 0$$

$$(ii)\quad \frac{d}{dt}|\gamma| > 0 \tag{4.10}$$

where γ is the articulation angle, given by:

$$\gamma = \psi_{s1} - \psi_{s2} \tag{4.11}$$

The validity of the above necessary conditions to detect the onset of vehicle jackknife is investigated for various braking-in-a-turn maneuvers. The directional dynamics of the vehicle combination are investigated for various braking torque distributions.

In the second analysis, the braking is applied with a brake torque of 13.6 kN·m at the front axle (FB_1), 40.7 kN·m at the rear tractor axles (FB_2), and 13.6 kN·m at the semitrailer axles (FB_3). The approximate lateral force, the total side force developed at the drive axle tires, the average sideslip angle of the dual tire sets on the drive axles and the articulation angle response characteristics of the vehicle are presented in Figure 4.7. The sideslip and articulation angle continue to grow as the lateral forces increases. The approximate lateral force and the total side force developed at the drive axle tires approach identical peak values at the same time, as shown in Figure 4.7. It can be seen that both the necessary conditions related to onset of vehicle jackknife are satisfied. The time derivative of F_r approaches zero at approximately 0.5 second and the time derivative of the magnitude of the corresponding articulation angle is observed to be positive indicating the vehicle jackknife. It can also be observed that

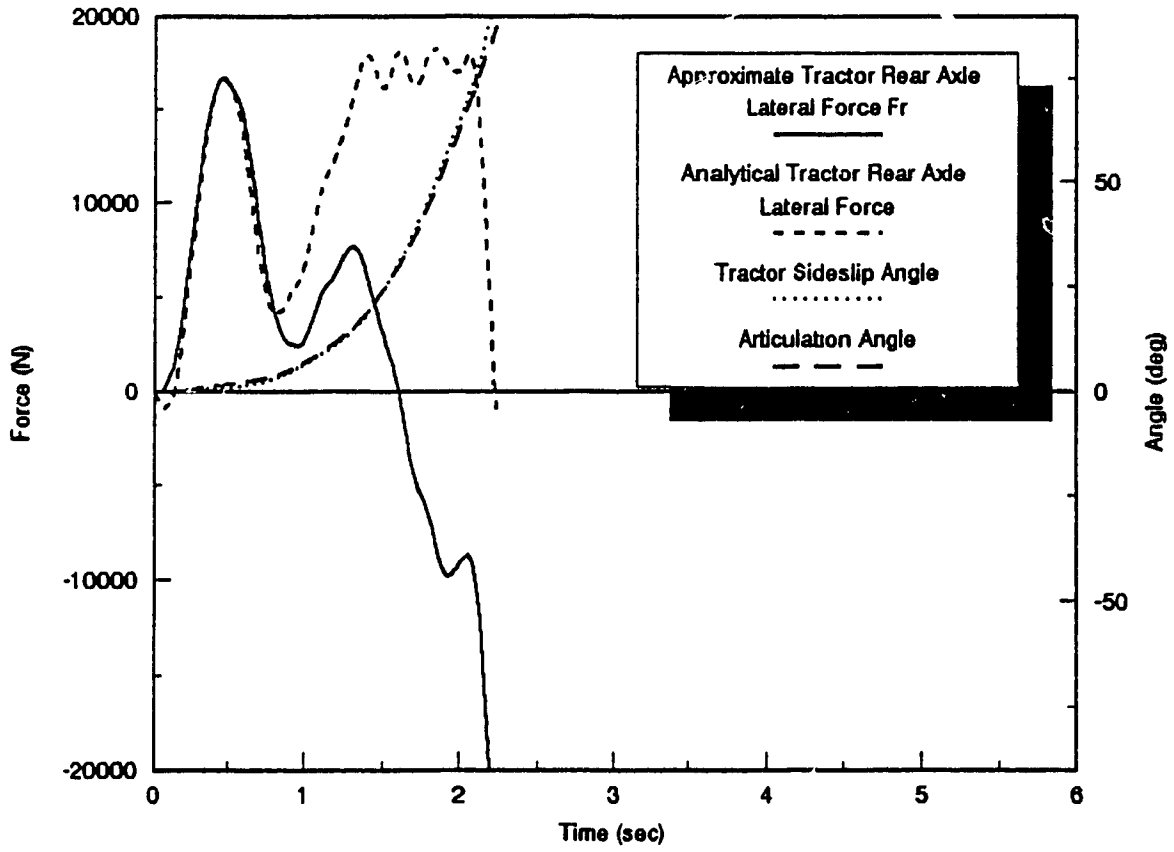

FIGURE 4.7: The Drive Axles Lateral Forces, Sideslip Angle and Articulation Angle Response Characteristics of the Tractor Subject to a Braking-in-a-Turn Maneuver (δ_1=1.7°, FB_1=13.6 kN·m, FB_2=40.7 kN·m, FB_3=13.6 kN·m)

the condition of vehicle jackknife is attained well before the articulation angle reaches a dangerous value. The onset of jackknife is detected while the articulation angle reaches only 2 degrees. It is further observed that the lateral force diverges quite rapidly as the articulation angle increases since the force exerted by the semitrailer on the tractor changes its direction of application. The two necessary conditions of tractor jackknife thus reveal that the detection of jackknife can be performed at relatively small articulation angles.

In the third analysis, braking is applied at the tractor rear axles only with a brake torque of 27.1 kN·m. The lateral forces, sideslip angle and articulation angle characteristics are presented in Figure 4.8. The approximate lateral force approaches a peak value slightly before the total side force saturates, as shown in Figure 4.8. As the lateral forces reach their maximum, the articulation angle continues to increase at a slow rate, thus initiating a mild jackknife. A maximum articulation angle of 15 degrees is attained, as shown in Figure 4.8. The two necessary conditions and thus the detection of the jackknife however are obtained when the articulation angle approaches 10 degrees at approximately 2 seconds.

In the fourth case, the front wheel steer angle is increased to 2.3 degrees and braking is applied to the rear tractor axles only with a brake torque of 40.7 kN·m. The lateral forces, sideslip angle and articulation angle response characteristics are presented in Figure 4.9. The lateral forces approach their peak values quite rapidly, while the articulation angle continues to grow. The two necessary conditions described in Equation (4.10) are thus satisfied initiating the vehicle jackknife. The vehicle jackknife is detected while the articulation

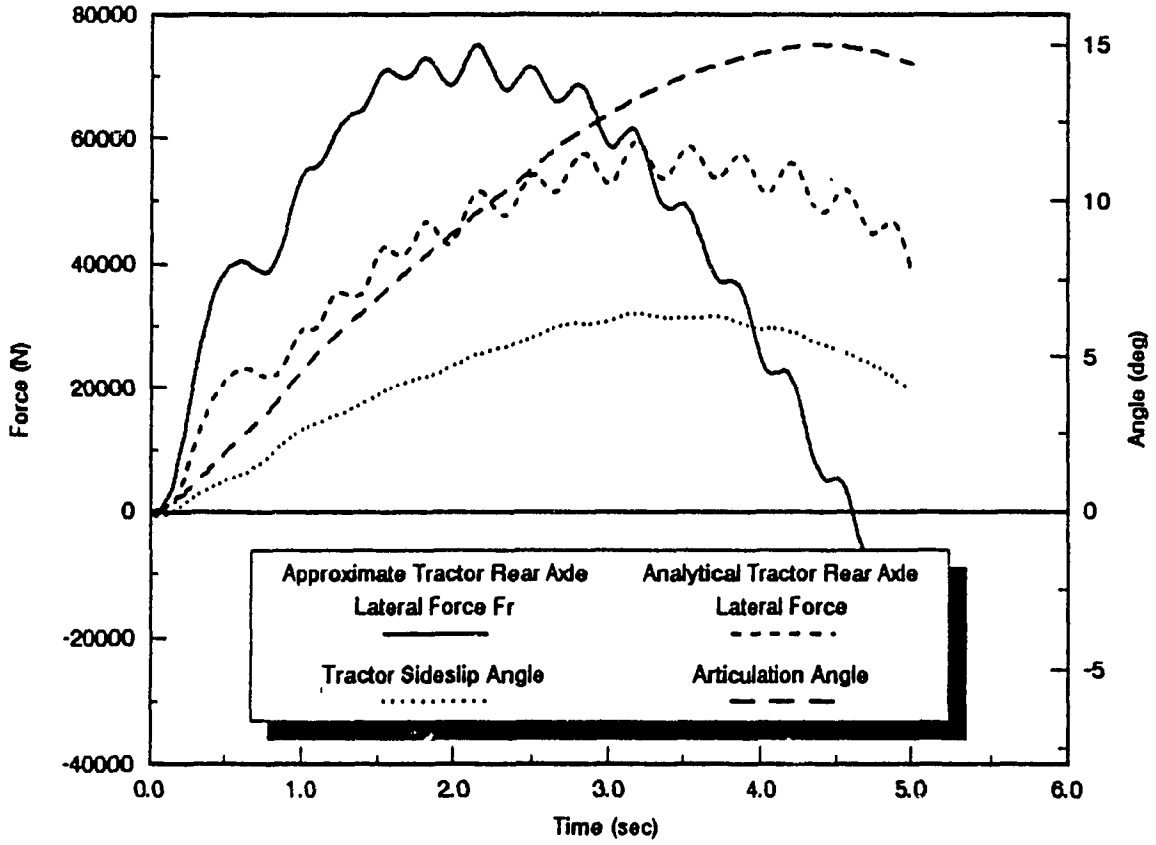

FIGURE 4.8: The Drive Axles Lateral Forces, Sideslip Angle and Articulation Angle Response Characteristics of the Tractor Subject to a Braking-in-a-Turn Maneuver (δ_1=1.7°, FB_1=0 kN·m, FB_2=27.1 kN·m, FB_3=0 kN·m)

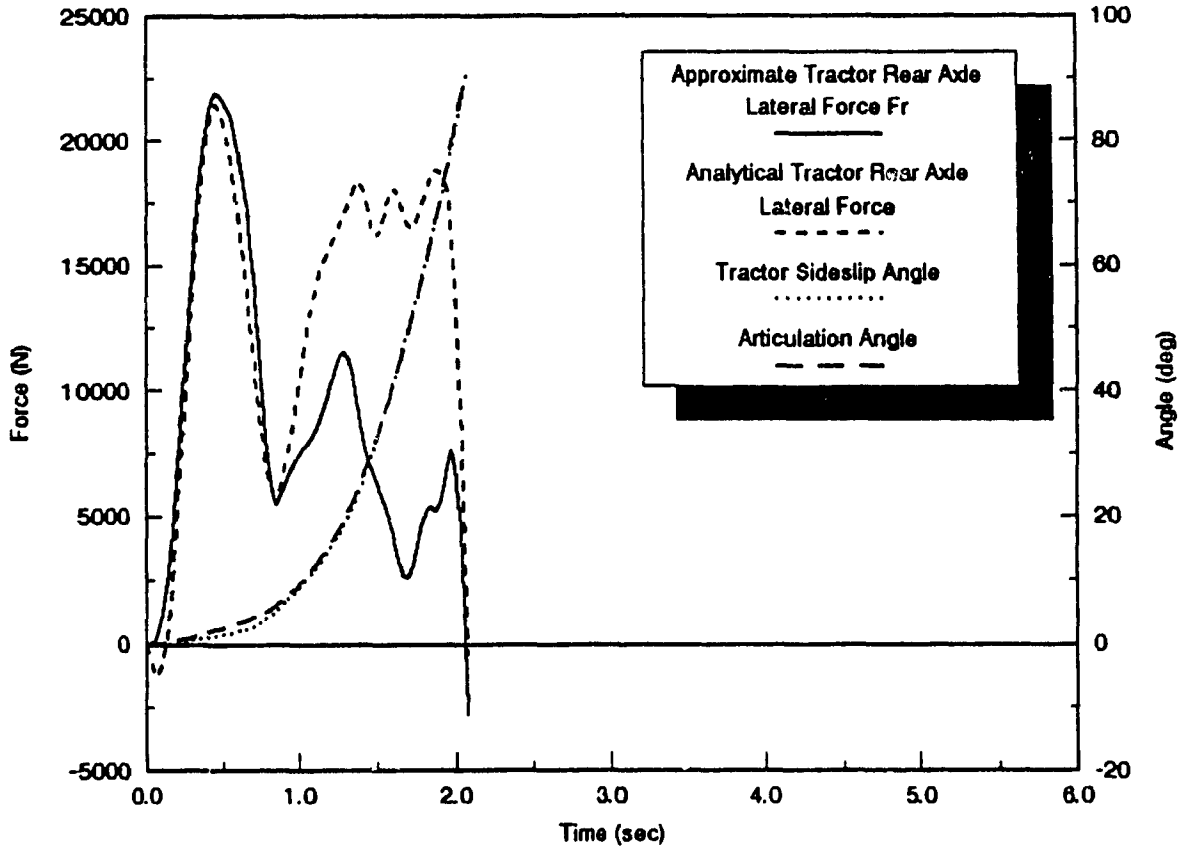

FIGURE 4.9: The Drive Axles Lateral Forces, Sideslip Angle and Articulation Angle Response Characteristics of the Tractor Subject to a Braking-in-a-Turn Maneuver (δ_1=2.3°, FB_1=0 kN·m, FB_2=40.7 kN·m, FB_3=0 kN·m)

angle is relatively small ($\cong$ 5 degrees at $t \cong 0.5$ s), as shown in Figure 4.9.

In the fifth case, the front wheel steer angle is maintained at 1.7 degrees, and the braking is applied to the tractor rear axles only with a smaller brake torque of 13.6 kN·m. As the lateral forces reach their maximum, the articulation angle increases at a slow rate, thus initiating an even milder jackknife, as shown in Figure 4.10. The maximum articulation angle is attained around 7.5 degrees, as shown in Figure 4.10. The detection of the jackknife condition is obtained while the articulation angle is relatively small ($\cong$ 6 degrees at $t \cong 2$ s).

In the sixth analysis, the front wheel steer angle is reduced to 0.6 degrees and the braking force is applied to tractor rear axles only with a brake torque of 10.8 kN·m. The lateral forces, sideslip angle and articulation angle response characteristics are presented in Figure 4.11. Figure 4.11 reveals that as the lateral force curves reach their maximum, the articulation angle also reaches its maximum, thus no jackknife is initiated. The maximum articulation angle attained is less than 2 degrees.

In the last case, the front wheel steer angle is kept at 0.6 degrees while the brake torque is applied to all the axles, 3.25 kN·m at the tractor front axle, 4.88 kN·m at the rear tractor and the semitrailer axles. The lateral forces, sideslip angle and articulation angle response characteristics are presented in Figure 4.12. As the lateral forces reach their maximum, the articulation angle approaches its maximum. The necessary conditions are thus not achieved indicating that the jackknife is not initiated. The maximum articulation angle attained is around 1.7 degrees.

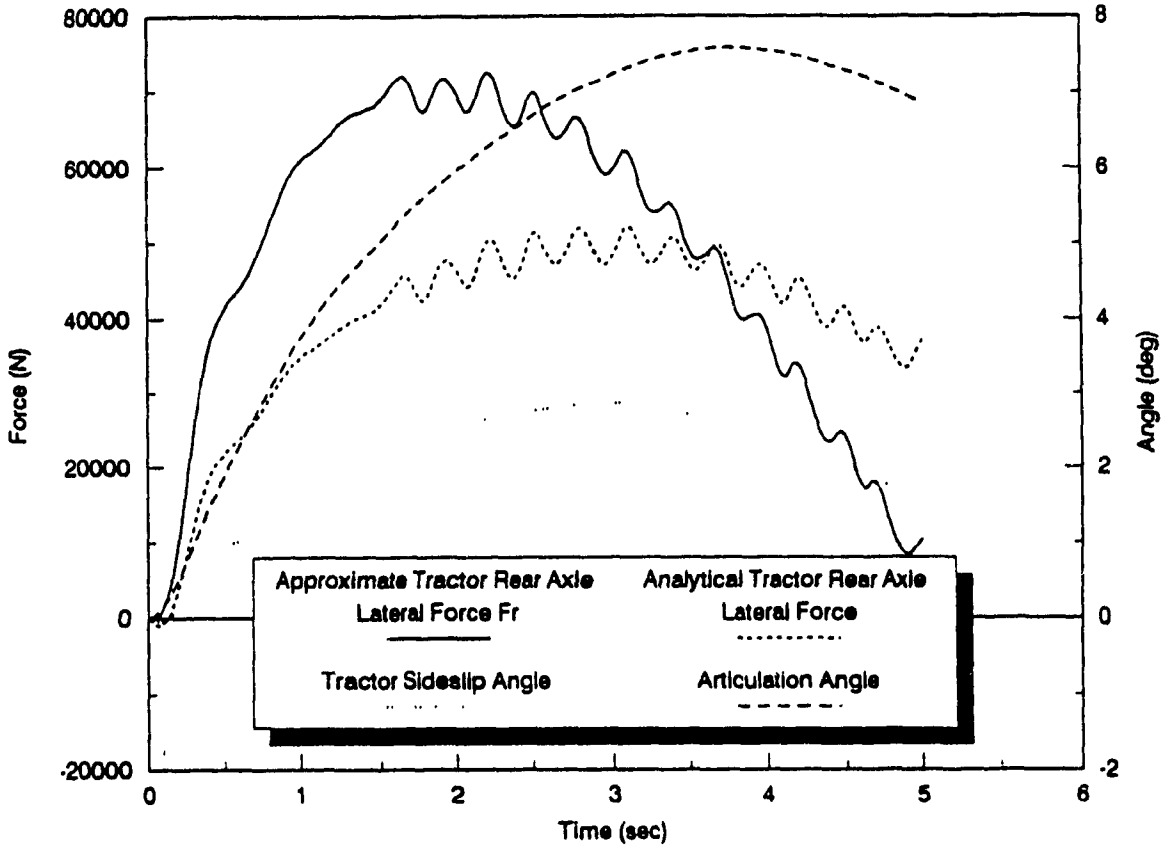

FIGURE 4.10: The Drive Axles Lateral Forces, Sideslip Angle and Articulation Angle Response Characteristics of the Tractor Subject to a Braking-in-a-Turn Maneuver (δ_1=1.7°, FB_1=0 kN·m, FB_2=13.6 kN·m, FB_3=0 kN·m)

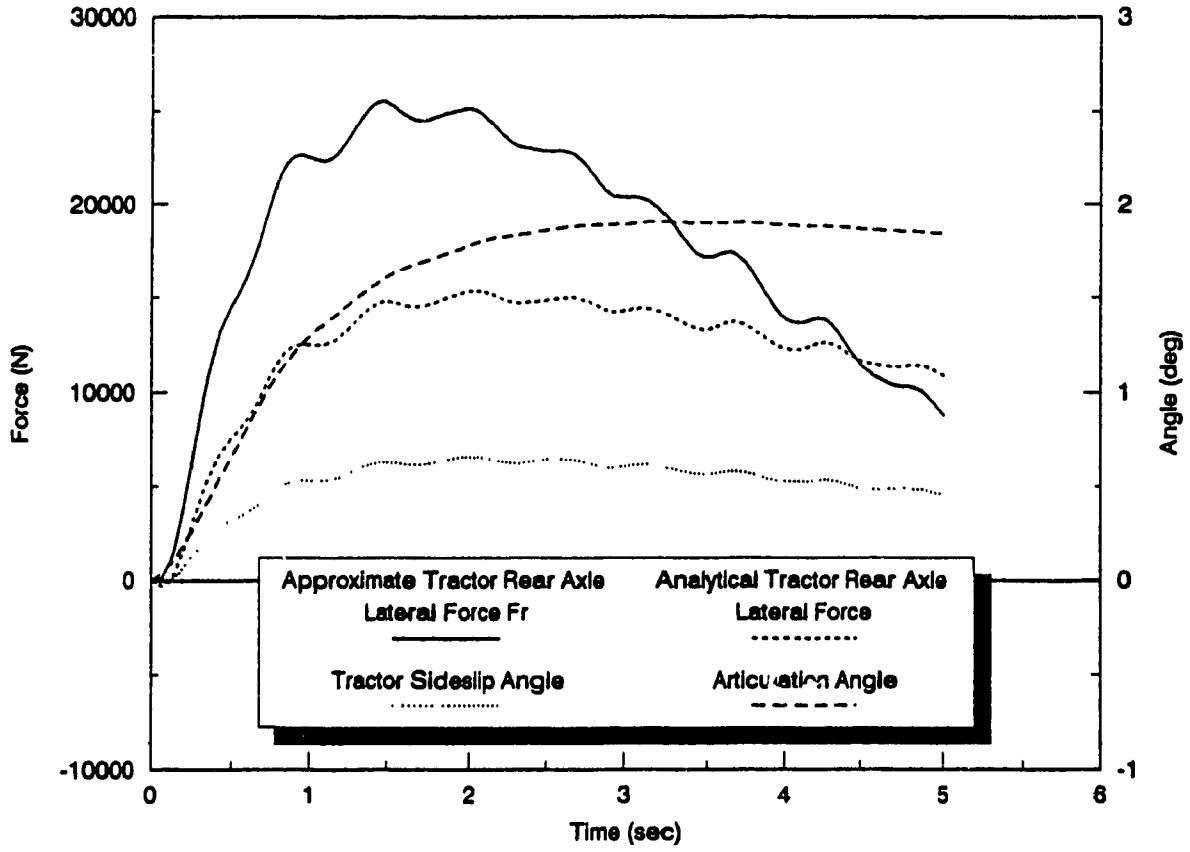

FIGURE 4.11: The Drive Axles Lateral Forces, Sideslip Angle and Articulation Angle Response Characteristics of the Tractor Subject to a Braking-in-a-Turn Maneuver (δ_1=0.6°, FB_1=0 kN·m, FB_2=10.8 kN·m, FB_3=0 kN·m)

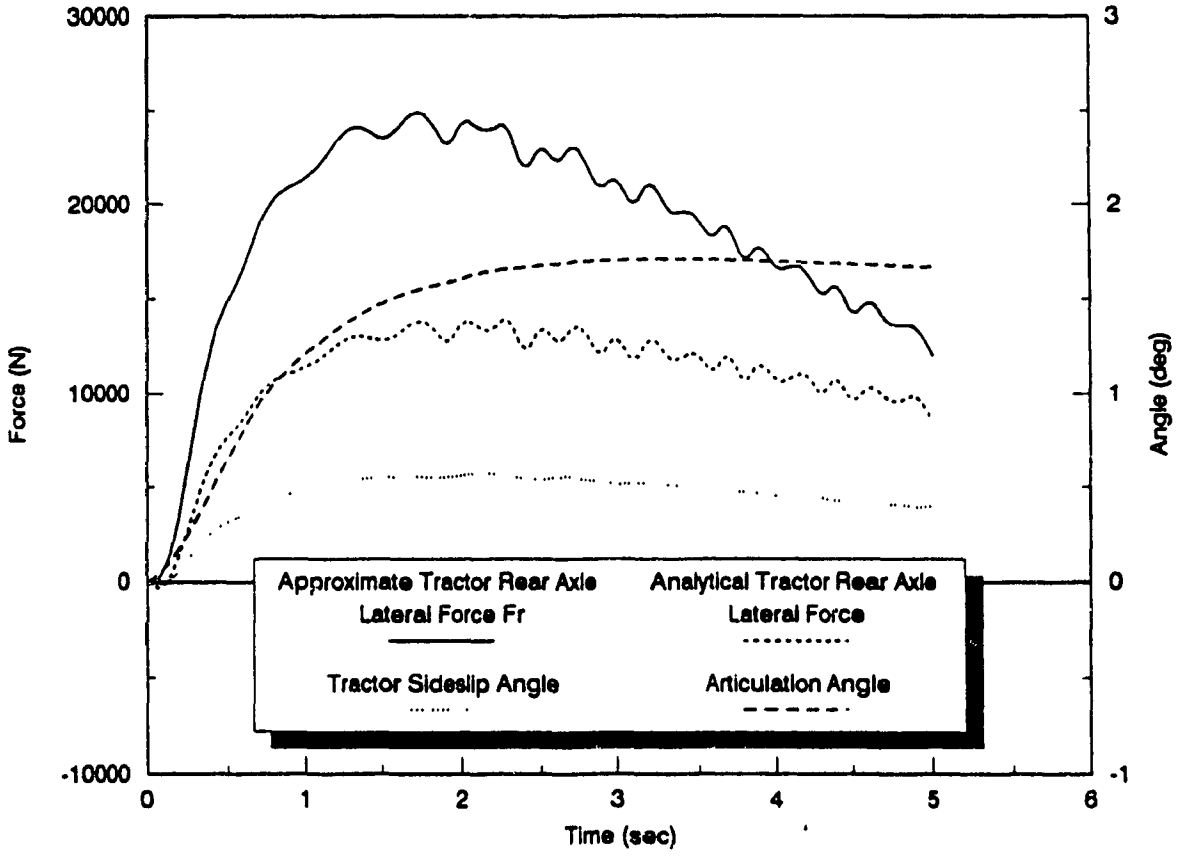

FIGURE 4.12: The Drive Axles Lateral Forces, Sideslip Angle and Articulation Angle Response Characteristics of the Tractor Subject to a Braking-in-a-Turn Maneuver (δ_1=0.6°, FB_1=3.25 kN·m, FB_2=4.88 kN·m, FB_3=4.88 kN·m)

From these analyses, it can be concluded that an estimate of the approximate tractor rear axle lateral force and articulation angle can defined the onset of jackknife accurately and well before the articulation angle reaches a critical value. The monitoring of the side force and the articulation angle has the potential for implementation in a real tractor-semitrailer combination. Such an implementation will require only simple measurement and signal processing. This implementation can detect the onset of vehicle jackknife condition arising from simultaneous braking and steering maneuvers as well as from the slippery road conditions.

4.7 SUMMARY

A three dimensional model of the articulated vehicle combination capable of simulating the steering and braking maneuvers is used to investigate the vehicle jackknife stability limits. The onset of jackknife during braking-in-a-turn maneuvers is described via the cornering force and the sideslip angles developed at the drive axles. In view of the complexities associated with measurement of side forces, the cornering force developed at the drive axles is related to an approximate lateral force derived from the yaw plane of the tractor. The sideslip angle developed at the drive axles is related to the articulation angle, which can be measured quite conveniently. The onset of tractor jackknife is described by the approximate lateral force and the articulation angle. The sensitivity of the approximate lateral force and articulation angle to variations in braking and steering parameters is investigated to determine their feasibility.

CHAPTER 5

DETERMINATION OF ONSET OF VEHICLE INSTABILITY

5.1 GENERAL

The number and severity of highway accidents involving heavy vehicles can be decreased considerably by reducing the number of accidents attributed to driver-vehicle interactions. Vehicle accidents caused by rollover and jackknife are often attributed to inadequate driver-vehicle interactions, such as high speed, rapid steering, rapid braking, etc The probability of such accidents can be reduced by providing an early warning to the driver pertaining to impending vehicle instabilities, such that the driver may take an appropriate corrective action.

Development of an early warning safety monitor requires a prior knowledge of response parameters that closely relate to the onset of vehicle instability. It is desirable to limit the number of these parameters to only a few, in order to facilitate manipulations, and to minimize the cost of on-line measurement and signal processing. The key parameters, related to onset of vehicle instability, should be directly measurable and the associated sensors should be reliable enough to operate in rough environment. In this chapter, the key parameters derived in Chapters 2 to 4 are further examined for their on-line acquisition and the design criteria are formulated towards development of an early warning safety monitor.

The early warning safety monitor can be realized with a microprocessor that can read and manipulate the signals from the sensors. The stability criteria are either computed or retrieved by the

microprocessor. The on-line measurements on the vehicle are assessed in relation to the stability criteria to detect the onset of any instability. The microprocessor based early warning safety monitor can then warn the driver of the impending danger.

5.2 ONSET OF ROLLOVER INSTABILITY DURING STEADY TURNING

Many research investigations conducted on the dynamics of articulated vehicles reveal that the vehicle rollover is strongly related to its rollover threshold during steady turning [24,32]. The rollover threshold defined as the magnitude of maximum lateral acceleration that the vehicle can withstand, is determined from the static roll plane model of the vehicle described in Chapter 2.

The model contains a comprehensive description of suspension and tire properties, such that an accurate estimation of the steady turning rollover threshold can be made. Computer simulations are carried out to establish the lateral acceleration and vehicle roll experienced during a steady turn. The calculations are terminated when the deflections of the trailer and tractor rear axles tires on the inside of the turn approach zero. The highest lateral acceleration achieved during the computation process is termed as the steady turning rollover threshold of the vehicle.

The steady turning rollover can be related to a number of vehicle response parameters, such as vertical load on the tires on the inside of the turn, roll angle of the composite axles and the lateral acceleration of the vehicle. The wheel lift-off can be detected when the vertical load on the tires on the inside of the turn approaches zero. Thus the onset of vehicle rollover can be detected via the normal load on the

tires. However, an on-line measurement of tire load is extremely difficult. Consequently, detection of rollover instability through tire loads is considered infeasible.

Alternatively, the vehicle rollover during steady turning is strongly related to the roll angle of the unsprung mass and the lateral acceleration, and these response parameters can be conveniently measured during the vehicle operation. Thus, it is concluded that the unsprung mass roll angle and the vehicle lateral acceleration merit further considerations in order to detect the onset of vehicle rollover during steady turns.

The rollover threshold and thus the rollover stability of the vehicle is strongly influenced by various vehicle parameters, such as vehicle geometry, axle loads, and stiffness properties of the suspension, tires and articulation mechanism. However, the vehicle weights and dimensions, regulated by the provincial governments, permit only small variations in vehicle geometry and axle loads, as listed in Table 5.1 [27]. Thus the variations in rollover threshold due to small variations in geometry and axle loads are considered insignificant.

The rollover threshold and thus the roll stability of the vehicle is strongly related to the compliance of the articulation mechanism, suspension and tires. Due to the weights and dimensions regulations, the vehicle width is limited to 2.44 meters. Vehicles with wider track (2.59-meter wide) have been recently proposed to attain higher load carrying capacities and stability limits. However, majority of the tractor-semitrailer vehicles on the road are still 2.44-meter wide. The center of gravity of a semitrailer loaded with median freight density is located at a height of approximately 2 meters. Thus, the rigid rollover

TABLE 5.1
WEIGHTS AND DIMENSIONS ACROSS CANADA
FOR FIVE-AXLE TRACTOR-SEMITRAILER [27]

Province	Typical Gross Combination Weight (kN)	Overall Length (m)	Tandem Axles Load (kN)	Tandem Axles Spread (m)
Québec	387-410	21	172 177	<1.50 >1.52
Ontario	392-428	23	169 176 187	1.30-1.40 1.52-1.60 >1.80
New Brunswick	356-387	20	157 162 167 177	1.22 1.37 1.52 1.83
Alberta	356-365	20	157	
Manitoba	356	20	157	
British Columbia	365-387	20	162 167	<1.50 1.50-1.85
Canada (proposed by RTAC)	387	23	167	1.20-1.85

threshold of the majority of the loaded tractor-semitrailers is estimated as 5.2 m/s^2 (0.53 g). The rollover threshold of a compliant vehicle, however, decreases as a function of the effective roll stiffness of the vehicle.

In view of the dependency of the rollover threshold limit on various vehicle parameters, a comprehensive database on currently used suspensions, tires and axle loads was compiled. Computer simulations were carried out to establish the range of compliance factors representing a broad class of tires and suspensions. The rollover thresholds of tractor-semitrailer combinations of twenty-four different configurations with three different values of center of gravity height of the trailer are computed to determine the range of compliance factors.

Computer simulations on the steady turning response characteristics reveal that for a given loading condition and vehicle track width, the lateral acceleration corresponding to the rollover varies only slightly with variations in the properties of commercially available suspension. Moreover, the lateral acceleration corresponding to vehicle rollover is relatively insensitive to the torsional stiffness characteristics of the tractor chassis, and that of the articulation mechanism and trailer structure. Thus the vehicle's lateral acceleration can be directly related to the onset of vehicle rollover provided the sprung mass center of gravity height and the tire track width do not vary. In the majority of the freight vehicle combinations, the tire track width is held constant due to limits imposed on the maximum vehicle width. However, the sprung mass center of gravity height and thus the roll stability limits vary with varying loading conditions.

The rollover threshold of the compliant five-axle tractor-semitrailer vehicle is related to that of a rigid vehicle through a compliance factor C. The compliance factor is determined from the elastic properties of the suspension, tires and articulation mechanism. The compliance factor is always less than one and can be expressed as the ratio of rollover threshold of the compliant vehicle to that of the rigid vehicle. The compliance factors of selected vehicle configurations are evaluated as discussed in Chapter 2. The results of the study reveal the mean value as 0.72 with a standard deviation of 0.03. The threshold value of compliance factor is thus computed from:

$$C^{*} = \frac{1}{\alpha}(\bar{C}-3\sigma) \tag{5.1}$$

where C^{*} is the threshold value of the compliance factor and α is the safety factor. Assuming a safety factor of 1.1, the threshold value of compliance factor is achieved as 0.57.

For known values of trailer track width and center of gravity height, the rollover threshold of a rigid vehicle a_y^{*} can be computed using Equation 2.2. A safe value of vehicle lateral acceleration is then obtained as:

$$\bar{a}_y = C^{*} a_y^{*} \tag{5.2}$$

where $\bar{a}_y$ is the safe value of lateral acceleration related to onset of roll instability during steady turning. The lateral acceleration of the semitrailer during steady turning can be easily measured using a piezo-resistive accelerometer. The onset of vehicle rollover can be

detected by comparing the measured value of lateral acceleration to the precalculated safe limit, $\bar{a}_y$. In the event when the center of gravity height is unknown, the safe value of lateral acceleration is established assuming a center of gravity height of 2 meters.

5.3 ONSET OF ROLL INSTABILITY AT HIGHWAY SPEEDS

The vehicle rollovers occurring at highway speeds are far more fatal than those occurring during steady turns. Rollovers occurring at highway speeds pose unreasonable risk to the highway safety, safety of the drivers and passengers of light vehicles, and property in commerce. The rollovers occurring at high speeds are often caused by severe steering maneuvers, such as rapid lane change and evasive maneuvers. The three-dimensional yaw-roll model of the vehicle, developed in Chapter 3, contains comprehensive description of the suspension and tire properties, the directional dynamics and stability characteristics of the vehicle can thus be predicted quite accurately. The yaw-roll analysis program has been validated through a number of road tests conducted by UMTRI [1]. The three dimensional yaw and roll plane model of the articulated vehicle is simulated for lane change and evasive steering maneuvers, in order to identify the key parameters related to onset of vehicle rollover at highway speeds.

Lift-off of tires at the rearmost axle is often considered as the first noticeable phenomenon prior to vehicle rollover. Since tire loads are very intricate to measure, a measure of dynamic suspension loads is considered to detect the onset of tire lift-off and thus the vehicle rollover. However, the dynamic suspension loads are strongly related to the type of axle suspension, as discussed in Chapter 3. The variations

in dynamic loads due to air springs are considerably different than those due to the leaf springs, since the air springs are precharged and usually do not go into tension.

Alternatively the detection of tire lift-off is attempted via measuring the axle roll angle. The simulation results presented in Chapter 3 for various configurations clearly revealed that the wheel lift-off and thus the onset of vehicle rollover is directly related to the semitrailer's axle roll angle response. For the current suspension designs and varying values of center of gravity heights, the mean value and the standard deviation of axle roll angles are computed as 1.97 and 0.17, respectively, for 2.44-meter wide vehicles. The corresponding values for 2.59-meter wide vehicles are obtained as 1.78 and 0.19.

The lowest values of roll angle response of the 2.44-meter and 2.59-meter wide semitrailer's trailing axles are 1.55 and 1.38 degrees, respectively. Applying a safety factor of 1.1, the safe values of axle roll angles are obtained as 1.41 and 1.26 degrees, respectively. The axle roll angle can be measured directly using a miniature vertical gyroscope or a tilt sensor. A tilt sensor, however, will require appropriate correction for the lateral acceleration.

5.4 ONSET OF JACKKNIFE INSTABILITY

The tractor-semitrailers operation always involved the problem of jackknife before the instability can be observed directly. Tractor jackknife is a mode of instability in which the ratio of tractor yaw angle to semitrailer yaw angle approaches a large value. Compared with other modes of instabilities, the tractor jackknife is the most dangerous, most rapid, and least controllable by the driver.

The detection of onset of jackknife instability requires the determination of jackknife in a quantitative manner. The jackknife instability of the tractor-semitrailer combination is investigated via a vehicle model capable of simulating the braking and steering dynamics, developed by UMTRI [26]. The vehicle model incorporates the dynamics of the air brake system and a comprehensive tire-road friction model, and has shown to be capable of predicting the vehicle performance quite accurately [68]. The vehicle model was employed to evaluate the directional dynamics associated with braking-in-turn maneuvers.

Tractor jackknife is associated with saturation of the total side force produced by the drive axle tires. This saturation of the side force occurs when the magnitude of the sideslip angle at either drive axle tire continues to grow and the rate of change of the side force generated at the tire approaches zero. The measure of the total side force at the tractor rear axle is very intricate, an approximation of this force is obtained by summing the yaw moments about the front axle, as discussed in Chapter 4. This approximate side force, F_r, is expressed as:

$$F_r = \frac{m_1(\dot{v}_{S1} + r_{S1}u_{S1})x_{U1} - I_{ZZ1}\dot{r}_{S1} - F_{5y}(x_{U1}+x_5)}{x_{U1} + \frac{(x_{U2}+x_{U3})}{2}} \qquad (5.3)$$

The simulation results presented in Chapter 4 clearly demonstrated that this approximate side force is directly related to the true side force generated at the drive axle tires. The rate of change of the approximate and true side forces approach zero at the same time. The results presented in Chapter 4 also demonstrated that as the rate of

change of the side force approaches zero, a tractor jackknife is initiated as evidenced by the rapid increase in sideslip and articulation angles. The onset of tractor jackknife is thus expressed by the following two conditions:

$$\frac{d}{dt}(F_r) \cong 0$$
$$\frac{d}{dt}|\gamma| > 0 \qquad (5.4)$$

The approximate side force is a function of the lateral acceleration of the tractor, forward velocity, yaw rate and yaw acceleration of the tractor, and lateral force at the fifth wheel constraint. The quantity $(\dot{v}_{s1}+r_{s1}u_{s1})$ is, approximately, the absolute lateral acceleration of the tractor center of gravity. This acceleration can be measured using a piezo-resistive accelerometer located near the tractor's center of gravity and oriented in the $\vec{j}_{s1}$ direction. The quantity $\dot{r}_{s1}$ is the angular acceleration component about the $\vec{k}_{s1}$ axis (yaw acceleration of the tractor). The yaw acceleration can be measured by placing an additional accelerometer near the tractor rear axle and oriented in the $\vec{j}_{s1}$ direction. The yaw acceleration can then be evaluated from the two lateral accelerations and the longitudinal distance between the accelerometers. Let $a_1 \cong (\dot{v}_{s1}+r_{s1}u_{s1})$ be the lateral acceleration measured near the tractor's center of gravity and a_2 be the lateral acceleration measured near the tandem center. The yaw acceleration can thus be approximated from:

$$\dot{r} = \frac{a_2 - a_1}{b_2} \qquad (5.5)$$

where b_2 is the longitudinal distance between the two accelerometers. The quantity F_{5y} is the lateral component of the constraint forces acting on the tractor. This quantity can be measured by means of strain gauges or by a force transducer properly placed at the fifth wheel.

However, the measure of the sideslip angle is quite complex. The simulation results presented in Chapter 4 clearly revealed that the sign of the time derivative of the magnitude of the articulation angle is identical to that of the sideslip angle. Thus, the articulation angle, which is directly measurable using a goniometer, can be used to detect a growing sideslip angle. The onset of tractor jackknife can thus be detected by monitoring the dynamic behavior of the approximate side force and the articulation angle.

From the analysis carried out, it can be concluded that an estimate of the approximate tractor rear axle lateral force and the articulation angle can define the onset of jackknife accurately and well before the articulation angle reaches a critical value. The monitoring of side force and articulation angle has the potential for implementation in a real tractor-semitrailer and such an implementation will require only simple measurement and signal processing. This implementation can detect the onset of vehicle jackknife arising from braking as well as from the slippery road conditions.

5.5 DESIGN OF THE SAFETY MONITOR

An electronic monitoring system consists of three major components: a sensor, a signal processing unit, and a form of display device. In the following subsection the main components of the early warning system

are discussed. The circuit diagram of the proposed safety monitor is shown in Figure 5.1.

5.5.1 Microprocessor Board

The central processing unit is a microprocessor, which includes an arithmetic logic unit as well as registers for data and instruction storage, and a control unit. The board is based on the Z-80 microprocessor from Zilog which is an eight bits microprocessor of relatively advanced design and provides great versatility and high speed in an elegant simple configuration. It uses *n*-channel depletion-mode MOS (Metal Oxide Semiconductor) technology providing high element density and allows operation at 5 volts with a 4 megahertz clock. Clock signal and power supply use three pins, and the data bus and the 16 address lines use another 24 pins, leaving 13 pins of the 40 pins for the control signals. The instruction set includes 158 distinct instructions providing flexibility and extensive computing power. The combination of simplicity and versatility makes the Z80 attractive for the design of the early warning system.

The Z-80 requires a single phase 0 to 5 volts clock signal, generated by the 74LS04 oscillator circuit. Since the typical high-level output voltage of a TTL (Transistor-Transistor Logic) gate is only 3.3 volts and the minimum high level required at the Z-80 clock input is 4.4 volts, a 330 ohms pull-up resistor is thus required. When power is first applied to the system it is convenient to have the microprocessor reset itself without activating the reset switch. With the *RC* network connected to the reset input, the capacitor will hold the reset pin low for several time constants when power is first applied.

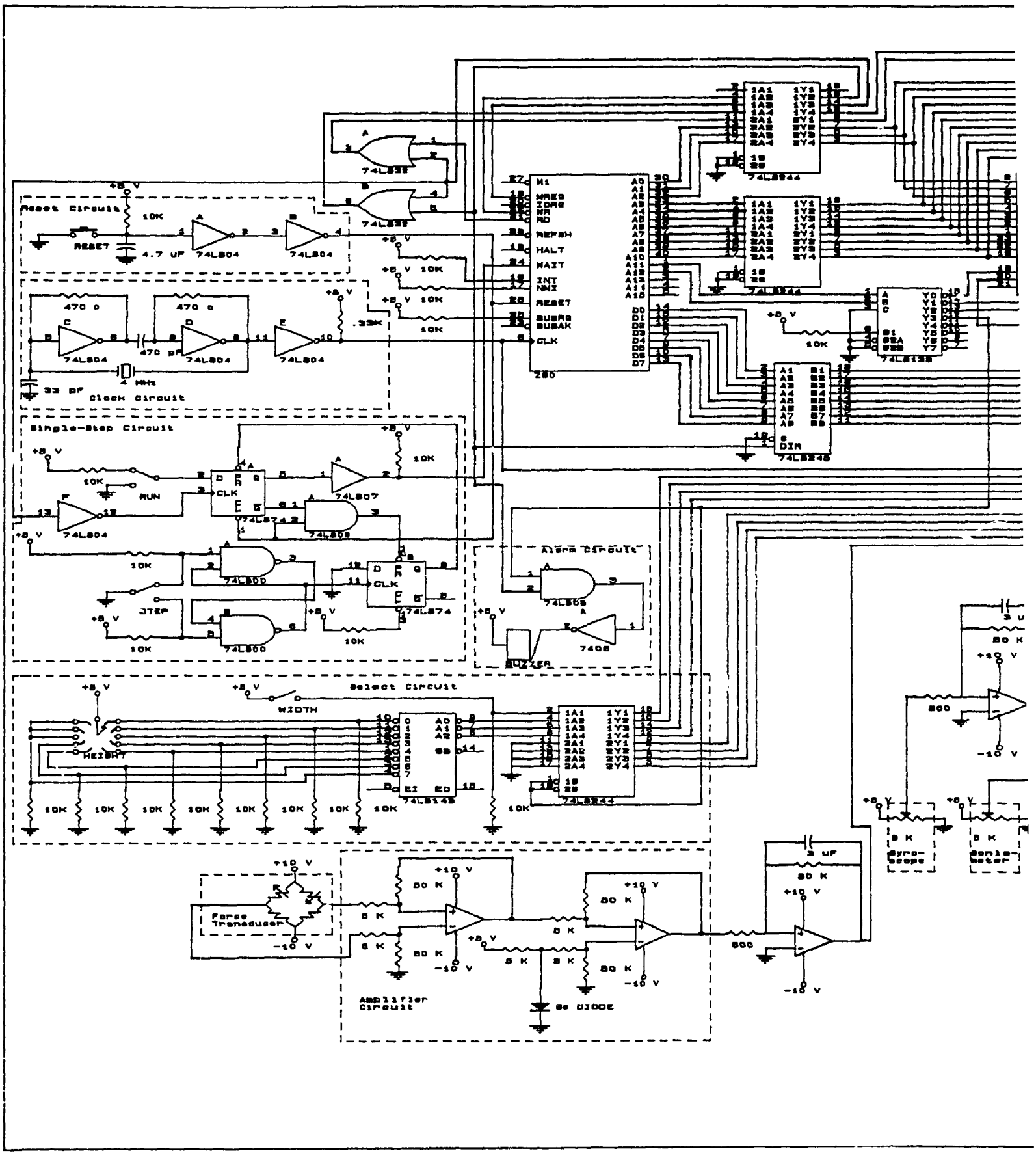

FIGURE 5.1: Circuit Diagram of the Proposed Safety Monitor

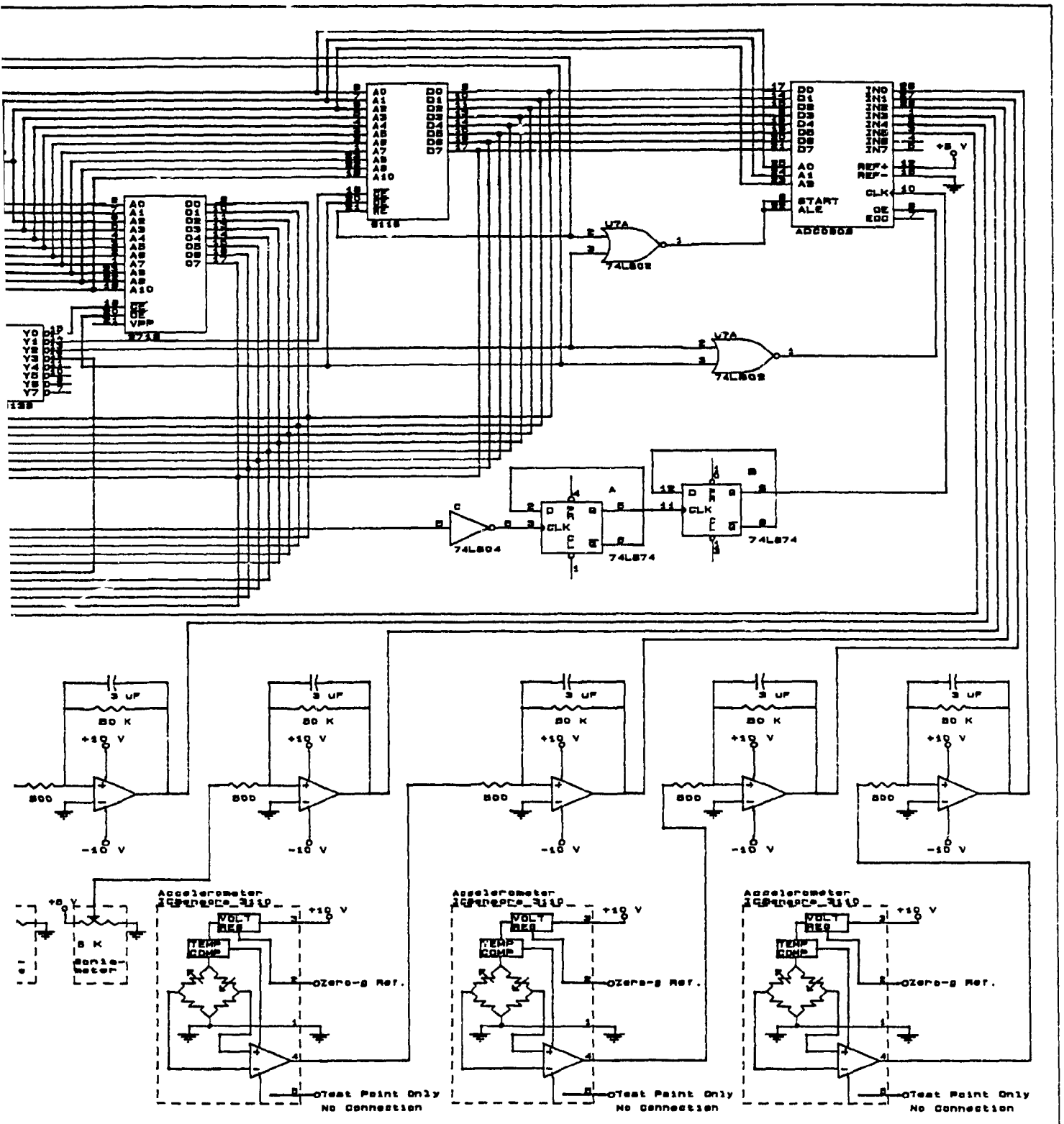

CONCAVE Research Center
Concordia University
Dept. Mech. Eng
1455 de Maisonneuve Ouest
H3G 1M8

Title: Early Warning System		
Size: C	Document Number: 1	REV: 1.3
Date: January 17, 1992	Sheet 1 of 1	

Because the reset signal obtained across the capacitor is a rising exponential and not a sharp square wave, a *Schmitt* trigger is used to yield a nearly square wave shape.

Microprocessors in general are MOS devices with very limited drive capabilities, thus bus buffering is required. The buffers with built-in *Schmitt* trigger and *tri-state* capability are employed to allow several transmitters to control the same bus line. The circuit is designed with a single-step circuit to test the hardware and to carry out diagnostics in the development stage by freezing the data on the microprocessor buses. The single-step circuit use the built-in *WAIT* state capability of the microprocessor. In the *WAIT* state the microprocessor idles, holding valid addresses, control signals, and data on its buses. The input-output are memory-mapped to reduce the number of chips and the complexity of the board. The program is stored in a two-kilobyte electrically programmable read-only memory chip (2716, 2K EPROM) and the computation results are stored in a two-kilobyte read-and-write static memory chip (6116, 2K SRAM).

5.5.2 Data Acquisition

The microprocessor can measure analog voltages by using a special interface component called an analog-to-digital converter. The integrated circuit ADC0808 from National Semiconductor provides nearly all the components needed to build a complete data acquisition system. At any given time, any one of the eight separate input signals can be sampled as selected by the three address input lines. The selected channel is converted to an 8-bit digital word after a typical conversion time of 100 microseconds. Tri-state output latches-buffers are built-in

to allow direct connection with the data bus. An external 5 volt reference voltage is required and this determines the absolute accuracy. A 1 megahertz signal is also provided by dividing the system clock by four. Internally the analog-to-digital converter uses the *successive approximations* technique for analog-to-digital conversion. A successive approximations register and analog comparators are all included on the chip. With the 5-volt reference, the input voltage range is limited to 0 to 5 volts

5.5.3 Sensors

Sensors are required to measure the vehicle response parameters related to onset of vehicle instability. An accelerometer, located at the semitrailer's sprung mass is required to measure the vehicle's lateral acceleration and to detect the onset of vehicle rollover during steady turning. Since the lateral motion of the vehicle is a low frequency phenomenon, it is desirable to select resistive accelerometers. A general purpose, solid-state piezo-resistive accelerometer with built-in amplification and temperature compensation, ICSensors 3110, is selected in view of its high resolution. The lightweight plastic housing provides easy attachment to the measurement surface. The accelerometer module consists of a silicon micro machined accelerometer, an amplifier, a signal conditioner, and a temperature compensation circuit. The accelerometer with a range of ± 9.81 m/s^2 provides a full scale output of ± 2 volts about a 2.5-volt offset. The accelerometer element is protected from shocks by over-range stops in the silicon micro-structure.

The detection of roll instability arising from high speed directional maneuvers requires the measurement of the roll angle response of the rearmost axle. The roll angle can be measured via a gyroscope attached to the axle. The VM02-0128-1 vertical gyroscope made by Humphrey with a range of ± 9 degrees can be employed. The miniature vertical gyroscope requires an input voltage of 28 volts D.C and comprises of an internal A.C. inverter for the gyroscope spin motor. The angle is measured by a 5000 ohms rotary potentiometer. The gyroscope can sustain shocks of up to 15 *g* and is packaged in a moisture proof case.

The detection of the onset of vehicle jackknife requires measurement of lateral and yaw acceleration of the tractor, articulation angle and the lateral force at the fifth wheel constraint. Two piezo-resistive accelerometers are mounted, one at the tractor chassis near the center of gravity and one near the tandem center of the drive axle, and the corresponding tractor's yaw acceleration is derived from the two lateral acceleration signals. \ strain gauge based low profile load cell (Omega LCH-20K) can be mounted to measure the lateral force at the fifth wheel constraint. The load cell provides a full scale output of 30 millivolts with a nominal excitation voltage of 10 volts D.C.. The articulation angle can be measured using a goniometer. The goniometer consists of a 5000 ohms rotary potentiometer and pulleys in a pull-cord arrangement.

5.5.4 Software

The software program is developed to compute the stability criteria and to determine the impending roll and jackknife instability from the

measured response variables. The software will provide the warning to the driver through an electronic buzzer when the onset of an instability is detected. The software reads the base parameters, such as vehicle width and the approximate center of gravity height of the trailer. The vehicle width is read from a switch which can be toggled between 2.44 meters and 2.59 meters. An eight-position rotary switch representing the approximate height of the semitrailer center of gravity can be set between 1.4 meters to 2.1 meters in 0.1 meter increments. The safe values of rollover threshold and the roll angle of the semitrailer's rearmost axle are then established by the software.

The analog-to-digital conversion is performed almost independently of the software calculating the onset of instability. The analog signals from the sensors are digitized using the analog-to-digital converter and stored in memory. The stored values are compared to the computed stability criteria to detect an impending instability. The lateral acceleration response of the semitrailer is compared to the safe value of lateral acceleration to detect a roll instability at low speeds. In the next step, the program scans the semitrailer's rearmost axle roll angle from the digitized output of the gyroscope and onset of roll instability is detected by comparing it with the safe value depending on the vehicle width. In the last step, the approximate side force is computed from the digitized signals of the two accelerometers fixed on the tractor and the force transducer fixed on the fifth wheel. The side force and measured articulation angles are filtered through a low-pass filter. The rates of change of the magnitude of articulation angle and the side force are computed. The two necessary conditions of jackknife are checked to determine impending tractor jackknife. If

onset of any instability is detected, the program will sound an electronic buzzer and continue its computations. Thus the software will continue to give the warning until the vehicle becomes directionally stable.

A listing of software written in Assembler language with the accompanying machine instructions is presented in Appendix I.

5.6 SUMMARY

The key measurable vehicle response parameters that describe the onset of vehicle instability are derived based upon the discussion presented in this chapter. The roll instability arising during a steady turn can be detected via the the semitrailer's lateral acceleration response, which can be easily measured using a piezo-resistive accelerometer. The onset of potential vehicle rollover at highway speeds is related to the roll angle response of the semitrailer's trailing axle. The axle roll angle can be measured using a miniature vertical gyroscope or a tilt sensor with appropriate lateral acceleration correction. An estimate of the approximate tractor rear axle lateral force and articulation angle can define the onset of tractor jackknife accurately. This approximate side force, calculated from the simple yaw plane model of the tractor, can be easily measured using two accelerometers and a force transducer. The articulation angle can be easily measured using a goniometer.

The onset of roll and jackknife instabilities can thus be detected via the measurement of semitrailer's lateral acceleration, trailing axle's roll angle, tractor's lateral and yaw accelerations, lateral constraint force, and articulation angle. The measured response signals

are manipulated to detect the onset of vehicle instability and to generate an early warning to the driver. The design of the proposed early warning system is presented with the description of the associated hardware and software.

CHAPTER 6

CONCLUSIONS AND RECOMMENDATIONS FOR FUTURE WORK

6.1 GENERAL

Since the introduction of electronic controls in the automotive industry, considerable efforts have been mounted to develop sensors and display devices to improve vehicle performance and driver comfort. Smart electronic control systems are now being developed to improve performance, economy and safety of heavy-duty trucks. Highway accidents involving heavy vehicles pose unreasonable risks to the safety of driver, vehicle in property in commerce. Important accident scenarios include: rollover due to sudden lane changes or high speed cornering, loss of directional control due to locked wheel during sudden stop. Of the major in-transit accident scenarios, only rollover and brake lock involve driver-vehicle interactions. The driver-vehicle interactions associated with rollover or brake lock present the potential for the recognition of impending hazardous situations using on-board measurements in order to allow the driver to take corrective action.

The overall objective of the thesis research was to contribute towards the development of an on-line safety monitor for heavy articulated vehicles that can provide an early warning of the impending instabilities. The development of an early warning safety monitor, however requires determination of dynamic response variables related to onset of roll and jackknife instabilities of the vehicle. The roll and jackknife stability limits of the five-axle tractor-semitrailer combinations are investigated via computer modeling and simulation to

determine directly measurable key parameters closely related to the onset of vehicle instabilities.

6.2 MAJOR HIGHLIGHTS OF THE INVESTIGATION

The major highlights of this investigation are summarized as follows:

(*i*) The steady turning roll stability limits of the vehicle combination are evaluated using a static roll plane model. The roll stability limits, described by the vehicle's rollover threshold lateral acceleration, are evaluated in view of various vehicle design and operational parameters.

(*ii*) A comprehensive database on suspension and tire properties is compiled to investigate the sensitivity of vehicle's rollover threshold to variations in suspension and tire properties.

(*iii*) The rollover threshold of the vehicle is related to the roliover threshold of a rigid vehicle and a compliance factor. Through computer simulation of various vehicle configurations, it is concluded that the vehicle rollover during steady turns can be detected via the vehicle's lateral acceleration response. The mean and the standard deviation values of the compliance factors are established for various vehicle configurations to further demonstrate that the lateral acceleration response is the key parameter related to the onset of vehicle rollover during steady turns.

(*iv*) The roll stability of vehicle combination corresponding to directional maneuvers executed at highway speeds is investigated through a three dimensional directional dynamic model of the vehicle. The computer simulations are carried out for lane change and evasive steering maneuvers at typical highway speeds.

(*v*) The onset of vehicle rollover is related to the response parameters, such as dynamic wheel load, dynamic suspension load and axle roll angle. The feasibility of these parameters is investigated in view of their acquisition and it is concluded that the roll angle response of the semitrailer's trailing axle provides the most reliable information concerning the onset of vehicle rollover at highway speeds.

(*vi*) The tractor jackknife behavior is investigated using the Phase IV model, developed by UMTRI. The directional response of the tractor-semitrailer vehicle is evaluated for simultaneous braking and steering maneuvers. The onset of tractor jackknife is related to the rate of change of cornering forces generated at the drive axle tires and the sideslip angle.

(*vii*) Recognizing tha the measurement of side forces and sideslip angles is quite complex, the onset of vehicle jackknife is described by an approximate side force computed from the yaw plane of the tractor. The vehicle jackknife is expressed by two necessary conditions

related to the rate of change of the approximate side force and the articulation angle.

(*viii*) The identified key parameters are discussed in view of their feasibility and ease of measurement. Design of an early warning safety monitor, and the associated hardware and software are presented.

6.3 CONCLUSIONS

Based upon the study, the following conclusions are drawn:

- The onset of roll instability of the vehicle can be directly related to the rearmost axle's wheel liftoff and thus the dynamic normal load acting on the rearmost axle's tires.
- The onset of vehicle jackknife is directly related to the cornering forces and sideslip angles developed at the drive axle's tires.
- The detection of vehicle instability via dynamic wheel loads, cornering forces and sideslip angles requires quite complex measurements.
- The vehicle's roll instability during steady turns can be related to vehicle's lateral acceleration response, which can be easily measured.
- The roll instability of the vehicle subject to directional maneuvers at highway speeds can be characterized via the roll angle response of the semitrailer axles.
- The cornering forces and sideslip angles developed at the drive axle tires are related to the approximate lateral force,

derived from the yaw plane, and the articulation angle, respectively.

- The approximate lateral force can be manipulated from the lateral force at the constraint, lateral acceleration response and the tractor geometry.
- The onset of vehicle jackknife is related to the rate of change of approximate side force and the articulation angle.
- An on-line monitoring of vehicle's lateral acceleration, lateral force at the fifth wheel constraint, rearmost axle's roll angle and articulation angle response characteristics provides the basis for warning the driver to take appropriate corrective action.
- An early warning safety monitor can be realized to minimize the number of highway accidents attributed to inadequate driver-vehicle interactions.

6.4 RECOMMENDATIONS FOR FURTHER WORK

The study presents the key parameters related to onset of instabilities in a five-axle tractor-semitrailer combination and their acquisition. The realization of a comprehensive and reliable early warning safety monitor will require further testing and simulations. The following recommendations are made to realize the early warning safety monitor for heavy vehicle combinations:

a. The proposed safety monitor should be built and tested in the laboratory along with the software.

b. Field tests should be conducted to establish (*i*) the

reliability of the safety monitor and (*ii*) driver's reactions to the warning.

c. Studies on development of low cost and reliable sensors can certainly accelerate the implementation of such safety monitor. Specifically, the highly expensive and fragile gyroscope required to measure the axle roll angle needs to be replaced by a low cost and rugged roll angle sensor.

d. The influence of cross-slope of highways and ramps on the key parameters related to onset of vehicle instabilities needs to be investigated in order to ensure adequate operation of the safety monitor.

e. Vehicle configurations, such as tri- and quad-axle tractor-semitrailers, and B-trains should be investigated using the proposed methodology to derive the corresponding key parameters related to the onset of instability.

f. The effect of vehicle speed on the key parameters related to the onset of instability should be studied.

g. The models should be expanded to include the study of the effect of cargo shift, such as in partially filled tanker trucks, or improperly/unevenly loaded trucks to derive the corresponding key parameters related to the onset of instability.

h. Key parameters related to the onset of instability should also be studied for other types of trucks, such as trucks with and without trailers, trucks or tractors with dual front axles.

REFERENCES

1. Robert D. Ervin and Guy Yoram, The Influence of Weights and Dimensions on the Stability and Control of Heavy Duty Trucks in Canada, portions of a draft Report, University of Michigan Transportation Research Institute, 1986.

2. Robert D. Ervin, The Influence of Size and Weight Variables on the Roll Stability of Heavy Duty Trucks, SAE Paper 831163, 1983.

3. Robert E. Heglund, Truck Safety - An Agenda for the Future, SAE Publication No P-181, 1986, p. 154.

4. Hank Seiff, "Large Truck Accident Exposure in the U.S.", Symposium sur le Rôle des Poids Lourds dans les Accidents de la Circulation, OCDE, Montréal, Québec, 1987.

5. Robert M. Clarke, "Vehicle Factors in Accidents Involving Heavy Freight Vehicles", Symposium sur le Rôle des Poids Lourds dans les Accidents de la Circulation, OCDE, Montréal, Québec, 1987.

6. B. E. Horn, "OECD Emphasis on Highway Freight Transportation Issues and Truck Safety", Symposium sur le Rôle des Poids Lourds dans les Accidents de la Circulation, OCDE, Montréal, Québec, 1987.

7. P. Hamelin, "Risque d'Implication des Conducteurs de Poids Lourds dans les Accidents de la Circulation en Fonction de leurs 'Habitudes Temporelles de Travail' et de leurs Caractéristiques Professionnelles", Symposium sur le Rôle des poids Lourds dans les Accidents de la Circulation, OCDE, Montréal, Québec, 1987.

8. F. Vlk, "Lateral Dynamics of Commercial Vehicle Combinations - A Literature Survey", Vehicle System Dynamics, vol. 11, 1982, pp. 305-324.

9. A. G. Nalecz and J. Genin, "Dynamic Stability of Heavy Articulated Vehicles", International Journal of Vehicle Design, vol. 5, no. 4 1984, pp. 417-426.

10. P. S. Fancher, "The Static Stability of Articulated Commercial Vehicles", Vehicle System Dynamics, vol. 14, 1985, pp. 201-227.

11. F. Vlk, "Handling Performance of Truck-Trailer Vehicles: A State-of-the-Art Survey", International Journal of Vehicle Design, vol. 6, no. 3, 1985, pp. 323-361.

12. E. A. Susemihl and A. I. Krauter, "Jackknifing of Tractor-Semitrailer Trucks - Detection and Corrective Action", Journal of Dynamic Systems, Measurement, and Control, Transactions ASME, 1974, pp. 244-252.

13. G. R. Larocque *et al.*, Feasibility Study of a System Safety Monitor for Hazardous Material Trucking, SAE Paper 852357, 1985.

14. Robert D. Ervin *et al.*, Influence of Size and Weights Variables on the Stability and Control Properties of Heavy Trucks', Report UMTRI-83-10-2, University of Michigan Transportation Research Institute, 1983.

15. F. Vlk, "Stationar- und Ubergangsverhalten von Sattel- und Lastzugen bei der Kreisfahrt: Lineare Berechnungen", Vehicle System Dynamics, vol. 12, 1983, pp. 331-350.

16. I. Schmid, Engineering Approach to Truck and Tractor Train Stability, SAE paper 670006, 1967.

17. F. D. Snelgrove *et al.*, Performance Evaluation of Several Jackknife Control Devices, Report CVOS-TR-80-03, Ontario Ministry of Transportation and Communications, Toronto, Ontario, 1980.

18. C. Mallikarjunarao and P. Fancher, Analysis of the Directional Response Characteristics of Double Tankers, SAE Paper 781064, 1978.

19. H. K. Brewer and R. S. Rice, Tires - Stability and Control, SAE Paper 830561, 1983.

20. D. B. Johnson and J. C. Huston, Nonlinear Lateral Stability Analysis of Road Vehicles using Liapunov's Second Method, SAE Paper 841057, 1984.

21. P. M. Leucht, The Directional Dynamics of the Commercial Tractor-Semitrailers during Braking, SAE Paper 700371, 1970.

22. J. E. Bernard, A Digital Computer Method for the Prediction of the Directional Response of Trucks and Tractor-Trailers, SAE Paper 740138, 1974.

23. E. A. Susemihl and A. I. Krauter, Automatic Stabilization of Tractor Jackknifing in Tractor-Semitrailer Trucks, SAE Paper 740551, 1974.

24. C. Mallikarjunarao *et al.*,'Roll Response of Articulated Motor Trucks during Steady-Turning Maneuvers', Computational Method in Ground Transportation Vehicles, ASME Winter Annual Meeting, Nov. 1982, pp. 133-152.

25. C. B. Winkler *et al.*, Testing the Michigan Double-Bottom Tanker', SAE Paper 781066, 1978.

26. J. Y. Wong and M. El-Gindy, Computer Simulation of Heavy Vehicle Dynamics Behavior - Users Guide to UMTRI Models, Number 3, University of Michigan Transportation Research Institute, 1985.

27. Council of Ministers of Transportation and Highway Safety, The Memorandum of Understanding on Interprovincial Vehicle Weights and Dimensions, Summary Information, 1988.

28. J. Nuotio, "Heavy traffic transport on the Finnish road network", Symposium sur le rôle des poids lourds dans les accidents de la circulation, OCDE, Montréal, Québec, 1987.

29. Robert D. Ervin *et al.*, Future Configuration of Tank Vehicles Hauling Flammable Liquids in Michigan, Report UM-HSRI-80-73-2, University of Michigan Transportation Research Institute, 1980.

30. S. Rakheja *et al.*, "Roll Plane Analysis of Articulated Tank Vehicles during steady turning", Vehicle System Dynamics, no. 17, 1988, pp. 81-104.

31. Robert E. Heglund, Truck-Safety - An Agenda for the Future, SAE Publication No P-181, Handling/Stability Session, 1986.

32. D. W. G. Miller and N. F. Barter, "Roll-Over of Articulated Vehicles", Proceedings of the Institute of Mechanical Engineers, C203/73, 1973.

33. F. Uffelmann, "Automotive Stability and Handling Dynamics in Cornering and Braking Maneuvers", Vehicle System Dynamics, vol. 12, 1983, pp. 203-223.

34. M. J. Vanderploeg and J. E. Bernard, "Dynamics of Double Bottom Commercial Vehicles", International Journal of Vehicle Design, vol. 6, no. 2, 1985, pp. 139-148.

35. M. K. Verma and T. D. Gillespie, "Roll Dynamics of Commercial Vehicles", Vehicle System Dynamics, vol. 9, 1980, pp. 1-17.

36. C. C. MacAdam, A Computer-Based Study of the Yaw/Roll Stability of Heavy Trucks Characterized by High Centers of Gravity, SAE paper 821260, 1982.

37. W. B. Diboll and D. H. Hagen, "Lateral Stability of Road and Rail Trailers", Journal of Engineering for Industry, Transactions ASME, 1969, pp. 1069-1074.

38. T. E. Kashmerick, Vehicle Equipment Installation for Best Ride Match, SAE Paper 690766, 1969.

39. T. D. Gillespie and C. B. Winkler, "On the Directional Response Characteristics of Heavy Vehicles", 2nd IUTAM Symposium on Dynamics of Vehicles on Roads and Tracks, 1977, pp. 165-183.

40. R. L. Collins and J. P. Wong, "Stability of Car Trailer Systems with Special Regard to Trailer Design", Journal of Dynamic Systems, Measurement, and Control, Transactions ASME, 1974, pp. 236-243.

41. D. B. Johnson *et al.*, The Influence of Drawbar Flexibility and Roll Steer on the Stability of Articulated Vehicles, SAE Paper 790183, 1979.

42. J. C. Huston and D. B. Johnson, Relative Significance of Parameters Affecting Lateral Stability of Articulated Recreational Vehicles, SAE Paper 790184, 1979.

43. D. A. Crolla and F. D. Hales "The Lateral Stability of Tractor and Trailer Combinations", Journal of Terramechanics, vol. 16, no. 1, 1979, pp 1-22.

44. R. T. Klein and H. T. Szostak, Determination of Trailer Stability Through Simple Analytical Methods and Test Procedures, SAE Paper 790186, 1979.

45. E. C. Mikulcik, "Stability Criteria for Automobile-Trailer Combinations", Vehicle System Dynamics, vol. 9, 1980, pp. 281-289.

46. J. C. Huston and D. B. Johnson, Basic Analytical Results for Lateral Stability of Car/Trailer Systems, SAE Paper 820136, 1982.

47. P. S. Fancher, The Transient Directional Response of Full Trailers, SAE Paper 821259, 1982.

48. A. F. D'Souza and R. L. Eshleman, "Maneuverability Limits and Handling Criterion of Articulated Vehicles", Computational Methods in Ground Transportation Vehicles, ASME Winter Annual Meeting, Nov. 1982, pp. 117-132.

49. H.-C. Pflug, "Lateral Dynamic Behavior of Truck-Trailer Combinations due to the Influence of the Load", Vehicle System Dynamics, vol. 15, 1986, pp. 155-175.

50. S. Tousi *et al.*, "On the Stability of a Flexible Vehicle Controlled by a Human Pilot", Vehicle System Dynamics, vol. 17, 1988, pp. 37-56.

51. B. W. Mooring and J. Genin, "A Kinematic Constraint Method for Stability Analysis of Articulated Vehicles", International Journal of Vehicle Design, vol. 3, no. 2, 1982, pp. 190-201

52. S. Sankar *et al.*, "Effect of Wheel Slip on the Stability and Stopping Ability of a Road Vehicle", International Journal of Vehicle Design, vol. 3, no. 1, 1982, pp. 77-89.

53. H. K. Sachs and C. C. Chou, "On the Stability in the Sense of Liapunov of a Rubber Tire Vehicle", Journal of Dynamics Systems, Measurement, and Control, Transactions ASME, 1976, pp. 180-185.

54. J. C. Huston and D. B. Johnson, Effect of the Normal Force Dependence of Cornering Stiffness on the Lateral Stability of Recreational Vehicles, SAE Paper 800161, 1985.

55. H. B. Pacejka, "In-Plane and Out-of-Plane Dynamics of Pneumatic Tyres", Vehicle System Dynamics, vol. 10, 1981, pp. 221-251.

56. L. Segel and Robert D. Ervin, "The Influence of Tire Factors on the Stability of Trucks and Tractor Trailers", Vehicle System Dynamics, Vol. 10, 1981, pp. 37-59.

57. V. S. Verma *et al.*, "The Directional Behavior during Braking of a Tractor/Semi-Trailer Fitted with Anti-Locking Devices", International Journal of Vehicle Design, vol. 1, no. 3, 1980, pp. 195-220.

58. R. E. Nelson and J. W. Fitch, Optimum Braking, Stability and Structural Integrity for Longer Truck Combinations, SAE Paper 680547, 1968.

59. R. H. Johnston, "Speed Measurement by Radar for Anti-Lock Braking", International Conference on Automotive Electronics, IEE Conference Publication No. 181, 1979.

60. P. Feske and E. Petersen, Progress of the WABCO ABS for Commercial Vehicle in the North American Market, SAE Paper 861978, 1986.

61. H. Decker and R. Stock, BOSH-ABS-Designed for the User, SAE Paper 861977, 1986.

62. E. Göhring, Reliability of Daimler-Benz/WABCO Anti-Lock Systems - Five Years of Experience after Production Began, SAE Paper 880986, 1988.

63. E. Petersen, *et al.* Anti-Lock Braking Systems (ABS) with Integrated Drive Slip Control (ASR) for Commercial Vehicles, SAE Paper 861961, 1986.

64. D. Kramer *et al.*, Drive Axle Antilock for Heavy Vehicle Stability, SAE Paper 871572, 1987.

65. Paul A. Croce *et al.*, A Feasibility Study of a Sealed Safety Monitor for Trucks Carrying LNG and Other Hazardous Materials, Report DOE/EV/10502-1, 1982.

66. Peter Carracher, "Status of Technological Development of Heavy Freight Vehicles: Other Major Factor Influencing Traffic Safety", Symposium sur le Rôle des Poids Lourds dans les Accidents de la Circulation, OCDE, Montréal, Québec 1987.

67. C. C. Macadam *et al.*, A Computerized Model for Simulating the Braking and Steering Dynamics of Trucks, Tractor-Semitrailers, Doubles and Triples Combinations - User's Manual, Report UM-HSRI-80-58, University of Michigan Transportation Institute, 1980.

68. M. El-Gindy and J. Y. Wong, "Comparison of Various Computer Simulation Models for Predicting the Directional Responses of Articulated Vehicles", Vehicle System Dynamics, no. 16, 1987, pp. 249-268.

APPENDIX I

LISTING OF THE EARLY WARNING SAFETY MONITOR SOFTWARE

```
0000 F3            DI              ;DISABLE INTERRUPTS
0001 31FF0F        LD SP,0FFFH     ;LOAD HIGHEST ADDRESS IN STACK
0004 3A0018        LD A,(1800H)    ;LOAD THE SELECTOR VALUE IN A
0007 320008        LD (0800H),A    ;LOAD THE SELECTOR VALUE AT 0800
000A CB47          BIT 0,A         ;TEST FOR VEHICLE WIDTH
000C 2856          JR Z,N9         ;IF SWITCH INDICATES 96 INCHES
000E 3D            DEC A           ;
000F 281F          JR Z,N1         ;CHECK FOR 59 INCHE CG HEIGHT
0011 D602          SUB 2H          ;
0013 2822          JR Z,N2         ;CHECK FOR 63 INCHE CG HEIGHT
0015 D602          SUB 2H          ;
0017 2825          JR Z,N3         ;CHECK FOR 67 INCHE CG HEIGHT
0019 D602          SUB 2H          ;
001B 2828          JR Z,N4         ;CHECK FOR 71 INCHE CG HEIGHT
001D D602          SUB 2H          ;
001F 282B          JR Z,N5         ;CHECK FOR 75 INCHE CG HEIGHT
0021 D602          SUB 2H          ;
0023 282E          JR Z,N6         ;CHECK FOR 79 INCHE CG HEIGHT
0025 D602          SUB 2H          ;
0027 2831          JR Z,N7         ;CHECK FOR 83 INCHE CG HEIGHT
0029 3E70          LD A,70H        ;
002B 320208        LD (0802H),A    ;LOAD 106 IN/SEC**2 IN 0802H
002E 182F          JR N8           ;
0030 3EA6    N1    LD A,0A6H       ;
0032 320208        LD (0802H),A    ;LOAD 157 IN/SEC**2 IN 0802H
0035 1828          JR N8           ;
0037 3E9B    N2    LD A,9BH        ;
0039 320208        LD (0802H),A    ;LOAD 147 IN/SEC**2 IN 0802H
003C 1821          JR N8           ;
003E 3E92    N3    LD A,92H        ;
0040 320208        LD (0802H),A    ;LOAD 138 IN/SEC**2 IN 0802H
0043 181A          JR N8           ;
0045 3E89    N4    LD A,89H        ;
0047 320208        LD (0802H),A    ;LOAD 130 IN/SEC**2 IN 0802H
004A 1813          JR N8           ;
004C 3E82    N5    LD A,82H        ;
004E 320208        LD (0802H),A    ;LOAD 123 IN/SEC**2 IN 0802H
0051 180C          JR N8           ;
0053 3E7C    N6    LD A,7CH        ;
0055 320208        LD (0802H),A    ;LOAD 117 IN/SEC**2 IN 0802H
0058 1805          JR N8           ;
005A 3E75    N7    LD A,75H        ;
005C 320208        LD (0802H),A    ;LOAD 111 IN/SEC**2 IN 0802H
005F 3E14    N8    LD A,14H        ;
0061 320108        LD (0801H),A    ;LOAD 1.41 DEGREES IN 0801H
0064 3E01    N9    LD A,1H         ;
0066 CB47          BIT 0,A         ;RESET ZERO FLAG
```

```
0068 3A0008          LD A,(0800H)
006B CBC7            SET 0,A
006D 3D              DEC A              ;
006E 281F            JR Z,N10           ;CHECK FOR 59 INCHE CG HEIGHT
0070 D602            SUB 2H             ;
0072 2822            JR Z,N11           ;CHECK FOR 63 INCHE CG HEIGHT
0074 D602            SUB 2H             ;
0076 2825            JR Z,N12           ;CHECK FOR 67 INCHE CG HEIGHT
0078 D602            SUB 2H             ;
007A 2828            JR Z,N13           ;CHECK FOR 71 INCHE CG HEIGHT
007C D602            SUB 2H             ;
007E 282B            JR Z,N14           ;CHECK FOR 75 INCHE CG HEIGHT
0080 D602            SUB 2H             ;
0082 282E            JR Z,N15           ;CHECK FOR 79 INCHE CG HEIGHT
0084 D602            SUB 2H             ;
0086 2831            JR Z,N16           ;CHECK FOR 83 INCHE CG HEIGHT
0088 3E78            LD A,78H           ;
008A 320208          LD (0802H),A       ;LOAD 114 IN/SEC**2 IN 0802H
008D 182F            JR N17             ;
008F 3EB1      N10   LD A,0B1H          ;
0091 320208          LD (0802H),A       ;LOAD 168 IN/SEC**2 IN 0802H
0094 1828            JR N17             ;
0096 3EA6      N11   LD A,0A6H           ;
0098 320208          LD (0802H),A       ;LOAD 157 IN/SEC**2 IN 0802H
009B 1821            JR N17             ;
009D 3E9C      N12   LD A,9CH           ;
009F 320208          LD (0802H),A       ;LOAD 148 IN/SEC**2 IN 0802H
00A2 181A            JR N17             ;
00A4 3E94      N13   LD A,94H           ;
00A6 320208          LD (0802H),A       ;LOAD 140 IN/SEC**2 IN 0802H
00A9 1813            JR N17             ;
00AB 3E8B      N14   LD A,8BH           ;
00AD 320208          LD (0802H),A       ;LOAD 132 IN/SEC**2 IN 0802H
00B0 180C            JR N17             ;
00B2 3E84      N15   LD A,84H           ;
00B4 320208          LD (0802H),A       ;LOAD 125 IN/SEC**2 IN 0802H
00B7 1805            JR N17             ;
00B9 3E75      N16   LD A,75H           ;
00BB 320208          LD (0802H),A       ;LOAD 111 IN/SEC**2 IN 0802H
00BE 3E12      N17   LD A,12H           ;
00C0 320108          LD (0801H),A       ;LOAD 1.26 DEGREES IN 0801H
00C3 3E01            LD A,1H            ;
00C5 CB47            BIT 0,A            ;RESET ZERO FLAG
00C7 3A0308    N43   LD A,(803H)        ;LOAD PREVIOUS VALUE OF ACC#1
00CA CB7F            BIT 7H,A           ;CHECK FOR SIGN OF THE ACC
00CC 2804            JR Z,N18
00CE D680            SUB 80H            ;PUT ABSOLUTE VALUE OF ACC
00D0 1804            JR N19
00D2 47        N18   LD B,A
00D3 3E80            LD A,80H
00D5 90              SUB B
00D6 320908    N19   LD (809H),A        ;MULTIPLY ACCELERATION 1 BY 4
00D9 3E04            LD A,4H
```

```
00DB 320A08          LD (80AH),A
00DE CD3502          CALL UMUL8
00E1 3A0B08          LD A,(080BH)       ;LOAD ACC VALUE IN A
00E4 47              LD B,A             ;LOAD ACC VALUE IN B
00E5 3A0208          LD A,(0802H)       ;LOAD SAFE VALUE IN A
00E8 90              SUB B              ;SUBSTRACT CHECK IF ACC SAFE
00E9 3802            JR C,N24
00EB 1803            JR N25
00ED 320018    N24   LD (1800H),A       ;SOUND BUZZER LAT ACC EXC. SAFE
00F0 3A0708    N25   LD A,(0807H)       ;LOAD PREV. VALUE OF ROLL ANGLE
00F3 CB7F            BIT 7H,A           ;CHECK FOR SIGN OF THE ROLL ANG
00F5 2804            JR Z,N26
00F7 D680            SUB 80H            ;PUT ABSOLUTE VALUE OF ROLL ANG
00F9 1804            JR N27
00FB 47        N26   LD B,A
00FC 3E80            LD A,80H
00FE 90              SUB B
00FF 47        N27   LD B,A             ;LOAD ROLL ANGLE VALUE IN B
0100 3A0208          LD A,(0802H)       ;LOAD SAFE VALUE IN A
0103 90              SUB B              ;SUBSTRACT CHECK ANG EXC. SAFE
0104 3802            JR C,N28
0106 180C            JR N29
0108 320018    N28   LD (1800H),A       ;SOUND BUZZER ROLL ANG EXC. SAFE
010B 3A0018          LD A,(1800H)       ;LOAD CONVERTED VALUE OF ACC1
010E 320308          LD (0803H),A       ;SAVE IT IN MEMORY
0111 320118          LD (1801H),A       ;START CONVERSION ON ACC2
0114 3A0408    N29   LD A,(0804H)       ;LOAD PREV. VALUE OF LAT ACC#2
0117 CB7F            BIT 7H,A           ;CHECK FOR SIGN OF THE ACC
0119 2804            JR Z,N30
011B D680            SUB 80H            ;PUT ABSOLUTE VALUE OF ACC
011D 1804            JR N31
011F 47        N30   LD B,A
0120 3E80            LD A,80H
0122 90              SUB B
0123 6F        N31   LD L,A             ;EXTEND NEG ACC TO 16 BIT SIGNED
0124 87              ADD A,A
0125 9F              SBC A,A
0126 67              LD H,A
0127 1E04            LD E,4
0129 1600            LD D,0
012B CD4D02          CALL MUL16         ;MULTIPLY ACCELERATION BY 4
012E 221008          LD (0810H),HL      ;TRACTOR CG LAT ACC IN/SEC**2
0131 3A0018          LD A,(1800H)       ;LOAD CONVERTED VALUE OF ACC2
0134 320408          LD (0804H),A       ;SAVE IT MEMORY
0137 320218          LD (1802H),A       ;START CONVERSION ON ACC3
013A 3A0508          LD A,(0805H)       ;LOAD PREVIOUS VALUE OF ACC#3
013D CB7F            BIT 7H,A           ;CHECK FOR SIGN OF THE ACC
013F 2804            JR Z,N32
0141 D680            SUB 80H            ;PUT ABSOLUTE VALUE OF ACC
0143 1804            JR N33
0145 47        N32   LD B,A
0146 3E80            LD A,80H
0148 90              SUB B
```

```
0149 6F        N33   LD L,A            ;EXTEND NEG ACC TO 16 BIT SIGNED
014A 87              ADD A,A
014B 9F              SBC A,A
014C 67              LD H,A
014D 1E04            LD E,4
014F 1600            LD D,0
0151 CD4D02          CALL MUL16        ;MULTIPLY ACCELERATION BY 4
0154 221208          LD (0812H),HL     ;TRACTOR LAT ACC AT DRIVE AXLES
0157 3A0018          LD A,(1800H)      ;LOAD CONVERTED VALUE OF ACC3
015A 320508          LD (0805H),A      ;SAVE IT IN MEMORY
015D 320318          LD (1803H),A      ;START CONVERSION ON GONIOMETER
0160 3A0808          LD A,(0808H);     ;LOAD PREV.B VALUE OF LAT FORCE
0163 CB7F            BIT 7H,A          ;CHECK FOR SIGN OF LATERAL FORCE
0165 2804            JR Z,N34
0167 D680            SUB 80H           ;PUT ABSOLUTE VALUE OF LAT FORCE
0169 1804            JR N35
016B 47        N34   LD B,A
016C 3E80            LD A,80H
016E 90              SUB B
016F 6F        N35   LD L,A            ;EXTEND NEG LAT F TO 16 BIT SIG.
0170 87              ADD A,A
0171 9F              SBC A,A
0172 67              LD H,A
0173 1E9C            LD E,9CH
0175 1600            LD D,0
0177 CD4D02          CALL MUL16        ;MULTIPLY LATERAL FORCE BY 156
017A 3A0018          LD A,(1800H)      ;LOAD CONVERTED VALUE OF GONIO
017D 47              LD B,A
017E 3A0608          LD A,(0806H)      ;SAFE PREVIOUS VALUE OF ART ANG
0181 322008          LD (0820H),A
0184 78              LD A,B            ;SAVE IT IN MEMORY
0185 3A0608          LD A,(0806H)
0188 320418          LD (1804H),A      ;START CONVERSION ON GYROSCOPE
018B 221408          LD (0814H),HL     ;LATERAL FORCE IN LBS
018E 2A1008          LD HL,(810H)      ;LAT2 - LAT1 FOR ANG ACC
0191 A7              AND A
0192 ED4B1208        LD BC,(812H)
0196 ED42            SBC HL,BC
0198 221608          LD (0816H),HL     ;TRACTOR YAW ACC
019B 2A1008          LD HL,(0810H)     ;FR CALCULATION
019E 118507          LD DE,0785H
01A1 CD4D02          CALL MUL16
01A4 3A0018          LD A,(1800H)      ;LOAD CONVERTED VALUE OF GYRO
01A7 320708          LD (0807H),A      ;SAVE IT IN MEMORY
01AA 320518          LD (1805H),A      ;START CONVERSION ON FORCE TRAN.
01AD 221808          LD (0818H),HL     ;MT*AY*X1
01B0 2A1608          LD HL,(0816H)
01B3 11A604          LD DE,4A6H
01B6 CD4D02          CALL MUL16
01B9 3A0018          LD A,(1800H)      ;LOAD CONVERTED VALUE OF F  TRAN
01BC 320808          LD (0808H),A      ;SAVE IT IN MEMORY
01BF 320018          LD (1800H),A      ;START CONVERSION ON ACC#1
01C2 221A08          LD (081AH),HL     ;IZZ*WZ
```

```
01C5 2A1408          LD HL,(0814H)
01C8 1EAF            LD E,0AFH
01CA 1600            LD D,0
01CC CD4D02          CALL MUL16
01CF 221C08          LD (081CH),HL      ;F5Y*(X1+X5)
01D2 2A1808          LD HL (0818H)
01D5 A7              AND A
01D6 ED4B1A08        LD BC,(081AH)
01DA ED42            SBC HL,BC
01DC A7              AND A
01DD ED4B1C08        LD BC,(081CH)
01E1 ED42            SBC HL,BC
01E3 1EBE            LD E,0BEH
01E5 1600            LD D,0
01E7 CD6302          CALL SDIV16
01EA CB7C            BIT 7H,H
01EC 2807            JR Z,N36
01EE F9              LD BC,HL
01EF 210000          LD HL,0
01F2 A7              AND A
01F3 ED42            SBC HL,BC          ;PUT ABSOLUTE VALUE OF FR
01F5 F9        N36   LD DE,HL           ;SUBSTRACT OLD VALUE OF ABS FR
01F6 A7              AND A              ;FROM NEW VALUE OF ABS FR
01F7 ED4B1E08        LD BC,(081EH)
01FB ED42            SBC HL,BC
01FD ED531E08        LD (081EH),DE      ;FR
0201 202E            JR NZ,N37          ;IF DIFF IN FR=0 CHECK ART ANG
0203 3A0608          LD A,(806H)        ;LOAD PREVIOUS VALUE OF ART ANG
0206 CB7F            BIT 7H,A           ;CHECK FOR SIGN OF THE ART ANGLE
0208 2804            JR Z,N38
020A D680            SUB 80H
020C 1804            JR N39
020E 47        N38   LD B,A
020F 3E80            LD A,80H
0211 90              SUB B
0212 322108    N39   LD (0821H),A
0215 3A2008          LD A,(0820H)        ;LOAD OLD VALUE OF ART ANGLE
0218 CB7F            BIT 7H,A           ;CHECK FOR SIGN OF THE ART ANGLE
021A 2804            JR Z,N40
021C D680            SUB 80H
021E 1804            JR N41
0220 47        N40   LD B,A
0221 3E80            LD A,80H
0223 90              SUB B
0224 47        N41   LD B,A
0225 3A2108          LD A,(0821H)
0228 90              SUB B
0229 CB7F            BIT 7H,A
022B 2003            JR NZ,N42
022D 320018          LD (1800H),A       ;SOUND BUZZER ROLL ANG EXC. SAFE
0230 00        N42   NOP
0231 00        N37   NOP
0232 C3C700          JP N43
```

```
0235                                    ;SUBROUTINES
0235            UMUL8                   ;UNSIGNED MULTIPLICATION 8 BIT
0235 210908           LD HL,809H
0238 5E               LD E,(HL)         ;GET MULTIPLICAND
0239 1600             LD D,0            ;EXTEND TO 16 BITS
023B 23               INC HL
023C 7E               LD A,(HL)         ;GET MULTIPLIER
023D 210000           LD HL,0           ;PRODUCT=ZERO
0240 0608             LD B,8            ;COUNT = MULYIPLIER BIT LENGHT
0242 29         MULT  ADD HL,HL         ;SHIFT PRODUCT LEFT 1 BIT
0243 17               RLA               ;SHIFT MULTIPLIER LEFT 1 BIT
0244 3001             JR NC,CHCNT       ;IS CARRY FROM MULTIPLIER 1?
0246 19               ADD HL,DE         ;ADD MULTIPLICAND TO PRODUCT
0247 10F9       CHCNT DJNZ MULT
0249 220B08           LD (080BH),HL     ;SAVE PRODUCT IN MEMORY
024C C9               RET
024D            MUL16                   ;SIGNED MULTIPLICATION 16 BIT
024D 4D               LD C,L
024E 44               LD B,H
024F 210000           LD HL,0
0252 3E0F             LD A,15
0254 CB23       MLP   SLA E
0256 CB12             RL D
0258 3001             JR NC,MLP1
025A 09               ADD HL,BC
025B 29         MLP1  ADD HL,HL
025C 3D               DEC A
025D 20F5             JR NZ,MLP
025F B2               OR D
0260 F0               RET P
0261 09               ADD HL,BC
0262 C9               RET
0263            SDIV16                  ;SIGNED DIVISION OF 16 BIT
0263 7C               LD A,H
0264 32CC02           LD (SREM),A
0267 AA               XOR D
0268 32CB02           LD (SQUOT),A
026B 7A               LD A,D
026C B7               OR A
026D F27602           JP P,CHKDE
0270 97               SUB A
0271 93               SUB E
0272 5F               LD E,A
0273 9F               SBC A,A
0274 92               SUB D
0275 57               LD D,A
0276 7C         CHKDE LD A,H
0277 B7               OR A
0278 F28102           JP P,DODIV
027B 97               SUB A
027C 95               SUB L
027D 6F               LD L,A
027E 9F               SBC A,A
```

```
027F 94              SUB H
0280 67              LD H,A
0281 CD9E02     DODIV CALL UDIV16
0284 D8              RET C
0285 3ACB02          LD A,(SQUOT)
0288 B7              OR A
0289 F29202          JP P,DOREM
028C 97              SUB A
028D 95              SUB L
028E 6F              LD L,A
028F 9F              SBC A,A
0290 94              SUB H
0291 67              LD H,A
0292 3ACC02     DOREM LD A,(SREM)
0295 B7              OR A
0296 F0              RET P
0297 97              SUB A
0298 93              SUB E
0299 5F              LD E,A
029A 9F              SBC A,A
029B 92              SUB D
029C 57              LD D,A
029D C9              RET
029E            UDIV16
029E 7B              LD A,E
029F B2              OR D
02A0 2007            JR NZ,DIVIDE
02A2 210000          LD HL,0
02A5 54              LD D,H
02A6 5D              LD E,L
02A7 37              SCF
02A8 C9              RET
02A9            DIVIDE
02A9 4D              LD C,L
02AA 7C              LD A,H
02AB 210000          LD HL,0
02AE 0610            LD B,16
02B0 B7              OR A
02B1            DVLOOP
02B1 CB11            RL C
02B3 17              RLA
02B4 CB15            RL L
02B6 CB14            RL H
02B8 E5              PUSH HL
02B9 ED52            SBC HL,DE
02BB 3F              CCF
02BC 3801            JR C,DROP
02BE E3              EX (SP),HL
02BF            DROP
02BF 33              INC SP
02C0 33              INC SP
02C1 10EE            DJNZ DVLOOP
02C3 EB              EX DE,HL
```

```
02C4 CB11               RL C
02C6 69                 LD L,C
02C7 17                 RLA
02C8 67                 LD H,A
02C9 B7                 OR A
02CA C9                 RET
02CB            SQUOT   DS 1
02CC            SREM    DS 1
02CD            COUNT   DS 1
02CE
0000                    END
```